Heavy Quarkonium and QCD

Peacock, Anthony W

Heavy Quarkonium and QCD

Thesis submitted to the University of Durham
for the degree of Doctor of Philosophy by

Anthony W Peacock, BSc

October 1986

ACKNOWLEDGEMENTS

I would like to thank Alan Martin for his advice and guidance throughout the period of this research and for reading the manuscript, and also Kaoru Hagiwara and Martin Olsson for enjoyable collaborations.

I thank the members of the particle physics group at Durham - Alan Martin, Peter Collins, Fred Gault, Mike Pennington, Chris Maxwell, James Stirling, Mike Walley, Stuart Grayson, Nigel Glover, Anthony Allan, Neil Speirs, Martin Carter, King Lun Au, Simon Webb, Yanos Michopoulos, Nick Brown and Mohammed Nobarry - for providing a friendly and stimulating environment in which this work was carried out.

I am grateful to the Science and Engineering Research Council for financing this research and to Carole Walker for her excellent typing.

Finally, I would like to thank my family for their continual support and encouragement. This thesis is dedicated to my parents.

Heavy Quarkonium and QCD

Anthony W Peacock

Abstract

The sensitivity of the charmonium and bottomonium spectroscopy to the short distance part of the interquark potential is critically re-examined using the latest data. We confirm that the data cannot accommodate a QCD scale parameter ($\Lambda_{\overline{MS}}$) smaller than about 150 MeV, whereas we find no constraint on larger values of the scale parameter, contrary to a previous analysis. The effects of dynamical heavy quark masses in the loop correction to the perturbative potential is studied in detail and the effective four quark theory with a massive charmed quark is found to give an accurate description of the perturbative potential for quarkonia of mass up to about 250 GeV.

Predictions for the heavy quarkonium system of toponium are found to be very sensitive to the behaviour of the short-distance region of the potential and it is argued that the experimental determination of the mass and e^+e^- decay width of the 1S and 2S toponium resonances (of mass around 80 GeV) with accuracy anticipated at the forthcoming e^+e^- colliders should enable the QCD scale parameter to be determined to within ± 100 MeV.

The hadronic decays of the lowest S- and P-wave states of charmonium and bottomonium are examined in the light of recent experimental determination. All but the individual P-wave decays in charmonium can be adequately accounted for using reasonable values of the strong coupling constant and we are led to believe that the discrepancy lies with wavefunction corrections.

CONTENTS

* * * * * * * * * * *

CHAPTER 1

INTRODUCTION

1.1 Preamble

The history of particle physics has continually involved revealing new layers in the substructure of matter, which began with the discovery of atoms as the basic elementary constituents of chemical compounds and has led us to believe that at the current limits of resolution all matter is constructed of point-like spin 1/2 quarks and leptons. In addition, interactions between these particles - strong, weak and electromagnetic forces (neglecting gravity which is a small effect at current energies), all appear to be described by gauge theories and mediated by spin-1 gauge bosons. The gauge bosons of the Standard Model of interactions $SU(3)_C \times SU(2)_L \times U(1)_Y$, have all now been observed (although indirectly in the case of the strong force mediating gluons) thus lending support to the theoretical prejudices in favour of gauge theories.

The list of quarks and leptons is shown in Table 1.1, although the existence of the top quark is not yet established with absolute certainty, its discovery is confidently expected and indeed there is some evidence [1] for a top quark to exist in the mass range $30 < m_t < 50$ GeV.

In the next three sections we briefly discuss the ideas behind the gauge principle and the behaviour of the coupling constant in the electromagnetic and strong forces.

QUARKS			LEPTONS		
Flavour	Mass(GeV)	Q		Mass(GeV)	Q
Down,d	0.008	-1/3	e^-	0.0005	-1
Up,u	0.004	+2/3	ν_e	0	0
Strange,s	0.15	-1/3	μ^-	0.105	-1
Charm,c	1.5	+2/3	ν_μ	0	0
Bottom,b	4.9	-1/3	τ^-	1.8	-1
Top,t	?	+2/3	ν_τ	0	0

Table 1.1 : Masses and charges of the presently known quarks and leptons.

It is a property of all the gauge theories embodied in the Standard Model that there are unknown parameters that must be determined experimentally and in Section 1.5 we discuss the problems inherent in making a meaningful determination of the coupling in the strong force. As a possible testing ground for the ideas behind the strong force we consider heavy quark-antiquark bound states in Section 1.6. We motivate a non-relativistic description of such states and briefly discuss the interquark potential in Sections 1.7 and 1.8. Spin Dependent forces are analysed in Section 1.9 and the extent to which heavy quark-antiquark bound states are able to restrict the form of the interquark potential is reviewed in Section 1.10.

1.2 The Gauge Principle And Electromagnetism

The basis of the gauge principle, upon which all the components of the Standard Model rest, is the invariance of the fundamental Lagrangian under various local field transformations. These "symmetries" lead to conserved currents and thus to conserved charges, for example, the electric charge. The Lagrangian for a non-interacting spin 1/2 fermion ψ of mass m is;

$$L = i\bar{\psi}\gamma_\mu\partial^\mu\psi - m\psi\bar{\psi} \tag{1.1}$$

The Euler-Lagrange equations for this Lagrangian lead to the familiar Dirac equation

$$i\gamma_\mu\partial^\mu\psi - m\psi = 0 \tag{1.2}$$

This Lagrangian is invariant under the global phase transformation

$$\psi \rightarrow \exp(i\alpha)\psi \qquad \bar{\psi} \rightarrow \exp(-i\alpha)\bar{\psi} \tag{1.3}$$

and this leads, via Noethers Theorem, to the conserved current

$$j_\mu = \bar{\psi}\gamma_\mu\psi \tag{1.4}$$

The invariance under a global phase transformation implies that the phase, α , is unmeasurable and can be specified arbitrarily. A more general invariance occurs if the phase is allowed to vary at each space-time point, i.e. $\alpha \rightarrow \alpha(x)$. Lagrangians invariant under such a space-time dependent transformation are said to be locally gauge (or phase) invariant, and differ from eq. (1.1) in that an extra vector field must be introduced, resulting in a Lagrangian that describes spin 1/2 fermions interacting via the exchange of vector gauge bosons, i.e. Quantum Electrodynamics (QED).

$$L_{QED} = \bar{\psi}(i\gamma_\mu \partial^\mu \psi - m)\psi + e\bar{\psi}\gamma_\mu A^\mu \psi - (1/4)F_{\mu\nu}F^{\mu\nu} \qquad (1.5)$$

where ψ is the fermion field, A_μ is the gauge boson or photon and $F_{\mu\nu}$ is the electromagnetic field strength tensor defined by

$$F_{\mu\nu} = \partial_\mu A_\nu - \partial_\nu A_\mu \quad , \qquad (1.6)$$

and e is the electric charge of the fermion. The Lagrangian of eq. (1.5) is invariant under the local transformation

$$\psi \rightarrow \exp(i\alpha(x))\psi \quad , \qquad (1.7)$$

if A_μ transforms as

$$A_\mu \rightarrow A_\mu + (1/e)\partial_\mu \alpha(x) \qquad (1.8)$$

which is the usual gauge tranformation of the electromagnetic potential. The form of the fermion-photon coupling term is restricted by the fact it must exactly cancel the unwanted term generated by the local gauge transformation. The $F_{\mu\nu}F_{\mu\nu}$ term represents the kinetic energy of the photon and it is a direct consequence of local gauge invariance that a mass term for the photon $m^2 A_\mu A^\mu$ is not allowed.

The success of QED and the natural way in which both the photon-fermion coupling and masslessness of the photon arise suggests that local gauge invariance is a fundamental property and leads us to attempt descriptions of the strong and weak forces in a similar way.

1.3 The Strong Interaction

Quantum Chromodynamics (QCD) has now become widely accepted as the underlying theory of hadronic physics, and as such is an unquestionable ingredient of the Standard Model. The gauge transformations of QED, $\exp(i\,\alpha)$, form a unitary Abelian group U(1), and it is believed that QCD is based on the unitary non-abelian group $SU(3)_c$ of colour, in which, unlike the single generator of QED, QCD now has 8 generators and consequently 8 vector fields (gluons) which mediate the interaction. The quarks of the strong interaction lie in the triplet represenation of $SU(3)_c$ and the gluons lie in the adjoint. The QCD Lagrangian is;

$$L_{QCD} = \bar{q}(i\gamma_\mu\partial^\mu - m)q - g(\bar{q}\gamma_\mu T^a q)G^{\mu a} - (1/4)G^a_{\mu\nu}G^{\mu\nu a} \qquad (1.9)$$

where g is the strong coupling constant. The Lagrangian is invariant under local gauge transformations of the form

$$q \rightarrow \exp(i\alpha^a(x)T_a)q \quad , \qquad (1.10)$$

where q is a quark of mass m and where the eight generators of the group $T^a(a=1,..,8)$ form the SU(3) Lie Algebra

$$\left[T^a\ ,\ T^b\right] = if^{abc}T^c \quad . \qquad (1.11)$$

The gauge fields G^a_μ, in analogy to the photon field A_μ of QED, transform as a consequence of the local gauge invariance

$$G^a_\mu \rightarrow G^a_\mu - (1/g)\partial_\mu\alpha^a - f^{abc}\alpha^b G^c_\mu \qquad (1.12)$$

and the gluon field strength tensor has to have the form

$$G^a_{\mu\nu} = \partial_\mu G^a_\nu - \partial_\nu G^a_\mu - g f^{abc} G^b_\mu G^c_\nu \qquad (1.13)$$

As a result of the non-abelian nature of the group, (i.e. $f^{abc} \neq 0$), there are triple and quartic gluon interactions in the Kinetic energy term. Another way of expressing this is that in QCD the gluons carry the colour charge through which they couple to one another, unlike QED where the photon has zero electric charge. One direct consequence of these gluon self interactions is the different behaviour of the quark-gluon coupling in QCD as compared to the electron-photon coupling in QED.

1.4 The Running Coupling Constant

In QED, the electron-photon coupling, as depicted in Fig 1.1a, is determined in terms of the bare charge of the electron, e, that appears in the QED Lagrangian of eq. (1.5) or equivalently the fine structure constant, $\alpha \equiv e^2/4\pi$. However, higher-order vacuum polarisation corrections to this vertex, Fig 1.1b, tend to shield the bare charge of the electron, and a calculation of such diagrams gives the leading behaviour for α as

$$\alpha(Q^2) \simeq \alpha \left[1 + \left(\frac{\alpha}{3\pi} \ell n \frac{Q^2}{\mu^2} \right) + \left(\frac{\alpha}{3\pi} \ell n \left(\frac{Q^2}{\mu^2} \right) \right)^2 + \ldots \right] , \qquad (1.14)$$

where Q^2 is the momentum of the photon and μ is the arbitrary normalisation point at which α has been measured. It is convenient to define α as the value of the photon-electron-electron coupling in the limit of zero photon momentum when the electrons are on their mass shells

$$\alpha \equiv \alpha_{EM}(m_e^2) = 1/137 \qquad (1.15)$$

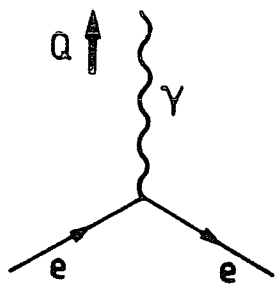

Fig 1.1a : The electron-photon vertex.

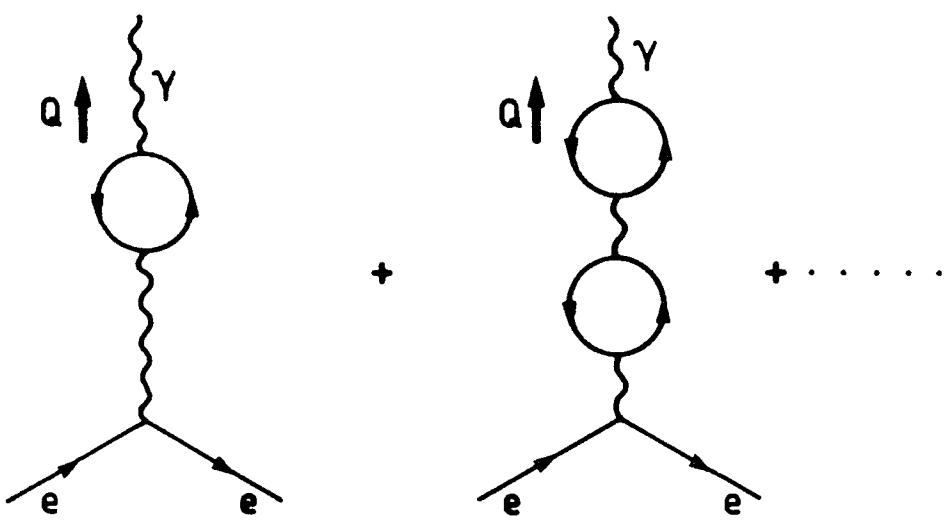

Fig 1.1b : Higher-order vacuum polarisation corrections to the bare vertex of Fig 1.1a.

Higher-order corrections produce a whole series of $[\ln(Q^2/\mu^2)]^n$ terms to leading order which can be resumed

$$\alpha(Q^2) \simeq \frac{\alpha_{EM}}{\left[1 - (\alpha_{EM}/3\pi)\ell n(Q^2/m_e^2)\right]} \qquad (1.16)$$

for $Q^2 >> m^2_e$. Thus the coupling in QED is not a constant at all but depends upon the energy of the photon, Q. As Q^2 increases, the photon sees more and more of the bare charge resulting in an increase of the coupling. The bare charge is thus ultraviolet divergent and it would seem that a breakdown of perturbation theory in QED is inevitable for large enough Q^2, however, gravitational effects will have modified the theory long before such a large Q^2 is reached and in fact a 10% effect would require $Q^2 \sim 10^{56}$ GeV, well out of the practical range.

Considering the equivalent gluon-quark coupling in QCD, Fig 1.2a, which is again determined in terms of the bare coupling, g, that appears in the QCD Lagrangian of eq. (1.9), or $\alpha_s \equiv g^2/4\pi$. Higher-order corrections to the bare vertex, Fig 1.2b, now include gluon self-interaction terms and calculating such diagrams, analogously to QED we find that the coupling of the gluon-quark vertex becomes

$$\alpha_s(Q^2) \simeq \alpha_s(\mu^2)\left[1 - \left(\frac{\alpha_s(\mu^2)}{2\pi} b_o \ell n \frac{Q^2}{\mu^2}\right) + \left(\frac{\alpha_s(\mu^2)}{2\pi} b_o \ell n \frac{Q^2}{\mu^2}\right)^2 + \ldots\right] , \qquad (1.17)$$

where b_o is a calculable constant and μ is again the arbitrary normalisation point at which α_s is measured. Summing the leading log terms gives

$$\alpha_s(Q^2) \simeq \frac{\alpha_s(\mu^2)}{\left[1 + (b_o/2\pi)\alpha_s(\mu^2)\ell n(Q^2/\mu^2)\right]} \qquad (1.18)$$

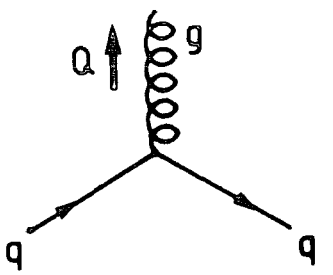

Fig 1.2a : The quark-gluon vertex.

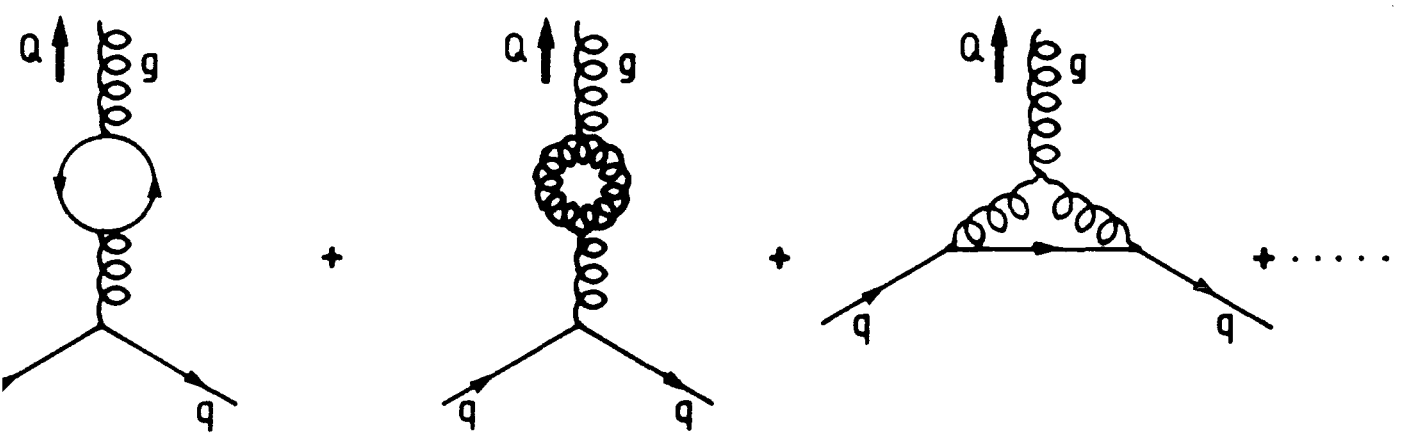

Fig 1.2b : Higher-order corrections to the bare vertex of Fig 1.2a including gluon self interaction terms.

Again the coupling in QCD depends upon the energy of the gluon, Q, however the precise dependence is controlled by the value of b_o. In QED, the equivalent to b_o is a negative quantity resulting in an ultraviolet divergent bare charge. However, in QCD, extra positive contributions to b_o arise due to gluon self interactions that are not present in QED. The value of b_o is found to be,

$$b_o = (11/6)N_C - (1/3)n_f \quad , \tag{1.19}$$

where N_C is the number of colours (=3), and n_f is the number of quark flavours that can contribute to fermion loops in the first diagram of Fig 1.2a. Thus we see that as long as $n_f < 16$, then $b_o > 0$ and it follows that $\alpha_s(Q^2) \to 0$ as $Q^2 \to \infty$, which is the opposite behaviour to that of QED. This property of the coupling in QCD is known as asymptotic freedom and is one of its most appealing features, implying that at very short distances coloured objects appear to be free. The discovery that QCD had this property is one of its major successes and offers a theoretical justification for the phenomenologically successful parton model. At large distances, or small Q^2, the coupling becomes large and we enter the regime of non-perturbative hadronic physics and although it is still a matter of conjecture whether this property leads to confinement, it offers an explanation for the non-observation of free quarks.

It is convenient to introduce a parameter Λ at this stage which parameterizises the Q^2 dependence of the coupling constant,

$$\Lambda^2 = \mu^2 \exp(-2\pi/\alpha_s(\mu^2)b_o) \quad , \tag{1.20a}$$

from which we can write, using eq. (1.18),

$$\alpha_s(Q^2) = 2\pi/(b_o \ell n(Q^2/\Lambda^2)) \quad . \tag{1.20b}$$

The parameter Λ of eq. (1.20b), now appears as a fundamental parameter, in much the same way as the fine structure constant α_{EM}, is for QED. Both quantities are not predicted by the theory but must be determined experimentally. The scale parameter Λ is introduced essentially due to the fact that there is no obvious definition for μ in eq. (1.17). In QED, μ is chosen as the electron mass and corresponds precisely to the region where the coupling is small and perturbation theory is expected to be reliable and readily accessible to experiment. However in QCD, this lower energy limit is excluded as a possible definition, as it is where the coupling is large and perturbation theory breaks down. Thus if QCD has a fundamental scale parameter we must consider how to obtain its value. Although such an evaluation may at first sight seem simple, in that all we need do is consider an observable process with a well defined momentum scale, Q, from which we can determine the coupling. Then from eq. (1.20b) we can simply read off Λ. However there is an ambiguity in the definition of the coupling constants, which in turn leads to problems in the precise definition of Λ when the perturbative calculation of a quantity in QCD is considered. This is known as the Renormalisation Scheme dependent problem.

1.5 Renormalisation Scheme Dependence

In order to determine the value of the QCD scale parameter Λ, we are restricted to use perturbation theory in order to calculate QCD predictions for a particular process. We write the predictions for an observable R as

$$R = a^N (1 + r_1 a + r_2 a + \ldots) , \quad N > 0, \tag{1.21}$$

where $a = \alpha_s(Q^2)/\pi$ and r_1, r_2, etc., are calculable higher order coefficients. In calculating these coefficients, divergences occur in the integrations over momenta flowing in closed loops of Feynman diagrams. There are a number of well established methods of dealing with such divergences. They essentially consist of identifying the source of the infinities and separating them out from the rest of the terms. Then by suitably defining a coupling constant in such a way that the infinities are either removed or absorbed in the definition, a finite answer remains.

For example, in the calculation of the quark-gluon vertex that was considered in Section 1.4, the higher-order corrections shown in Fig 1.2b, induce ultraviolet divergences due to the integrations of momenta flowing in closed loops. To control these divergences an ultraviolet momentum cutoff K is introduced in the integrals and in terms of K the coupling is,

$$\alpha_s(Q^2) = \alpha_s\left[1 - \left(\frac{\alpha_s}{2\pi} b_o \ell n \frac{Q^2}{K^2}\right) + \left(\frac{\alpha_s}{2\pi} b_o \ell n \frac{Q^2}{K^2}\right)^2 + \cdots\right], \qquad (1.22)$$

where α_s is defined from the bare coupling of the Lagrangian. Eq. (1.22) has no meaning as it diverges for $K \to \infty$. However, if we assume that we know the coupling $\alpha_s(Q^2)$ at $Q^2 = \mu^2$,

$$\alpha_s(\mu^2) = \alpha_s\left[1 - \left(\frac{\alpha_s}{2\pi} b_o \ell n \frac{\mu^2}{K^2}\right) + \left(\frac{\alpha_s}{2\pi} b_o \ell n \frac{\mu^2}{K^2}\right)^2 + \cdots\right], \qquad (1.23)$$

then both α_s and K of eq. (1.22) can be eliminated to give the result in eq. (1.17). It is essentially the fact that we have introduced the couple $\alpha_s(\mu^2)$ which removes the divergence.

There are in fact, an infinite number of such ways in which the divergences can be removed, leaving an arbitrary finite remainder and which lead to different values of r_i in eq. (1.21). Some of the more frequently used schemes of dealing with the divergences are outlined below:

(a) Minimal Subtraction Scheme [2]

In this scheme the loop integrals are evaluated in n-dimensions and it is found that the divergences appear as singularities of the form $1/(n-4)$ and hence only appear in 4-dimensions. These terms are separated and dropped. On returning to 4-dimensions the result is finite and $\alpha_{MS}(Q^2)$ along with Λ_{MS} are defined.

(b) Modified Minimal Subtraction Scheme [3]

Again the loop integrals are evaluated in n-dimensions and, in addition to the singularities, factors of $\ell n 4\pi$ and γ_E (Euler's Constant), which appear as artifacts of the calculation, are also dropped. The scheme defines $\alpha_{\overline{MS}}(Q^2)$, along with $\Lambda_{\overline{MS}}$

(c) Momentum-space Schemes [4]

The coupling in this scheme $\alpha_{MOM}(Q^2)$ is defined as the value of the three gluon-vertex (or quark-quark-gluon vertex) when the invariant masses of the particles are $-Q^2$. $\alpha_{MOM}(Q^2)$ is not related to any physical process and practical calculations in this scheme prove to be very difficult.

The coupling between any two schemes are related by a perturbative expansion

$$\alpha_2 = \alpha_1(1 + c\alpha_1) \qquad (1.24)$$

where the coefficient c is known for any two of the three schemes shown above. From eq. (1.24) it is clear that the value of r_1 in eq. (1.21) will depend on the particular scheme being used, and if this is the only coefficient known, we cannot be sure which scheme best approximates the true value of the physical quantity. It follows then, that there is an ambiguity in the precise definition of the fundamental scale parameter relevant for a physical process.

We further note that if none of the higher coefficients for a physical process are known then Λ is arbitrary up to a rescaling $\Lambda \to \Lambda' = x\Lambda$ Introducing a rescaling of Λ in the leading order equation for the coupling eq. (1.20b), is only manifest as a higher order effect, and can be absorbed into the unknown coefficient r_1.

The Renormalisation Scheme dependent problem we have discussed here, resulting in an ambiguity of the physical value of Λ , is essentially due to the fact that we have been limited to a truncated perturbation expansion with which to confront a physical process. The renormalisability of QCD ensures that the prediction for a physical quantity does not depend on the particular scheme provided we calculate to all orders, implying that a single value of Λ should result no matter what scheme is used. However, such a calculation to all orders is impossible in a finite amount of time, so the problem remains.

There are many physical processes from which the value of Λ can be extracted, and an extensive review is given in ref. [20].

Some examples are the ratio of hadronic to muon pair-production total cross-sections in e^+e^- annihilations and a study of the QCD corrections to the lowest-order expressions for parton densities within hadrons for both deep inelastic scattering and lepton pair-production experiments. In each process a quantity R, of the form eq. (1.21), relevant to the physical observable is calculated to at least next-to-leading order of QCD for a variety of schemes, in order to analyse the relevance of the Renormalisation scheme dependence problem for the particular process.

The accuracy to which the value of the coupling constant, α_s , relevant to a process and scheme, can be determined is dependent upon the accuracy to which the observable R is obtained experimentally. In fact, it can be seen from eq. (1.20b) that extreme accuracy of α_s is required if an accurate determination of Λ is to be achieved, due to the exponential sensitivity between the two quantities.

The processes analysed in ref. [20] typically indicate values of α_s around 0.2 and lead to the fact that the range, Λ = 0.2-0.5 GeV, will satisfy most determinations, although no single value is entirely consistent with all processes. To study in detail the accuracy to which the value of the QCD fundamental scale parameter, Λ , can be determined, we consider systems of heavy quark-antiquark pairs, bound by the QCD force and which are readily accessible to accurate experimental observation. The relevant calculable quantity, R, to this system is the interquark potential describing the binding force between the quark pair, from which α_s can be obtained. However, we first consider the properties of the bound-state system itself.

1.6 Heavy Quarkonia

Initially the underlying quark picture of strongly interacting particles was viewed as a convenient mathematical tool with which to classify the large spectrum of these particles found in accelerator experiments in the 1950's and 1960's, and up until November 1974 all particles could be explained in terms of 3 quarks (u, d, s) where the only allowed combinations are of three quarks (qqq) to form baryons or a quark and an antiquark (qq) to form mesons.

The discovery of a new particle in e^+e^- collisions at the Stanford Linear Accelerator and its simultaneous observation at the Brookhaven AGS in collisions of 28 GeV protons on a beryllium target;

$$\text{SLAC} : \quad e^+e^- \rightarrow \psi \rightarrow \text{hadrons}, e^+e^-, \mu^+\mu^- \tag{1.25}$$

$$\text{BNL} : \quad p + \text{Be} \rightarrow J + \text{anything}, \quad J \longrightarrow e^+e^- \tag{1.26}$$

heralded the beginning of a new era in particle physics and was to firmly establish the existence of quarks as constituents of matter. The new particle, which has become commonly known as the J/ψ, was seen as a very sharp resonance at a mass of around 3.1 GeV and was immediately recognised as being exceptional due to its very small width of 67 keV. (A 3 GeV state would, a priori, be expected to have a width of some hundreds of MeV). Also, by increasing the beam energies at SLAC, a second resonance was observed at a mass of around 3.7 GeV within a few weeks of the first discovery, and named ψ'

Many possible explanations of these states immediately followed, however their properties could all be understood in a rather natural manner if one assumes that these particles are bound states of a new heavy quark, the charmed quark. The production mechanism at SLAC then implies that both these states are vector mesons with the same quantum numbers as that of the photon, see Fig 1.3. Since no narrow $J^{PC} = 1^{--}$ resonances were found below the J/ψ it is identified as the ground state and the ψ' as its first excited partner.

Such a charmed quark (of charge +2e/3) had been postulated some years previously by Glashow, Iliopoulous and Maiani [5], in order to suppress strangeness - changing weak neutral currents, and carried a new quantum number, C for charm, which like strangeness, would be additively conserved in strong and electromagnetic interactions.

The startling property of the J/ψ was its extreme narrowness which, with hindsight, can be understood in analogy with the suppressed decay of the ϕ particle, a bound state of a strange and anti-strange (ss) quark, into non-strange hadrons. On grounds of phase space alone, it should be energetically more favourable for the ϕ to decay into three pions, composed of up and down quarks only, than for it to decay into two Kaons, each containing a strange quark. Yet experimentally it is found

$$\frac{\Gamma(\phi \to 3\pi)}{\Gamma\ \phi \to KK)} \simeq \frac{1}{5} \qquad (1.27)$$

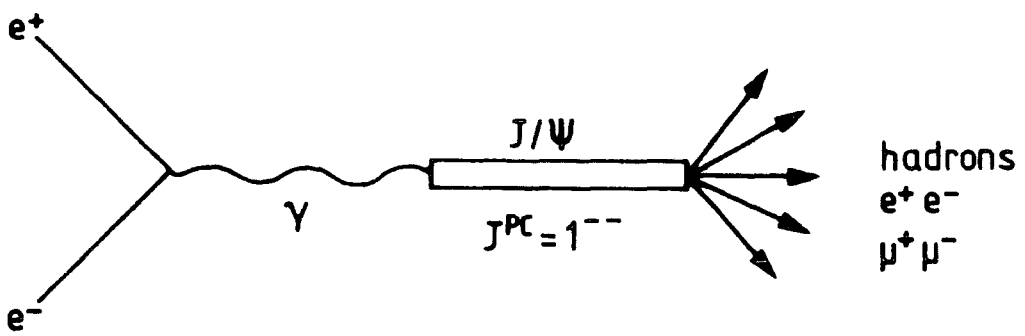

Fig 1.3 : The production mechanism for the J/ψ resonance produced in e^+e^- colliding beam experiments, via a virtual photon. The J/ψ then decays into leptons or quarks (which subsequently form hadrons in the final state).

Motivated by this suppression, the OZI rule [6] was proposed which states that decay processes with disconnected quark lines between initial and final states are suppressed in comparison to those with connected quark line diagrams. These two decay modes of the ϕ are shown in Fig 1.4. In the context of QCD, the OZI suppression can be viewed in terms of the reduced rate at which the quark-pair annihilate to form a multigluon intermediate state, as in Fig 1.4a, compared to the rapid creation of a quark-pair from the vacuum, as in Fig 1.4b.

The equivalent diagrams for the decay of the J/ ψ are shown in Fig 1.5. By the OZI rule, the decay in Fig 1.5b is favoured, however, this channel is forbidden by energy conservation as both the J/ ψ (3.1) and ψ' (3.7) lie below the threshold for the production of particles with open charm, i.e. $2M_D$ = 3.75 GeV. Fig 1.5a is therefore the only allowed hadronic decay and its suppression results in a long lifetime or equivalently a narrow width for the J/ ψ . In fact, the suppression is greater than seen for the ϕ due to the fact that the charm quark is heavier than the strange. Asymptotic freedom then tells us that the J/ ψ couples less strongly to gluons than the ϕ,

$$\alpha_s(m_\psi) < \alpha_s(m_\phi) \qquad (1.28)$$

The interpretation of the J/ψ and ψ' as bound states of a charm quark and anti-quark pair leads to clear experimental predictions, as other states should be expected.

Indeed further states have now also been discovered by studying the decays of these resonances produced in e^+e^- collisions. The analysis of the cascade decays

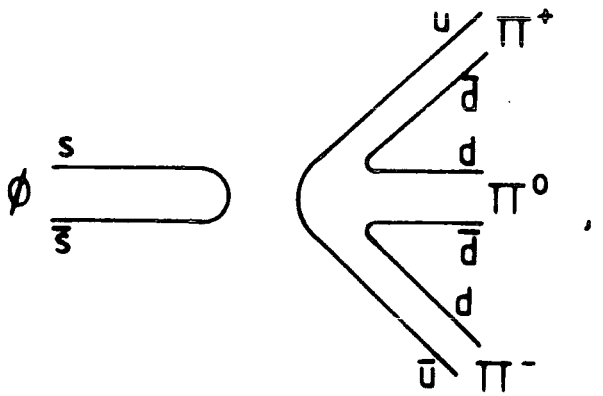

Fig 1.4a : OZI rule suppressed decay mode of $\phi \rightarrow 3\pi$

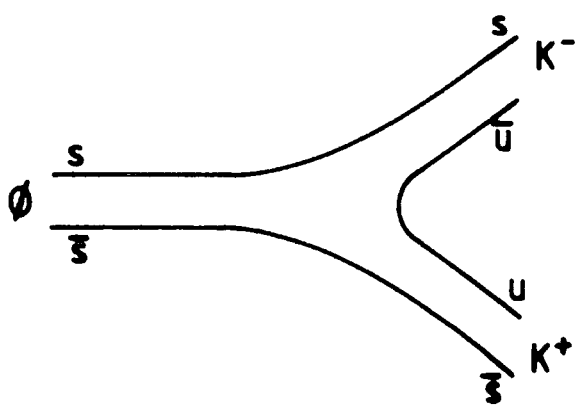

Fig 1.4b : OZI rule allowed decay mode of $\phi \rightarrow K^+K^-$

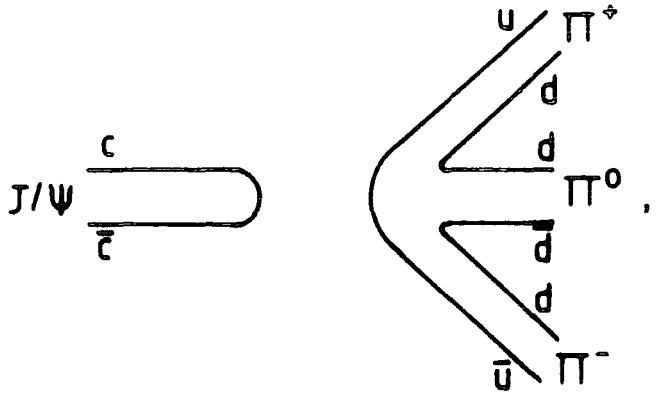

Fig 1.5a : OZI rule suppressed decay mode of $J/\psi \to 3\pi$

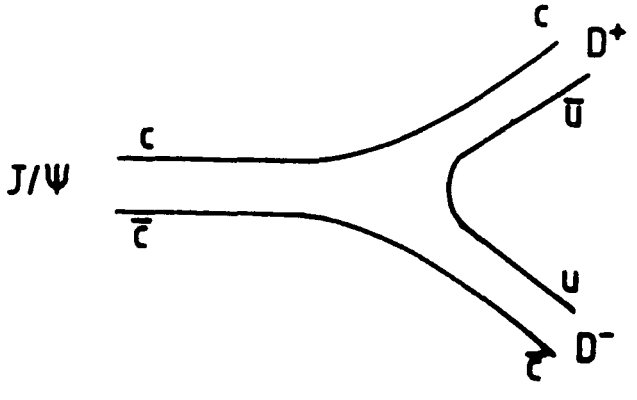

Fig 1.5b : OZI rule allowed decay mode of $J/\psi \to D^+D^-$

$$\psi' \rightarrow \gamma\gamma\psi \longrightarrow e^+e^- \qquad (1.29)$$

and the inclusive photon spectrum

$$\psi' \rightarrow \gamma + \text{anything} \quad , \qquad (1.30)$$

led to the discovery of cc χ states as well as η_c and η_c' which are interpreted as the P wave states and S wave spin-singlet partners to the J/ ψ and ψ' respectively, and indeed the discovery of these states has confirmed the interpretation of the spectroscopy in terms of qq bound states.

The cc or charmonium spectroscopy of states below threshold for DD pair production is shown in Fig 1.6a. Heavier states are also observed but decay very rapidly and have broad widths, characteristic of the lighter hadrons. The decay products of these heavier states are particles containing a single charmed quark plus another lighter quark, as seen by the decay in Fig 1.5b. Such hadrons carry the charm quantum number and can only decay weakly into normal hadrons. As such these particles provide a good testing ground for the weak interactions.

In Fig 1.6b, the charmonium spectrum can be compared to that of positronium, the bound state system of an electron and a positron. Apart from the difference in energy scales, the two spectroscopies are seen to be very similar, again providing strong evidence for believing that charmonium results from the binding of a heavy quark and anti-quark pair and leads us naturally to try and apply a non-relativisitic potential model description of such states.

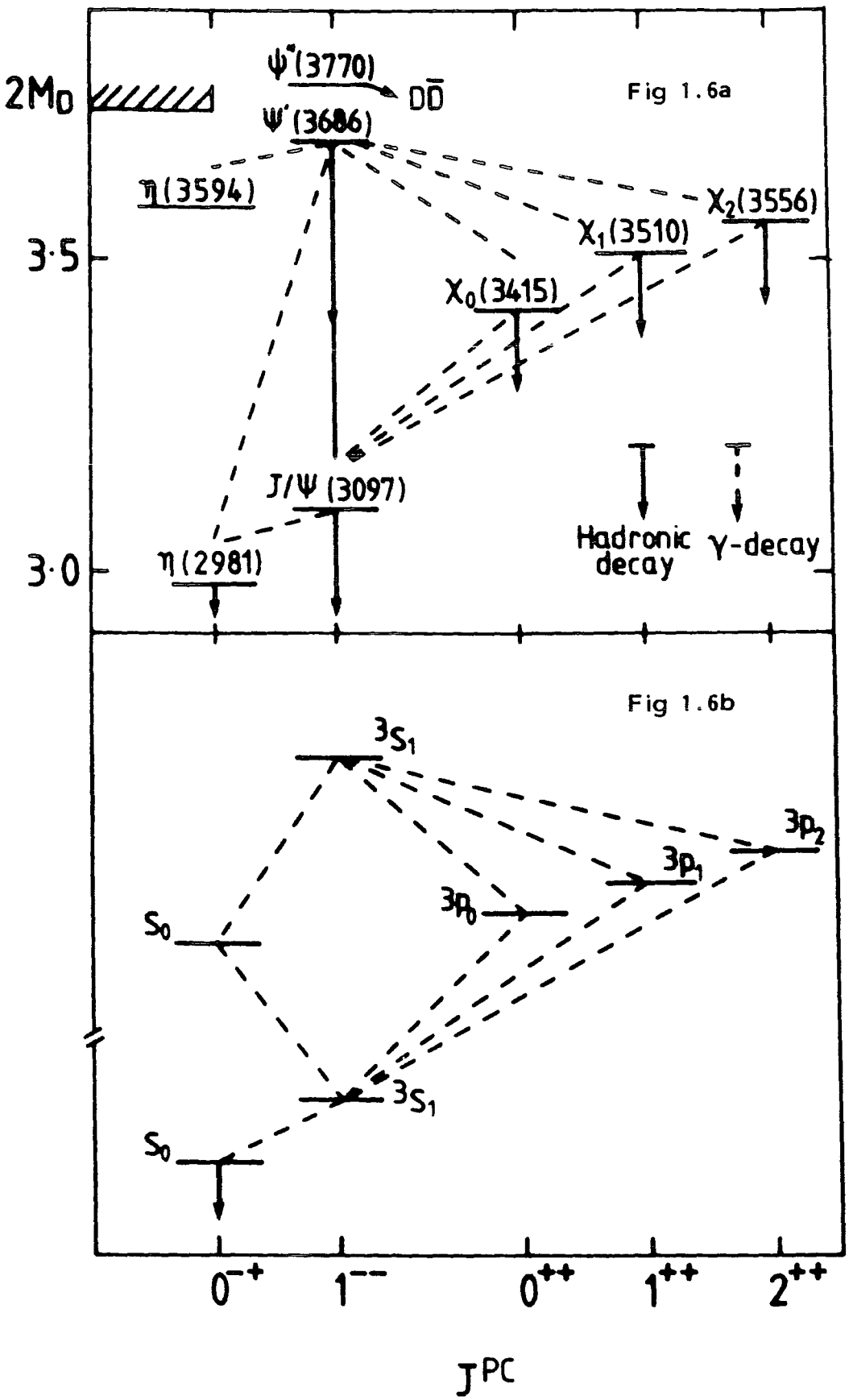
2M_D
3·5
3·0
ψ''(3770)
DD̄
ψ'(3686)
η(3594)
χ2(3556)
χ1(3510)
χ0(3415)
J/ψ(3097)
η(2981)
Hadronic decay
γ-decay
Fig 1.6a
Fig 1.6b
3S1
3p2
3p1
3p0
S0
S0
3S1
0−+
1−−
0++
1++
2++
JPC

Fig 1.6a : The observed charmonium spectrum. The transitions and states shown have all be observed. Another state is expected $^1P_1(J^{PC} = 1^{+-})$ and awaits discovery. The threshold for D^+D^- decay is indicated and the particles below this cannot decay into charmed mesons. The states with $J^{PC} = 1^{--}$ can be directly produced by e^+e^- colliders.

Fig 1.6b : The positronium spectrum, labelled in the conventional spectroscopic manner $^{2S+1}L_J$ where S, L and J are the total intrinsic spin, orbital and total angular momentum of each e^+e^- state respectively, in the non-relativistic classification.

To justify such a treatment we note that the observed spectrum in charmonium is similar to what would be expected from a non-relativistic analysis and also that the mass of the charmed quark is large compared to the typical hadronic energy scale. To see this more clearly we consider the Fourier Transformation of the running coupling constant, eq. (1.20), into co-ordinate space,

$$\alpha_s(r) = 2\pi/(b_o \ell n(1/\Lambda^2 r^2)) \quad . \tag{1.31}$$

The typical hadronic length is of the order 1 fermi $\equiv 5\ GeV^{-1}$, to which we associate an energy scale being that for which the coupling becomes of order unity,

$$r_c \sim \Lambda^{-1} \ , \quad \text{i.e.} \quad \Lambda \sim 200 \quad \text{MeV} \quad . \tag{1.32}$$

This is equivalent to saying that quarks inside particles of dimensions 1 fermi will typically have a momentum of about 200 MeV. The non-relativistic approximation is then valid provided the mass of the system is large compared to this momentum scale which for charm, $m_c = 1.5$ GeV, should be a reasonable approximation.

In 1977, following the discovery of the charmonium system, similar narrow resonances in the mass range 9.5 - 10.5 GeV were observed, and attributed to the bound states of a still heavier bottom quark, of charge $-e/3$. This system appeared in direct analogy with the charmonium spectrum and is shown in Fig 1.7 for those states below the open flavour threshold, although again higher mass broad states have also been identified. As the mass of this bottom quark, $m_b \simeq 5$ GeV, is much heavier than that of the charm quark, a non-relativistic treatment should be even more appropriate for bottomonium.

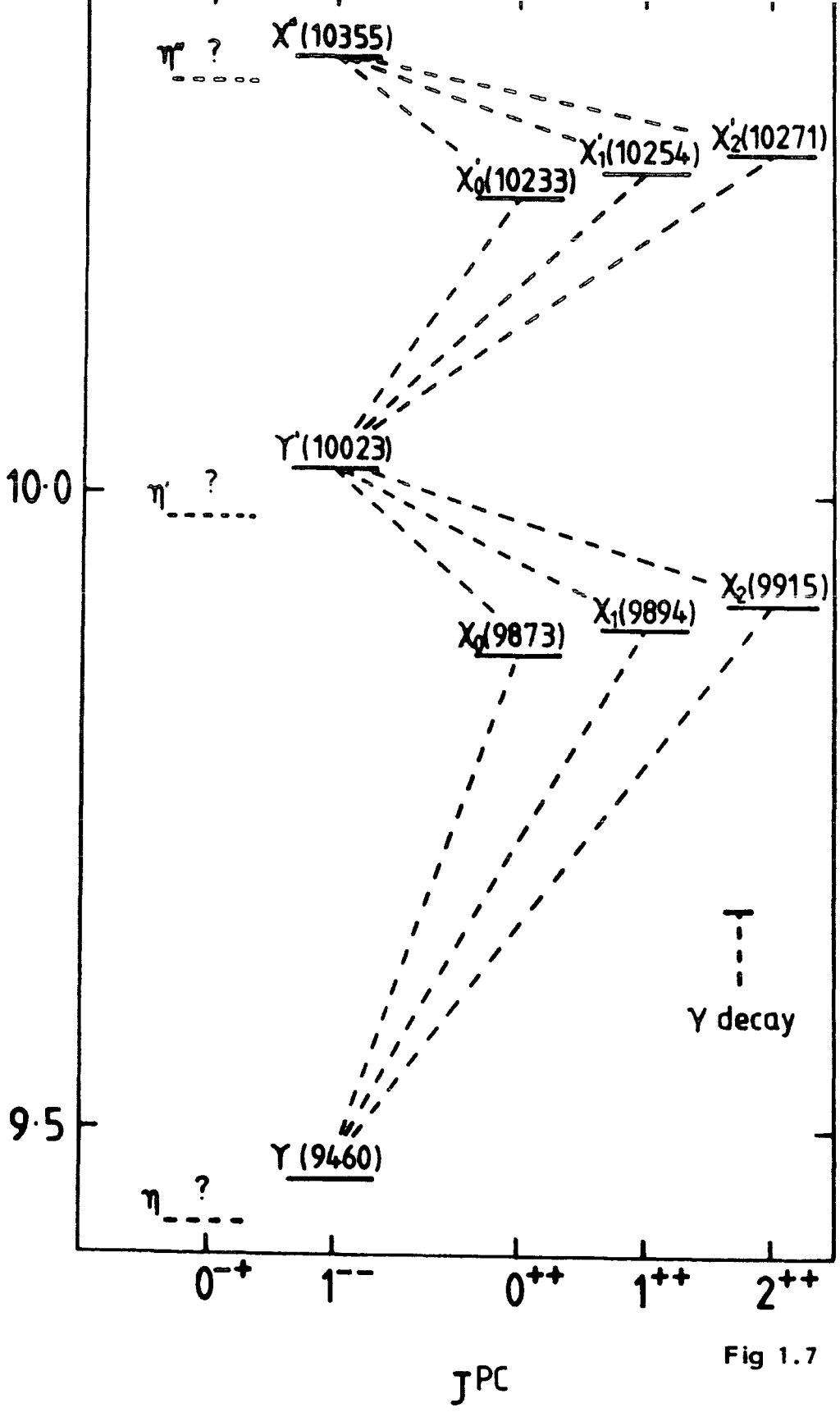

Fig 1.7

Fig 1.7 : The observed bottomonium spectrum. The dotted levels denote the spin-singlet S waves, which along with the $^1P_1$ states have not been observed. Only those states below open flavour threshold are shown.

The mass spectrum of charmonium and bottomonium, collectively known as heavy quarkonia, can be computed in the non-relativistic approximation using Schrodinger's equation and as such provides an ideal testing ground for the quark model and the strong interaction which binds these systems together.

1.7 Non Relativistic Quantum Mechanics

On the basis of the previous discussion it would be hoped that a good description of the charmonium and bottomonium spectroscopies is possible in terms of the Schrodinger equation.

Neglecting spin-dependence until Section 1.9, we write the 3-dimensional Schrodinger equation for a qq pair as

$$-\frac{\hbar^2}{2\mu}\nabla^2\Psi(r) + \left[V(r) - E_{n\ell}\right]\Psi(r) = 0 \quad , \tag{1.33}$$

where μ is the reduced mass of the system ($=m_q/2$), r is the relative quark separation $\Psi(r)$ is the Schrodinger wavefunction, V(r) is the interaction potential between the quark and antiquark and $E_{n\ell}$ are the allowed eigenvalues giving the possible masses of the qq bound states. Although we have kept the constant h in eq. (1.35), in all that follows we shall use natural units with

$$\hbar = c = 1 \quad . \tag{1.34}$$

For a central potential, the angular dependence of eq. (1.33) can be eliminated by writing

$$\Psi(r) = R_{n\ell}(r)\, Y_{\ell m}(\theta,\phi) \quad , \tag{1.35}$$

where $R_{n\ell}(r)$ is the radial wavefunction and $Y_{\ell m}(\theta, \phi)$ are the spherical harmonics. The radial equation is then

$$-\frac{1}{2u}\left(\frac{d^2}{dr^2}+\frac{2}{r}\frac{d}{dr}\right)R_{n\ell}(r)-\left[E_{n\ell}-V(r)-\frac{\ell(\ell+1)}{2\mu r}\right]R_{n\ell}(r)=0 \qquad (1.36)$$

and the radial wavefunction is normalised such that

$$\int_0^\infty dr\ r^2\left|R_{n\ell}(r)\right|^2=1 \quad . \qquad (1.37)$$

Then for an input potential V(r), the solution of eq. (1.36) gives the mass of the state

$$M_{n\ell}(qq)=2m_q+E_{n\ell}(m_q,V(r)) \quad . \qquad (1.38)$$

Obviously, the main problem now in making a quantitative analysis of the heavy quarkonia spectroscopy is the choice of interaction potential, V(r). So far this potential has not yet been computed from first principles and so we must rely upon models which incorporate as many QCD features as possible.

1.8 The Quarkonium Potential

Before we discuss specific models of the quarkonium potential, we first consider constraints that the observed quarkonia spectroscopies of Fig 1.6a and Fig 1.7, impose on the form of the potential. In positronium, the form of the interaction potential underlying the spectroscopy is of the pure Coulomb-type, $V(r) \sim 1/r$, in which neglecting fine structure effects the 2S and 1P levels are degenerate. Likewise for an Oscillator potential, $V(r) \sim r^2$, the 1P level is predicted to be exactly midway between 2S and 1S levels. In the spectroscopies of charmonium and bottomonium, the P wave level is found to be neither degenerate with, nor exactly midway between, the S-wave levels, indicating that the quarkonium potential has a form somewhat intermediate between the $1/r$ Coulomb and the r^2 Oscillator potentials.

A wide variety of quarkonium potentials have been proposed in order to describe the binding force between the quark and antiquark in charmonium and bottomonium. They essentially fall into two classes:

1. QCD-like Models

This class of model is motivated by the known value of the potential energy of two infinitely heavy (i.e. static) colour sources in a colour singlet state, separated by a distance, R. For single gluon exchange, which is the first-order calculation, the static qq potential is

$$V(r) \underset{r<<\Lambda}{\sim} -\frac{4}{3}\frac{\alpha_s(r)}{r} \quad , \tag{1.39}$$

and corresponds to a static Coulomb field at short distances, see Fig 1.8a. We see that due to the logarithms introduced by the running coupling constant of (eq. 1.31), that the QCD Coulomb field is not as singular as the pure Coulomb field of QED. At large separations, when the coupling becomes strong and perturbative theory is no longer valid, the colour lines of force extending between the two sources couple together as a consequence of the gluon self interactions, see Fig 1.8b, and we find:

$$V(r) \underset{r>>\Lambda}{\sim} Kr \quad . \tag{1.40}$$

In this class of models the behaviour of the potential at intermediate distances is chosen ad hoc.

The simplest choice for a potential of this type was first introduced by the Cornell Group [7]

$$V(r) = -\frac{4}{3}\frac{\alpha_s}{r} + br \quad , \quad \alpha_s = \text{constant} \quad . \tag{1.41}$$

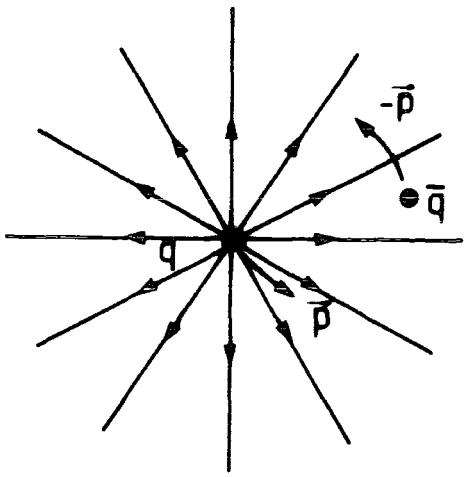

Fig 1.8a : Short-distance field configuration of the $q\bar{q}$ potential showing the Coulomb-type interaction motivated by single gluon exchange. P denotes the momentum of the quark (or antiquark) in the bound state.

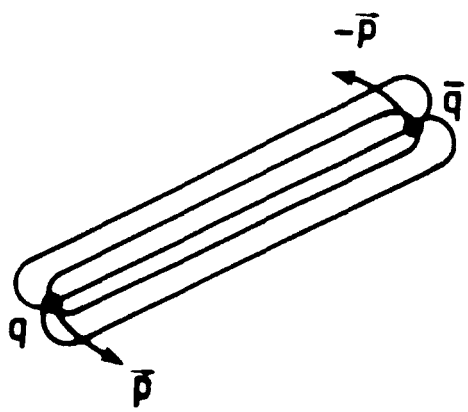

Fig 1.8b : The large distance expected field configuration of the $q\bar{q}$ potential showing the linear increase of binding energy with separation. This picture is motivated by the self coupling of the colour flux lines of force due to gluon exchange.

More sophisticated models have been proposed which incorporate the running of the coupling constant as well as next-to-leading order calculations for the static qq potential [8].

2. Empirical Models

Models without any theoretical bias have been proposed to empirically describe quarkonia spectroscopy. A celebrated example is that due to Martin [9],

$$V(r) = A + Br^{0.1} \quad , \tag{1.42}$$

although many others exist.

We plot in Fig 1.9 a variety of quarkonium potentials resulting from a fit to data. The potentials are seen to essentially agree in the range $0.1 < r < 1$ fermi, where neither limit of QCD-like models applies. The presently known charmonium and bottomonium data do not constrain the form of the potential at larger or smaller distances, but simply demonstrate the consistency of QCD-like models with experiment rather than prove their existence.

1.9 Spin Dependent Effects

First-order relativistic corrections to this non-relativistic approximation result in spin dependent forces which induce, for example, a separation of the triple P wave levels, and remove the degeneracy of the singlet and triplet S wave states. If in the non-relativistic approximation the mass of a level is predicted to be at m_L, then after including $O(v^2/c^2)$ corrections the mass becomes dependent on the spin configuration and can be written

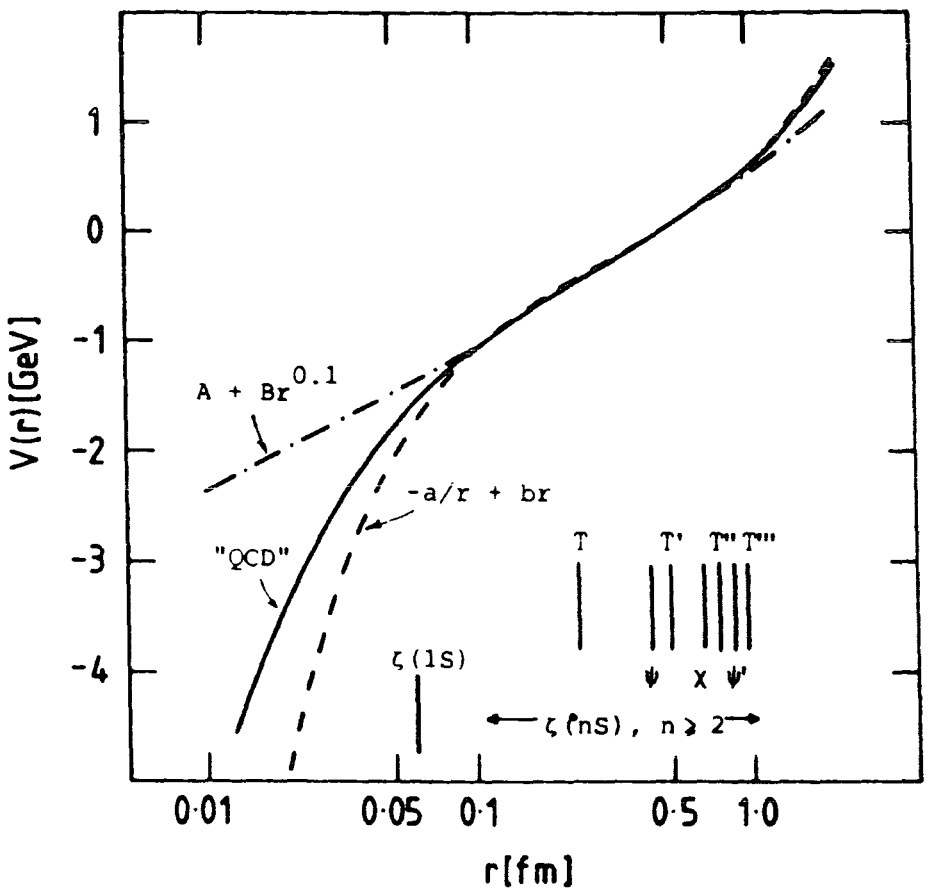

Fig 1.9 : A comparison of a variety of quarkonium potentials which successfully describe $c\bar{c}$ and $b\bar{b}$ spectra. The quarkonia states are shown at their mean square radii. This figure is adapted from a figure in ref [14].

$$m(^{2S+1}L_J) = m_L + m_H\langle S_1 . S_2\rangle + m_{SO}\langle L.S\rangle + m_T\langle \hat{r}.S_1\hat{r}.S_2 - (1/3)S_1.S_2\rangle \quad (1.43)$$

where S_1, S_2 refer to the spin operator of each quark and L is the orbital angular momentum operator between the quarks. The correction terms are written in direct analogy to these calculated for positronium [10], but modified such that the relevant interactions between magnetic fields and magnetic dipole moments refer to the qq system. The quantities m_H, m_{SO} and m_T represent hyperfine, spin orbit and tensor interactions respectively and depend upon the specific form of the quarkonium potential (see Ref [11]), and for a calculation in perturbation theory also depend upon the non-relativistic wave function of the Schrodinger equation, eq. (1.36). In order to determine the importance of such effects to the form of the short-distance region of the potential we consider quantitative estimates of these splittings in presently known and in any heavier quarkonium system that may be found.

Consider first the hyperfine force represented by m_H and which removes degeneracy between the triplet and singlet S wave states. This force is due to the interaction between the spins of the two quarks and as such is considered to be of short-range. Choosing the interquark potential to be the Cornell type of eq. (1.41) with which to make predictions we find the hyperfine splitting to be [12]

$$\Delta(n^3S_1 - n^1S_0) = \frac{8}{9}\frac{\alpha_s}{m_q^2}|R_{nS}(0)|^2 \quad (1.44)$$

where $R_{ns}(0)$ is the value of the radial n - S wavefunction at the origin. In charmonium the 1S hyperfine splitting between the ψ and η_c is predicted to be

$$\Delta(\psi - \eta_c) = 92 \text{ MeV} \quad , \tag{1.45}$$

which compares favourably with the experimental splitting of 116 MeV. In bottomonium eq. (1.44) predicts

$$\Delta m^{b}_{h.f.s.} = 32 \text{ MeV} \quad , \tag{1.46}$$

and for a quark qq system of mass around 80 GeV predicts

$$\Delta m_{h.f.s.}(80 \text{ GeV}) = 15 \text{ MeV} \quad . \tag{1.47}$$

These splittings are somewhat over-estimated since the Coulomb type singularity of the Cornell potential should be softened by logarithmic corrections arising from the running of the coupling constant in the one gluon exchange interaction. However it can be seen that this effect reduces considerably with increasing quark mass.

Indeed it will be essentially impossible to resolve this $\sim$ 10 MeV splitting in the forthcoming toponium experiments.

Consider next the fine-structure splitting repesented by m_{SO}. The total effect on the IP state (neglecting tensor interactions) is

$$\Delta m_{f.s.} = m(1^3P_2) - m(1^3P_0) \tag{1.48}$$

In going from the cc to the bb system, the splitting scales like the square of the quark velocity in the ground state [13]

$$\frac{\Delta m^{b}_{f.s.}}{\Delta m^{c}_{f.s.}} = \frac{v^2_b}{v^2_c} \tag{1.49}$$

where the quark velocity, v_q^2, is written in terms of the average total kinetic energy, $\langle T \rangle = \langle r\, dV/dr \rangle (1/2)$ available to the quarks as,

$$v_q^2 = 1 - \left[1 + \langle T \rangle / 2mc^2\right]^{-2} \qquad (1.50)$$

Experimentally it is found $\Delta m_{f.s.} = 141$ MeV and $\Delta m_{f.s.} = 42$ Mev and using the potential of ref. [14] the quark velocities are $v_c^2 = 0.23$ and $v_b^2 = 0.08$ checking the consistency of eq. (1.49). Estimating that for a heavy qq system of mass around 80 GeV $v^2 (m_q = 80\ \text{GeV}) = 0.01, \ldots, 0.02$ then by scaling we find

$$\Delta m_{f.s.}(80\ \text{GeV}) \simeq (5 - 10)\ \text{MeV} \quad , \qquad (1.51)$$

again beyond the resolution of forthcoming experiments. We thus conclude that in order to explore the short-distance behaviour of the quarkonium potential, below that which has already been fixed by charmonium and bottomonium, it is sufficient to analyse only the spin-averaged quarkonia data, in which spin-dependent corrections are eliminated.

To obtain the spin-averaged result we multiply each state of a given orbital angular momentum multiplet by its degeneracy and average over all possible state. For example, in the charmonium 1S state we write

$$\frac{3m_\psi + m_\eta}{4} = m_S \quad , \qquad (1.52)$$

where m_S is the non-relativistic result.

1.10 Preview

It is the aim of this work to consider the extent to which heavy quarkonia are able to test the theory of the strong interactions (QCD) which binds quarks into hadrons, and to make a meaningful determination of Λ, the fundamental scale parameter of the theory.

In order to do this we consider a QCD-like interquark potential which incorporates the next-to-leading order calculation for the static qq perturbative potential, valid at short distances, and fit to the cc and bb data for various values of Λ. Any constraint imposed on the value of Λ, by the data, can then be obtained by comparing the potential resulting from the fit with the short distance perturbative behaviour as a function of Λ.

It has been shown [14] that although cc and bb data do not determine a preference for the QCD form, they do impose a lower bound on Λ. A conclusion of $\Lambda > 0.1$ GeV is found by the following argument. The next-to-leading calculation is assumed to be reliable in the region $r < r_0$, where $r_0 \Lambda = 0.1$. For $\Lambda = 0.1$ GeV, the regions determined by the data and for which the calculation is assumed to be reliable, overlap for $0.1 \lesssim r \lesssim 0.2$ fm, and as the data demand a slope almost double that predicted by QCD, values of $\Lambda \sim 0.1$ GeV are rejected. A similar analysis [15] including the fact that small deviations in the perturbative result are allowed due to higher order corrections, concludes $\Lambda > 0.15$ GeV. Thus it appears the sensitivity to Λ only arises if we require the potential to approximate the perturbative behaviour at short distances.

To increase the sensitivity to Λ and indeed pin down a specific value, the experimentally constrained region of the potential must be extended to shorter distances such that a greater degree of overlap, with the perturbative result, can be considered.

It is well known [14, 16] that toponium spectroscopy, the bound states of the heavy top quark-antiquark pair, is sensitive to the short distance region of the potential. We see in Fig 1.10 the probability distributions $u^2(r)$ for the 1S state of toponium of mass 80 GeV compared to the equivalent distributions in charmonium and bottomonium. As expected the toponium system should be able to probe more deeply into the short-distance region (where QCD perturbation theory is relevant) and indeed will constrain the quarkonium potential down to distances of $r \sim 0.2\ \mathrm{GeV}^{-1}$. We study the sensitivity that hypothetical toponium data should impose on the value of Λ by making predictions for the data sample and including errors that are expected from future e^+e^- experiments. The effects of relativistic corrections can be suppressed by omitting cc data from the analysis.

The structure of this work is as follows. In Chapter 2 we discuss the details of the next-to-leading order perturbative QCD potential that we use in our analysis, and examine the effect of heavy quark loops (m_c, $m_b \neq 0$). Chapter 3 describes how we incorporate the intermediate and long-distance contributions into the potential in such a way that $\Lambda_{\overline{MS}}$ is constrained only by the short distance behaviour of the perturbative contribution to the potential and discuss the results of confronting this potential to the $c\bar{c}$ and $b\bar{b}$ data.

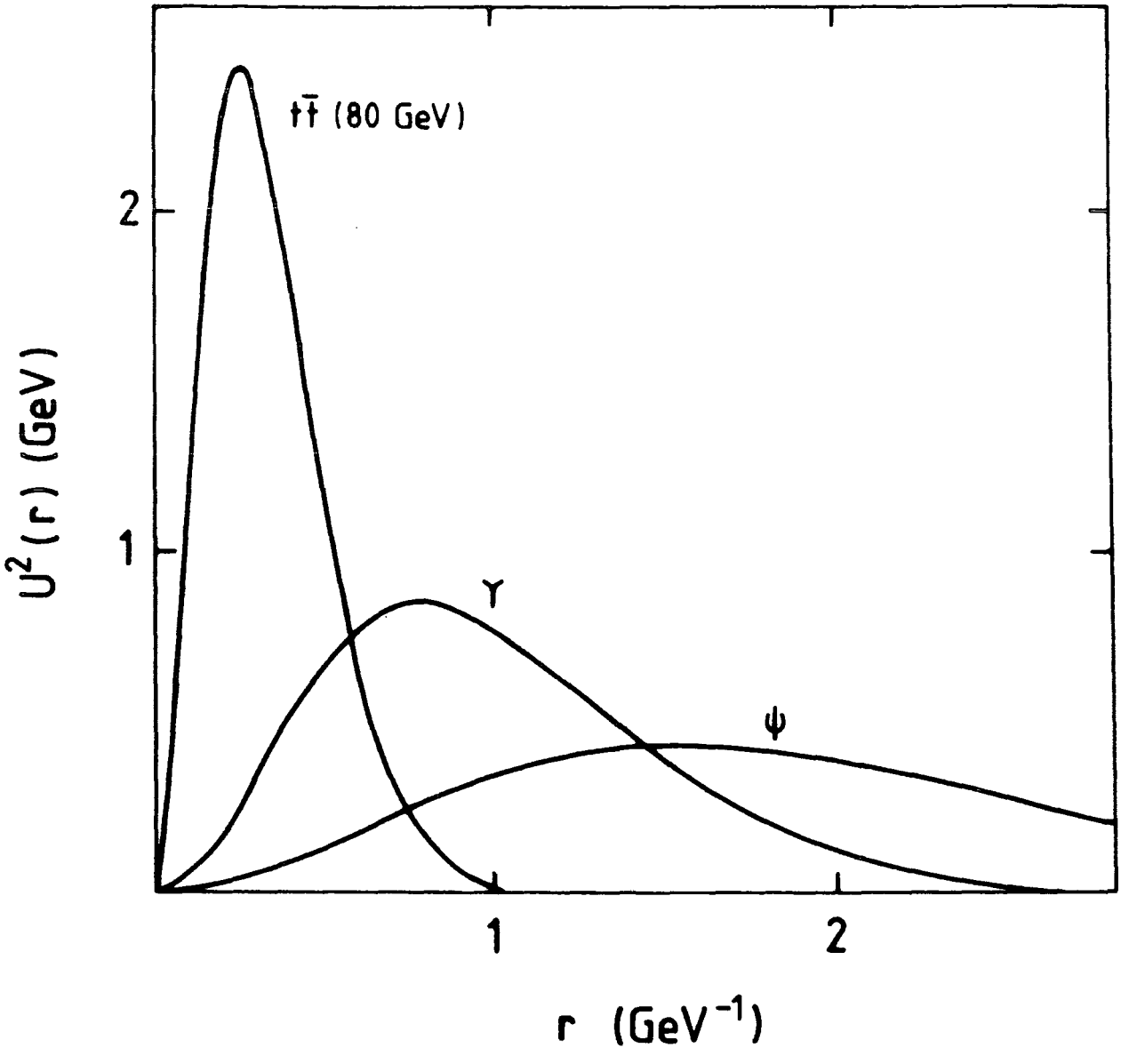

Fig 1.10 : Probability distributions $u^2(r)$ for the 1S states of toponium (m_{1S} = 80 GeV) bottomonium and charmonium to show the extent to which a toponium system, of this mass, should be expected to probe the short-distance region.

We examine the sensitivity to the value of $\Lambda_{\overline{MS}}$ and obtain consistent comparisons with other potentials that have been used to describe cc and bb data. In Chapter 4 we discuss toponium expectations and predictions and the accuracy to which experimental information on toponium will be able to determine the value of $\Lambda_{\overline{MS}}$. In Chapter 5 we return to the analysis of the cc and bb spectroscopy and discuss hadronic decay widths of S and P wave states in the light of recent measurement and notice that wavefunction distortion effects seem to be important for light P wave decays. Chapter 6 contains a summary and our main conclusions.

CHAPTER 2

The Perturbative Potential

Our objective is to study the constraints imposed on the QCD perturbative potential by heavy quarkonia data. We must therefore, critically review the short-distance static potential between a colour-singlet pair of colour triplet sources, calculated at the next-to-leading order in QCD perturbation theory, and examine the region of its validity. First, in Sub Section 1, we discuss the perturbative potential in massless QCD and estimate the errors that may arise from higher order corrections. Then, in Sub Section 2, we study the effects of massive quark loops.

2.1.1 Perturbative Potential In Massless QCD

The QCD perturbative expansion for the static potential [17] should be valid at small enough interquark separation since, due to asymptotic freedom [18], the effective coupling constant decreases with decreasing r. The finite part of the one loop contribution to the static potential has been calculated by several groups [19] in pure gauge theories and by Billoire [8] who includes massless quark loop contributions. The potential in momentum space, where the coupling constant is renormalised in the modified minimal subtraction ($\overline{MS}$) scheme, and where there are n_f massless quarks can be expressed as:

$$V(\vec{q}) = -4\pi^2 C_F \frac{a}{q^2}\left\{ 1 + a\left[C_A\left(\frac{11}{12}\ell n\frac{\mu^2}{q^2} + \frac{31}{37}\right) - T_F n_f\left(\frac{1}{3}\ell n\frac{\mu^2}{q^2} + \frac{5}{9}\right)\right] + O(a^2)\right\}, \tag{2.1}$$

with

$$a \equiv \alpha_s(\mu)_{\overline{MS}}/\pi \ , \tag{2.2}$$

$$T_F = 1/2 \tag{2.3}$$

$$C_F = 4/3 \tag{2.4}$$

$$C_A = 3 \tag{2.5}$$

(2.3)–(2.5): Colour Factors

The coupling, α_s is renormalised in the modified minimal subtraction ($\overline{MS}$) scheme [3] and μ is the unit of mass introduced in the dimensional regularisation [2].

It is a straightforward procedure to make the appropriate 3 dimensional Fourier Transform (See Appendix A) to express the potential in co-ordinate space

$$V(r) = -\pi C_F \frac{a}{r} [1 + a(b_o \ \ell n \ \mu r + A) + O(a^2)] \tag{2.6}$$

with

$$b_o = \frac{11}{6} C_A - \frac{2}{3} n_f T_F \ , \tag{2.7}$$

$$A = b_o \gamma_E + \frac{31}{37} C_A - \frac{5}{9} n_f T_F \ . \tag{2.8}$$

$$\gamma_E = - \int_0^\infty e^{-t} \ \ell nt \ dt = 0.5772... \tag{2.9}$$

The renormalisation group improvement of this equation amounts to recognising that there is an invariance of eq. (2.6) to a change of scale μ such that under this change the coupling will satisfy the renormalisation group equation (RG)

$$\mu \frac{\partial a}{\partial \mu} = -a^2 [b_o + b_1 a + O(a^2)] \tag{2.10}$$

with

$$b_1 = \frac{17}{12} C_A{}^2 - \frac{5}{6} C_A n_f T_F - \frac{1}{2} C_F n_f T_F \tag{2.11}$$

which, neglecting the $O(a^2)$ term, has an exact solution expressed by:

$$\Lambda_{\overline{MS}}^{(n_f)} = \mu \exp\left\{ -\frac{1}{b_o a} + \frac{b_1}{b_o^2} \ell n \left[\frac{2}{b_o} \left[\frac{1}{a} + \frac{b_1}{b_o} \right] \right] \right\}. \qquad (2.12)$$

This equation defines the μ - independent QCD scale parameter $\Lambda_{\overline{MS}}^{(n_f)}$.

We have thus specified the perturbative potential in co-ordinate space for n_f flavours of massless quarks, eq. (2.6), totally defined in terms of the constant $\Lambda_{\overline{MS}}^{(n_f)}$. However, to make a meaningful determination of Λ, by confronting the perturbative potential to data, we need to consider the effects of higher-order corrections.

2.1.2 Higher Order Corrections To Perturbative Potential

The two crucial questions that we need to consider are up to what distance r and with what accuracy is the truncated expansion of the perturbative potential in massless QCD eq. (2.6) valid? These questions are intimately related to the problem of choosing a good renormalisation scheme in which to formulate the problem as discussed in the introduction [20]. We need to look at the $O(a^2)$ terms of eq. (2.6) and decide on a criterion to determine the maximum value of r to which we should believe the perturbative expansion, beyond which the $O(a^2)$ terms may cause a breakdown in the perturbation series.

Here we adopt the conservative approach of Ref. [21]. Given a perturbation expansion for a physical quantity, R:-

$$R = a(\mu)^m \left\{ 1 + \sum_{k=1}^{n} C_k(\mu) [Na(\mu)]^k + O(a(\mu)^{n+1}) \right\}, \qquad (2.13)$$

where $Na(\mu) = N\alpha_s(\mu)/\pi$ is a natural expansion parameter in large N theories [22] with N = 3 for QCD, then if there is no a priori reason to expect this series to breakdown, we can assume that there exists an optimal scale μ_{OPT} at which the coefficients of the series satisfy

$$|C_k(\mu_{OPT})| < K = 0(1) \quad \text{for} \quad k=1,...n. \tag{2.14}$$

In practice however, only the first coefficient c_1 will be known, and in such a case the first guess μ_1 for the optimal scale is [23]

$$C_1(\mu_1) = 0 \ . \tag{2.15}$$

The RG invariance of the physical quantity R relates the first and second coefficients at the two scales by:

$$C_2(\mu_1) = C_2(\mu_{OPT}) - \frac{b_1}{Nb_o} C_1(\mu_{OPT}) \ . \tag{2.16}$$

Our assumption (2.14), and noting that $b_1/Nb_o \simeq 0.5$ for $n_f = 4$, implies that the fractional error of the estimate

$$R = a(\mu_1)^m \tag{2.17}$$

is given by

$$\left|\frac{\Delta R}{R}\right| \simeq |C_2(\mu_1)|[Na(\mu_1)]^2 < K[Na(\mu_1)]^2 \ . \tag{2.18}$$

The important observation here is that the choice (2.15) does not introduce artificially large corrections so long as there exists an optimal perturbation expression satisfying (2.14).

We would like to apply the above argument to the special case in hand, where the perturbative potential eq. (2.6) is the physical quantity under consideration. We have

$$V_P(r) = -C_F \frac{\alpha_s(\mu_1)_{\overline{MS}}}{r} \tag{2.19}$$

Where we have chosen μ_1 such that the next-to-leading order coefficient vanishes

$$\mu_1 = \frac{1}{r} \exp(-A/b_o) \ , \tag{2.20}$$

and that the fractional error from higher order terms is

$$|\Delta V_p(r)/V_p(r)| < K\left|\frac{N}{\pi}\alpha_s(\mu_1)_{\overline{MS}}\right|^2 \ . \tag{2.21}$$

The factor K is of order 1 and, lacking more information, we take $K = 1$. With the large colour factor ($N^2 = 9$) already included, this choice may seem rather conservative but in confronting the perturbative potential, determined totally by the value of Λ to data any constraint or conclusion drawn should not be expected to depend on this value of K, as it determines an upper limit to the fractional error expected from higher order corrections. However, lacking a calculation of the coefficient $c_2(\mu)$ of the expansion, $K = 1$ must seem the most reasonable choice. The only available perturbation series to three-loops in QCD are those of unphysical quantities; the RG functions in the $\overline{MS}$ scheme [24], an effective change in a special momentum (MOM) scheme [25] and its β function [26]. In all these perturbation series the factor K is less than unity for moderate values ($\lesssim 10$) of n_f.

The perturbative potential of (2.19) only gives a good approximation to the full quarkonium potential for those values of r for which the fractional error, given by eq. (2.21) is small. To determine a criterion that restricts the perturbative potential to a region of space within which the fractional error does not become unacceptably large we plot the fractional error as a function of $r\,\Lambda_{\overline{MS}}$ in Fig. 2.1.

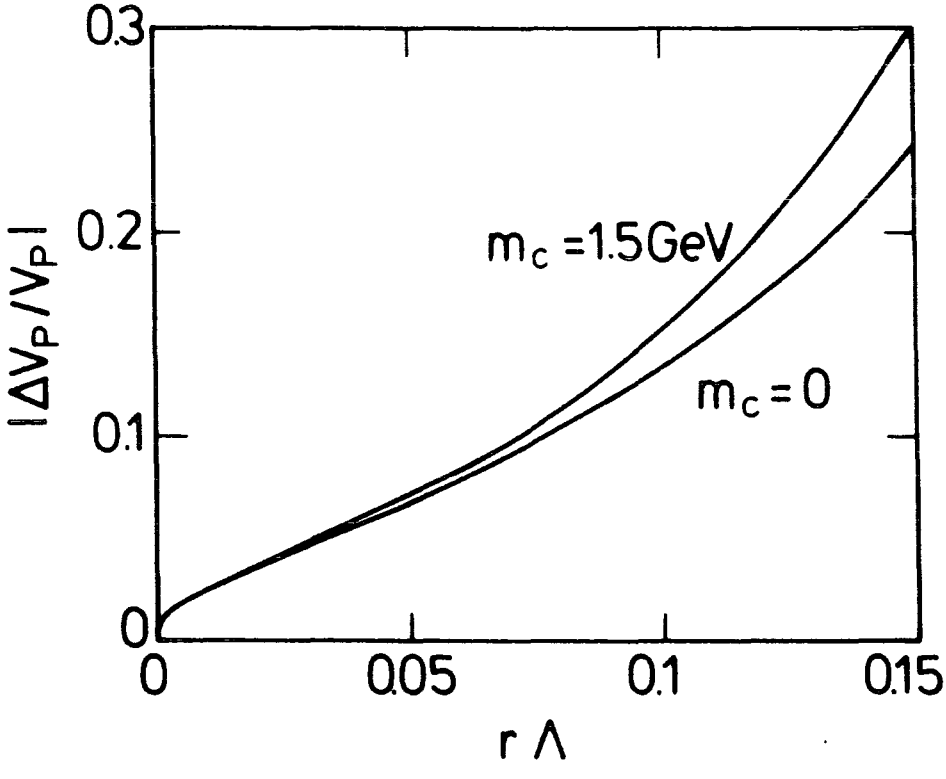

Fig 2.1 : The fractional error in the perturbative potential (calculated from eq. (2.21) with K=1) as a function of $r\Lambda$ for $\Lambda = \Lambda^{(4)}_{\overline{MS}} = 0.2$ GeV. The plot is essentially the same for other values of Λ. The $m_c = 1.5$ GeV curve is calculated using eq. (2.35) in the place of eq. (2.8).

Thus, for example, we expect V_p to be within 10% of the true potential for values of r satisfying

$$r\Lambda_{\overline{MS}}^{(4)} \lesssim 0.08 \ . \qquad (2.22)$$

We see from this that potentials with small values of $\Lambda_{\overline{MS}}^{(4)}$ should be expected to be valid over quite large regions before the perturbative expression is destroyed by these corrections.

An estimate of the magnitude of higher order corrections must be implicit in any confrontation of perturbation theory predictions with experimental data, and if in the case of quarkonium there is to be any meaningful constraints to be put upon $V_p(r)$ by the data, then there must be some degree of overlap between the region over which the expression for $V_p(r)$ is taken to be valid and the region relevant to the data. However, we cannot conclude that a certain value of Λ is favoured by the fact that a phenomenologically successful potential has the correct $r \to 0$ behaviour, if the potential deviates too much from the perturbative form, for that value of Λ , within its expected region of validity. Conversely, it is unjustified to rule out a value of Λ by requiring the exact onset of the perturbation potential as r is decreased below a certain value, as even at very short distances we must allow for changes in the potential arising from possible higher order corrections. In order to make an objective judgement of how a phenomenological potential reproduces the desired perturbative form for a given value of Λ , we shall make use of the error estimate eq. (2.21) with K = 1 in the short distance region specified by the inequality (2.22).

2.1.3 Two Technical Notes

We consider here two technical, but general, remarks of the determination of the QCD scale parameter, Λ .

i. For a given value of $\Lambda_{\overline{MS}}^{(n_f)}$, eq. (2.12) determines the trajectory of $a \equiv \alpha_s/\pi$. The trajectory, or the value of α_s at a certain value of μ , is calculated very efficiently by using an iterative solution as follows [27].

$$a(\mu) \equiv \frac{\alpha_s(\mu)_{\overline{MS}}}{\pi} = \frac{b_o}{b_1} F\left\{\frac{b_1}{b_o^2 \ln(\mu/\Lambda_{\overline{MS}}^{(n_f)}) + b_1 \ln(2b_1/b_o^2)}\right\} \quad (2.23a)$$

with

$$F(x) = \lim_{n\to\infty} F^{(n)}(x) \quad (2.23b)$$

where

$$F^{(1)}(x) = x , \quad (2.23c)$$

$$F^{(n)}(x) = [1/x + \ln(1 + 1/F^{(n-1)}(x))]^{-1} \quad \text{for } n=2,3 \ldots \quad (2.23d)$$

This iterative solution converges very rapidly for small x.

ii. In the literature there often appears another definition of $\Lambda_{\overline{MS}}^{(n_f)}$ namely,

$$a(\mu) \equiv \frac{\alpha_s(\mu)_{MS}}{\pi} = \frac{2}{b_o \ell n(\mu/\Lambda')}\left[1 + \frac{2b_1 \ell n \ell n(\mu/\Lambda')}{b_o^2 \ell n(\mu/\Lambda')}\right] \quad (2.24)$$

with

$$\Lambda' \equiv \Lambda_{\overline{MS}}^{'(n_f)}$$

Although the two definitions of Λ eq. (2.12) and eq. (2.24) are formally equivalent in the next-to-leading order, they lead to numerically different values of the Λ parameter for a given value of the strong coupling constant, at a given scale.

Due to the exponential sensitivity of Λ on the coupling constant, the numerical difference may be significant. We choose the definition of eq. (2.12) because it is identical to the numerical solution of the RG equation in the next-to-leading order. Numerical solutions of the RG equation is often the only practical way of obtaining the running coupling constant in the wider range of renormalisation schemes, including all mass dependent schemes.

2.2.1 Heavy Quark Loop Effects

It is well known that quark masses can be neglected in loop corrections to the static potential when [28]

$$r^2 m_q^2 \ll 1 \qquad (2.25)$$

is satisfied, whereas the effects of heavy quark loops are neglected when [29]

$$r^2 m_q^2 \gg 1 \ . \qquad (2.26)$$

The systems that we shall ultimately be confronting our potential against, are charmonium, bottomonium and eventually toponium ($m_t = 40$ GeV) whose lowest lying 1S states are sensitive to the potential in the region around $\langle r^2 \rangle^{1/2} = 2.2$, 1.1 and 0.35 GeV^{-1} respectively. For the three quarkonium systems, we show in Table 2.1 the sensitivity that the respective 1S states have to charm, bottom and top quark loop effects.

The first row of Table 2.1 indicates the $b\bar{b}$ and $t\bar{t}$ spectroscopies probe regions where

$$m_c^2 \langle r^2 \rangle = O(1) \qquad (2.27)$$

and hence we must include the effects of massive charmed quark loops in their description.

	$c\bar{c}$	$b\bar{b}$	$t\bar{t}$
$m_c^2\langle r^2\rangle$	10.9	2.72	0.28
$m_b^2\langle r^2\rangle$	121	30.3	3.06
$m_t^2\langle r^2\rangle$	7744	1936	196

Table 2.1 : Sensitivity of 1S-state to heavy quark loops.

The sensitivity to bottom quark loops is only seen in $t\bar{t}$, although even here the effects appear to be small and we shall discuss them later in the chapter. Top quark loops are too heavy to have any effect on the spectroscopies and essentially totally decouple. We shall first consider, quantitatively the effect of charmed quark loops in the perturbative potential.

2.2.2 Charm Quark Loop Effects

Such effects were first investigated in Ref. [15]. The perturbative potential in massive quark theory has an identical form to eq. 2.1 except that now there is an extra term, the vacuum polarisation function, which explicitly depends on the quark masses. In momentum space the potential is written as:

$$V(\vec{q}) = -4\pi^2 C_F \frac{a}{q^2}\left\{1 + a\left[C_A\left(\frac{11}{12}\ln\frac{\mu^2}{q^2} + \frac{31}{37}\right) - T_F\sum_{q=1}^{n_f}\left(\frac{1}{3}\ln\frac{\mu^2}{q^2} + F\left(\frac{m_q^2}{q^2}\right)\right)\right] + O(a^2)\right\} \qquad (2.28)$$

The vacuum polarisation function:

$$F(x) = -\frac{1}{3}\ln x + \frac{5}{9} - \frac{4}{3}x - \frac{1}{3}(1-2x)h\,\ln\left(\frac{h+1}{h-1}\right) \qquad (2.29)$$

with $h = (1+4x)^{\frac{1}{2}}$, completely determines the mass dependence in the one loop order. The limiting behaviour of small and large quark masses of this function is:

$$F(x) = -\frac{1}{3}\ln x - \frac{1}{15x} + O(x^{-2}) \quad \text{for} \quad x >> 1 \qquad (2.30a)$$

$$F(x) = \frac{5}{9} - 2x + O(x^2) \quad \text{for} \quad x << 1\ , \qquad (2.30b)$$

The large logarithms induced by treating heavy quarks in loops of eq. (2.30) shows that the minimal subtraction scheme is not well suited for treating such effects.

The 3 dimensional Fourier Transform of the potential to co-ordinate space (See Appendix A) can be performed using the approximation for the vacuum polarisation function of:

$$F(x) \simeq -\frac{1}{3}\ell n(x + e^{-5/3}) \tag{2.31}$$

which is accurate to within 5% over the whole range of x values ($0 \leq x \leq \infty$). In co-ordinate space the potential is then found to have an identical form to eq. (2.6) except that the coefficient A now becomes a function of $m_q r$,

$$A(r) = b_o\gamma_E + \frac{31}{37}C_A + \frac{2}{3}T_F \sum_{q=1}^{n_f}[\gamma_E + \ell n(m_q r) - Ei(-e^{5/6}m_q r)] \tag{2.32}$$

where Ei(-x) is the exponential integral

$$Ei(-x) = -\int_x^\infty \frac{dt}{t} e^{-t} . \tag{2.33}$$

For $m_q r \ll 1$, the factor in the square bracket in eq. (2.32) reduces to $^{-5}/6$ reproducing eq. (2.6) in the massless theory. However, for $m_q r \gg 1$, the square bracket diverges logarithmically signalling the breakdown of infra red decoupling in the $\overline{MS}$ scheme. This divergence however has a simple solution. We notice that provided we stay in the region where the condition

$$r^2 m_b^2 \gg 1 \tag{2.34}$$

is satisfied, then we can use a 4-flavour effective light quark theory [30] ($n_f = 4$), thereby neglecting bottom and top quark loop effects totally. We have seen already that condition (2.34) will hold at least down to a quarkonium system of mass around 80 GeV. The coefficient (2.32) becomes:

$$A(r) = b_o\gamma_E + \frac{31}{37}C_A + \frac{2}{3}T_F\left[-\frac{5}{2} + \gamma_E + \ell n(m_c r) - Ei(-e^{5/6}\, m_c r)\right] \tag{2.35}$$

Where b_o is given by eq. (2.7) with $n_f = 4$ and we have set $m_u = m_d = m_s = 0$. The expression for the potential (2.19) remains valid but where now the scale is chosen to be:

$$\mu_1 = \frac{1}{r} \exp(-A(r)/b_o) \qquad (2.36)$$

The fractional error in the perturbative potential can still be estimated from eq. (2.21) provided that effects of bottom quark loops are neglected. The result as a function of Λr is also shown in Fig. 2.1, where we see that the error is less than 10% provided.

$$r\Lambda_{\overline{MS}}^{(4)} < 0.07 \ . \qquad (2.37)$$

2.2.3 Effective Quark Theories

The use of effective light particle theories as an approach to taming the logarithmic divergences introduced by calculating in the $\overline{MS}$ scheme results in the division of the full QCD theory into a number of effective QCD theories, each labelled by the number of flavours and related by the matching conditions [31], which in the $\overline{MS}$ are written as:

$$\frac{\alpha_s^{(n_f-1)}(\mu)_{\overline{MS}}}{\pi} = \frac{\alpha_s^{(n_f)}(\mu)_{\overline{MS}}}{\pi}\left[1 + \frac{1}{3} T_F \ln \frac{\mu^2}{m_{n_f}^2} \frac{\alpha_s^{(n_f)}(\mu)_{\overline{MS}}}{\pi}\right] . \qquad (2.38)$$

Using this idea of the effective theory, allows us to form $n_f = 3,4,5$ and 6 - flavour theories each being related by a matching of the running coupling constant at a quark threshold.

Each effective n_f - flavour theory is determined by keeping only the first n_f quarks and finding $\Lambda_{\overline{MS}}^{(n_f)}$ through the condition

$$\alpha_s^{(n_f-1)}(\mu=m_f) = \alpha_s^{(n_f)}(\mu=m_f) \ . \qquad (2.39)$$

For example, using $\Lambda_{\overline{MS}}^{(4)} = 0.2$ GeV and with $m_{u,d,s} = 0$, $m_c = 1.5$, $m_b = 5$ and $m_t = 40$ GeV we find:

$$\left(\Lambda_{\overline{MS}}^{(3)}, \Lambda_{\overline{MS}}^{(4)}, \Lambda_{\overline{MS}}^{(5)}, \Lambda_{\overline{MS}}^{(6)}\right) = (0.25, 0.2, 0.13, 0.06) \text{ GeV} \qquad (2.40)$$

which with $b_0(n_f)$ and $b_1(n_f)$ given by eq. (2.7) and eq. (2.11) respectively, determines the trajectory $\alpha_s^{(n_f)}(\mu)$ versus μ. In Fig. 2.2, we show the flavour dependence of $\Lambda_{\overline{MS}}$ as a function of the 4 flavour effective theory.

The use of effective theories in QCD now allows us to consider the sensitivity of the perturbative potential to charm quark loops. We calculate $V_{\underline{p}}(r)$ in each of the following effective theories:-

i. 4 flavour, using $\Lambda_{\overline{MS}}^{(4)} = 0.2$ GeV and $m_c = 1.5$ GeV

ii. 4 flavour, using $\Lambda_{\overline{MS}}^{(4)} = 0.2$ GeV and $m_c = 0$ GeV

iii. 3 flavour, using $\Lambda_{\overline{MS}}^{(3)} = 0.25$ GeV

In each case we take $m_u = m_d = m_s = 0$ and only consider the region of $V_{\underline{p}}(r)$ which will be most sensitive to the 1S state of toponium, $0.2 \lesssim r \lesssim 0.5\ \text{GeV}^{-1}$. The resulting potentials from each approach are compared in Fig. 2.3. In practice setting $m_c = 0$ does not have a large effect on the toponium predictions as we see that the 2S-1S energy difference for a toponium system around 80 GeV will only be increased by 5 MeV on taking $m_c = 0$ rather than $m_c = 1.5$ GeV. Alternatively, by requiring a given 2S-1S energy difference, setting $m_c = 0$ will decrease the value of $\Lambda_{\overline{MS}}^{(4)}$ by about 20 MeV. The effective 3 flavour theory matches the two 4-flavour theories at different points due to the change in scale introduced by including the charm quark mass, but we expect it to become increasingly less accurate at shorter distance due to the neglect of heavy quark effects.

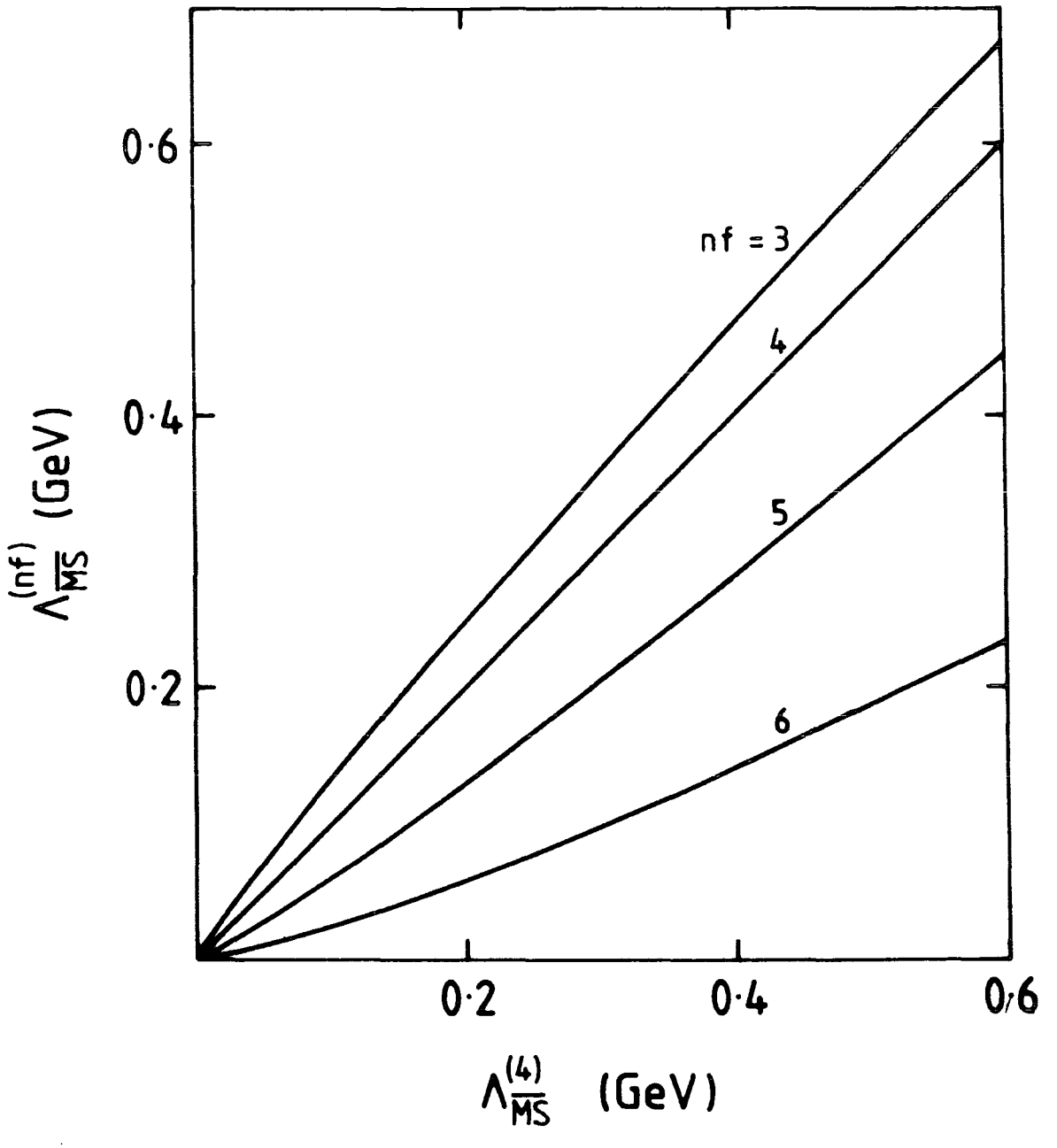

Fig 2.2 : Flavour dependence of $\Lambda_{\overline{MS}}$ as a function of the 4-flavour effective theory. The effective theories are related by eq. (2.38) assuming m_c = 1.5 GeV, m_b = 5 GeV, m_t = 40 GeV.

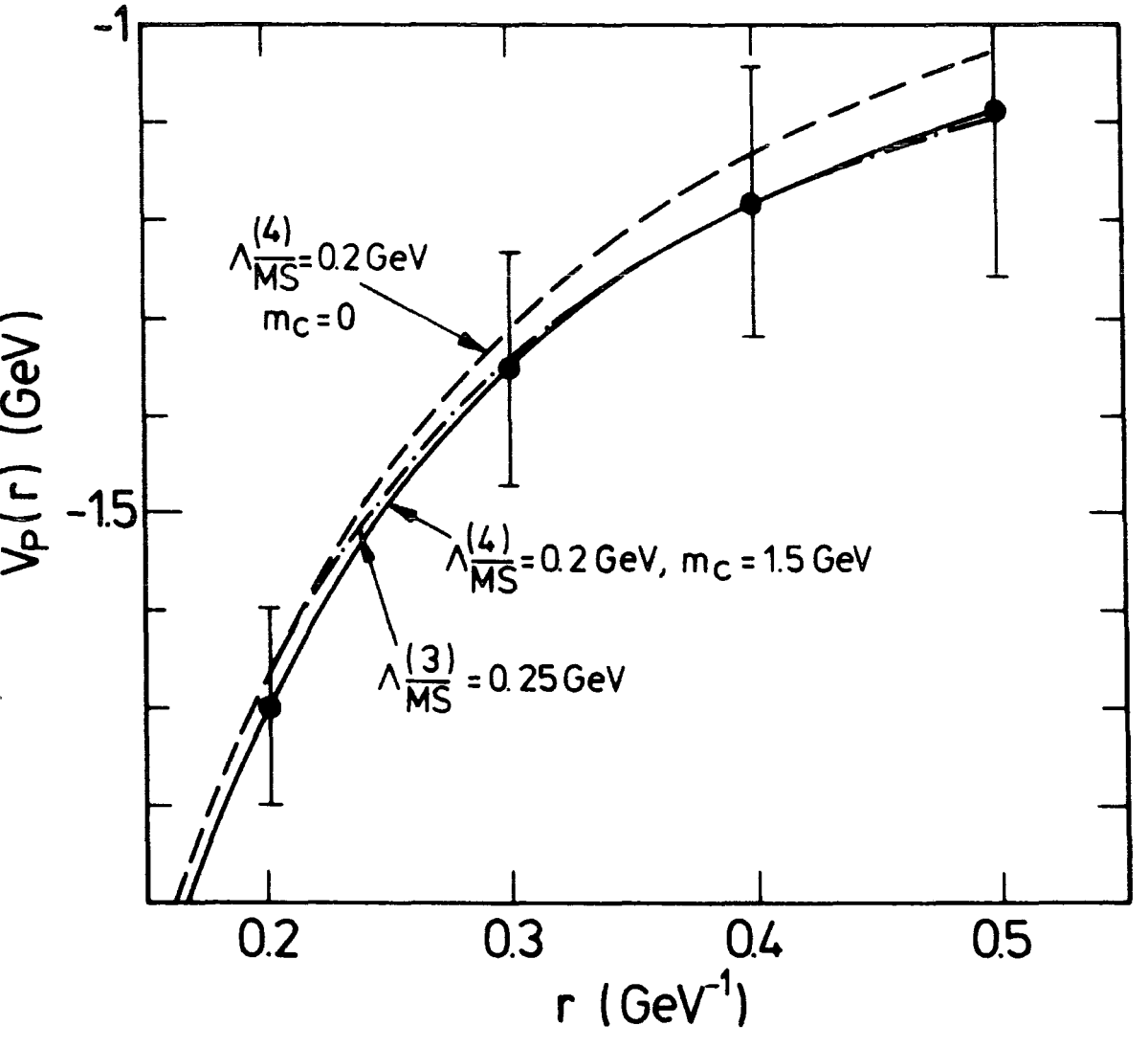

Fig 2.3 : The behaviour of the perturbative potential for $\Lambda^{(4)}_{\overline{MS}}$ = 0.2 GeV using an expanded scale to show the differences resulting from setting m_c = 0 and from changing n_f = 4 to n_f = 3 effective theory. The errors are calculated using eq. (2.21) with K=1.

We could have also used 5-flavour or 6-flavour effective theories to calculate the perturbative potential in this region by simply keeping 5 or 6 quarks in eq. (2.32), but we cannot expect the results to be in any way meaningful due to large logarithms. We shall consider next analysing the errors introduced by working in the effective theory, and also how to include bottom and top quark loop effects without logarithmic divergences.

2.2.4 Bottom Quark Loop Effects

In dealing with the heavy quark loop effects of bottom, and indeed top, we have already noted the inherent failure in the $\overline{MS}$ scheme calculation due to the presence of large logarithms in eq. (2.32) in the regions $r^2m^2_b>>1$ and $r^2m^2_t>>1$. In these regions we would expect the heavy quarks to decouple from the theory and indeed the infra red decoupling theorem [29] tells us that there always exists a renormalisation scheme in which the perturbation series, at a given mass scale, is insensitive to the physics at higher energies. Momentum-space subtraction (MOM) renormalisation schemes are the most natural examples of this category, where the only errors we need worry about are simply higher order corrections, unlike the effective flavour theories where heavy quark contributions and a truncation of the series for the matching condition are additional errors. Although we encounter more sources of error working in the $\overline{MS}$ effective theories, we need only work with mass-independent renormalisation schemes, whereas the price we must pay for a manifest decoupling of heavy quarks is that the renormalisation group equations (RG) become mass dependent and need to be solved numerically.

To determine the effects of bottom quark loops, we must calculate the full massive perturbative potential in this MOM scheme and by comparing this result to that obtained from each of the effective n_f - flavour theories calculated from eq. (2.32), we are able to study quantitatively, the region of validity of each effective theory.

2.2.5 Perturbative Potential In MOM Scheme

In Perturbation Theory, the renormalised coupling constant in two different renormalisation schemes are related to each other by a perturbation expansion. Specifically, the relation between the coupling constant in the $\overline{MS}$ and MOM schemes is written in the n-loop order as:

$$\left(\frac{\alpha_s}{\pi}\right)_{MS} = \left(\frac{\alpha_s}{\pi}\right)_{MOM}\left[1 + \sum_{k=1}^{n} c^{(k)}_{MOM}\left(\frac{\alpha_s}{\pi}\right)^k_{MOM}\right] \qquad (2.41)$$

where the coefficients $c^{(k)}_{MOM}$ depend in general upon the gauge parameter and the dimensionless ratio of quark masses and the renormalisation point, μ. However, the next-to-leading order coefficient $c^{(1)}_{MOM}$ is only known for a particular MOM scheme defined at the symmetric Euclidean point of the gluon-ghost-ghost vertex in the Landau gauge [32]. The coefficient is written as:

$$c^{(1)}_{MOM} = -\frac{187}{144}C_A + T_F \sum_{q=1}^{n_f} F\left(\frac{m_q^2}{\mu^2}\right) \qquad (2.42)$$

where F(x) is the vacuum polarisation function given by eq. (2.29). Using this, we see that in the MOM scheme, the perturbative potential is written in an identical form to eq. (2.6) but where A is now r and μ dependent, and where we have kept only next-to-leading order terms.

$$A = A_{MOM}(r) = A_{\overline{MS}}(r) - \frac{187}{144}C_A + T_F \sum_{q=1}^{n_f} F\left(\frac{m_q^2}{\mu^2}\right) \qquad (2.43)$$

Here $A_{\overline{MS}}(r)$ is given by eq. (2.32) with the sum taken over all flavours ($n_f = 6$). From eq. (2.43) we see immediately that the large logarithms in $A_{\overline{MS}}(r)$ and $F(x)$ when $m_q r >> 1$ exactly cancel up to terms of the form $\ell n(\mu r)$ and indeed the heavy quark behaviour of this equation is $(m_q r)^{-2}$ in accordance with the decoupling theorem [29]. The optimisation of the full theory is carried out just as in eq. (2.19), with the subscript replacement $\overline{MS} \rightarrow MOM$, however as A_{MOM} is now dependent on the scale μ also, we need to solve

$$b_o(n_f)\ell n(\mu r) + A_{MOM}(r,\mu)\Big|_{\mu=\mu_1} = 0 \quad , \tag{2.44}$$

to obtain the optimisation scale, μ_1 , which has to be done numerically. The scale dependence of the coupling constant $\alpha_s(\mu_1)_{MOM}$ is governed by the RG equation (2.10) but where now the coefficients b_o and b_1 depend on the dimensionless ration m_q / μ , [32]

$$b_o\left(\frac{m_q}{\mu}\right)_{MOM} = \frac{11}{6} C_A - \frac{2}{3} T_F \sum_{q=1}^{n_f} B_o\left(\frac{m_q^2}{\mu^2}\right) \tag{2.45a}$$

with

$$B_o(x) = 1 - 6x + \frac{12x^2}{h}\ell n\left[\frac{h+1}{h-1}\right] \qquad h = (1+4x)^{\frac{1}{2}} \tag{2.45b}$$

and

$$b_1\left(\frac{m_q}{\mu}\right)_{MOM} = \frac{17}{12} C_A^2 - \left(\frac{5}{6} C_A + \frac{1}{2} C_F\right) T_F \sum_{q=1}^{n_f} B_1\left(\frac{m_q^2}{\mu^2}\right) \tag{2.46a}$$

with

$$B_1(x) \simeq \frac{-0.4557x + 0.26995}{x^2 + 2.1742x + 0.26995} \tag{2.46b}$$

The trajectory $\alpha_s(\mu)_{MOM}$ versus μ in the full theory is determined by noting that for $\mu >> m_t$ the β function in the MOM and $\overline{MS}$ ($n_f = 6$) schemes becomes identical and that the couplings in each are related by a shift in the momentum scale [33]

$$\alpha_s(\mu)_{MOM} = \alpha_s^{(6)}(\mu e^{-t})_{\overline{MS}} \qquad \text{for } \mu >> m_t \tag{2.47a}$$

with [32]

$$t = (187C_A - 80n_fT_F)/[24(11C_A - 4n_fT_F)] \; . \tag{2.47b}$$

We have determined the trajectories in the effective theories as discussed in Section 2.2.3 and each is compared in Fig 2.4. However we should note that both the solution of the RG equation and the solution to find the optimisation scale μ_1 must be done numerically in the MOM scheme. These numerical tasks make working in this scheme too time consuming for practical interest. The most sensible approach to obtain a suitable workable potential, is to compare each of the effective theories in turn with the full theory and determine the best approximation in the region of interest. The predictions of the effective n_f-flavour theories normalised to that of the full theory are shown in Fig 2.5. We see that the effective theories which include heavy quark loop effects, $n_f = 5$ and $n_f = 6$, deviate considerably from the full theory due to the large logarithms in the region $r^2 m_q^2 >> 1$. The error bars are an estimate of the higher-order correction terms in the MOM scheme given by (2.21) and with K=1.

To decide which of the effective theories is the best approximation to the full theory we consider Fig 2.1, where for $\Lambda^{(4)}_{\overline{MS}} = 0.2$ GeV, we should only believe the perturbative potential so long as or $r < 0.5\ \text{GeV}^{-1}$. Toponium systems of mass around 80 GeV should be expected to probe down to distances of $r \sim 0.2\text{-}0.3\ \text{GeV}^{-1}$, so if data is to impose any constraint over the perturbative potential in its region of validity, we need to have the most accurate description possible at least over the region

$$0.2 < r < 0.5 \quad \text{GeV}^{-1} \tag{2.48}$$

From Fig 2.5 we see that the potential calculated in the $n_f = 4$ effective theory with $\Lambda^{(4)}_{\overline{MS}} = 0.2$ GeV gives the best approximation to the full theory in the region

$$0.08 \lesssim r \lesssim 0.5\ \text{GeV}^{-1}\ , \tag{2.49}$$

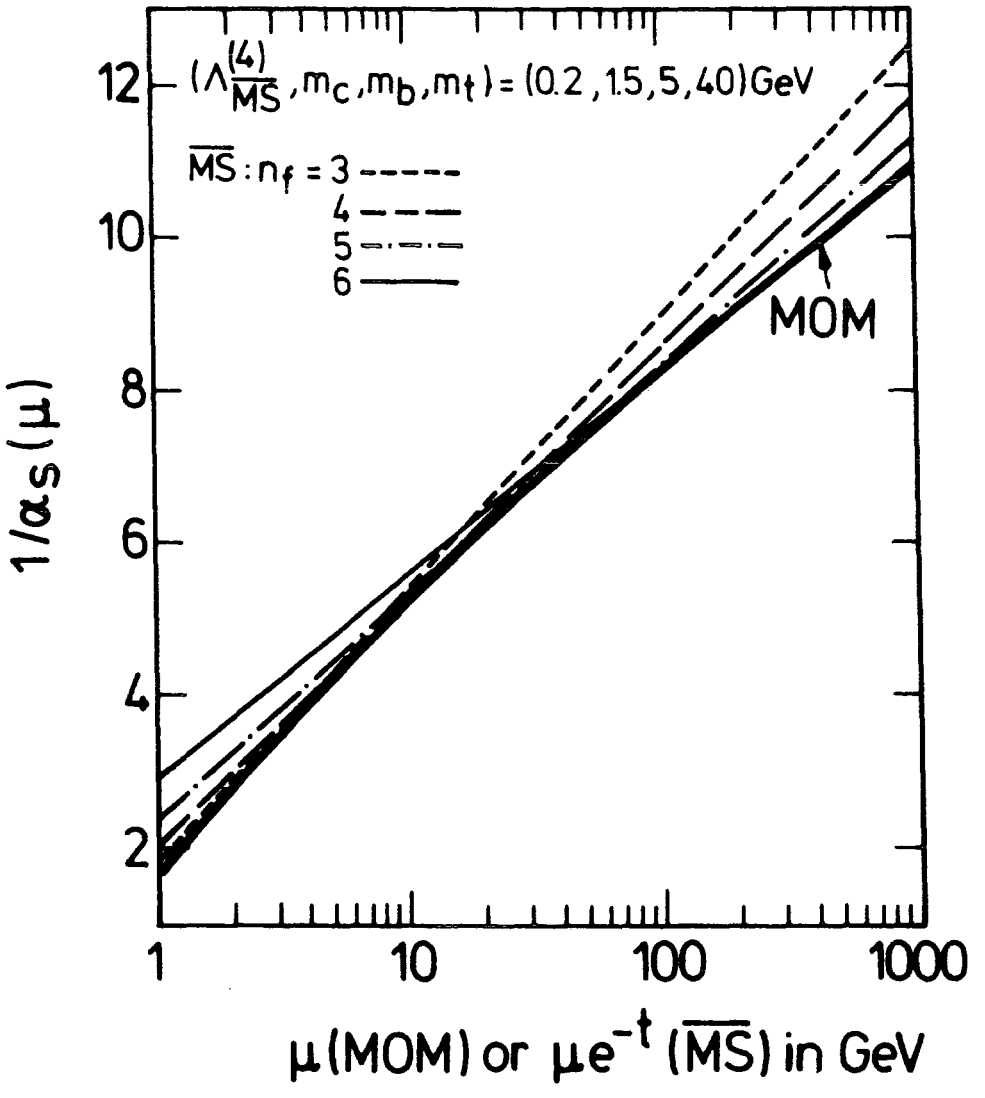

Fig 2.4 : The trajectories α_s versus μ or $\mu \exp(-t)$ (see eq. (2.47)) for the MOM scheme and the effective n_f-flavour theories in the $\overline{MS}$ scheme. All the curves correspond to taking $(\Lambda^{(4)}_{\overline{MS}}, m_c, m_b, m_t) = (0.2, 1.5, 5, 40)$ GeV.

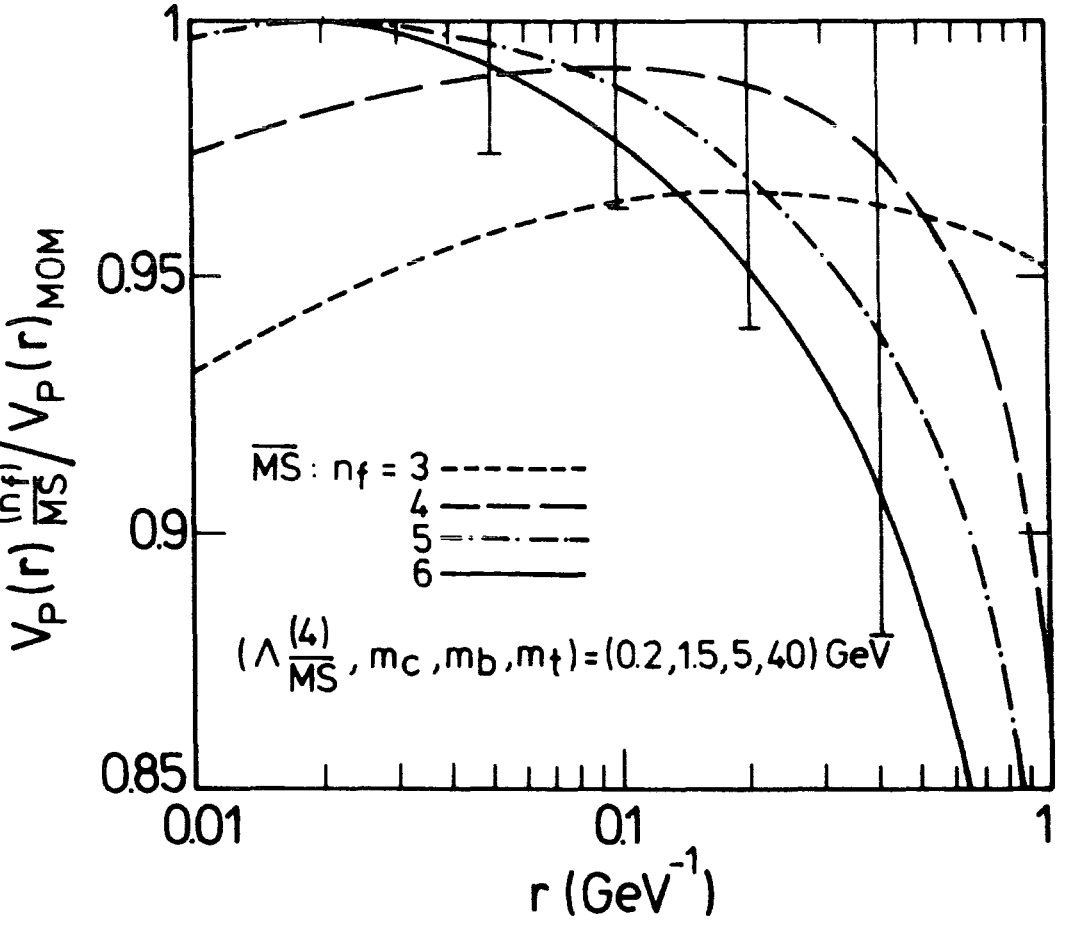

Fig 2.5 : The perturbative potential in the effective n_f-flavour theories renormalised in the $\overline{MS}$ scheme normalised to the perturbative potential of the full theory renormalised in the MOM scheme for $(\Lambda^{(4)}_{\overline{MS}}, m_c, m_b, m_t)$ = (0.2, 1.5, 5, 40) GeV. The error bars correspond to eq. (2.21) with K=1.

which includes the entire range of the perturbative potential that can be constrained by heavy quarkonium data. Indeed to feel the effects of bottom quark loops a quarkonium system would have to probe the short distance region $r < 0.08\ GeV^{-1}$. In Fig 2.6 we plot $\langle r^2 \rangle^{\frac{1}{2}}$ for the 1S state against a quark mass m_q of the system, and masses of $m_q > 250$ GeV would be required before such effects could be observed. Such quarkonium systems would instantly decay via weak interactions and cannot be observed [34, 12].

In conclusion, we have examined the form of the perturbative potential both in massless QCD and including heavy quark loop effects and have estimated the magnitude of higher order correction terms in both. We have found that the effective 4-flavour theory with a massive charm quark gives the best description of the short distance potential for any forseeable heavy quarkonium phenomenology. We now proceed to investigate how this short distance perturbative result governed by the value of $\Lambda \equiv \Lambda^{(4)}_{\overline{MS}}$ can be incorporated into a functional form for the full interquark potential.

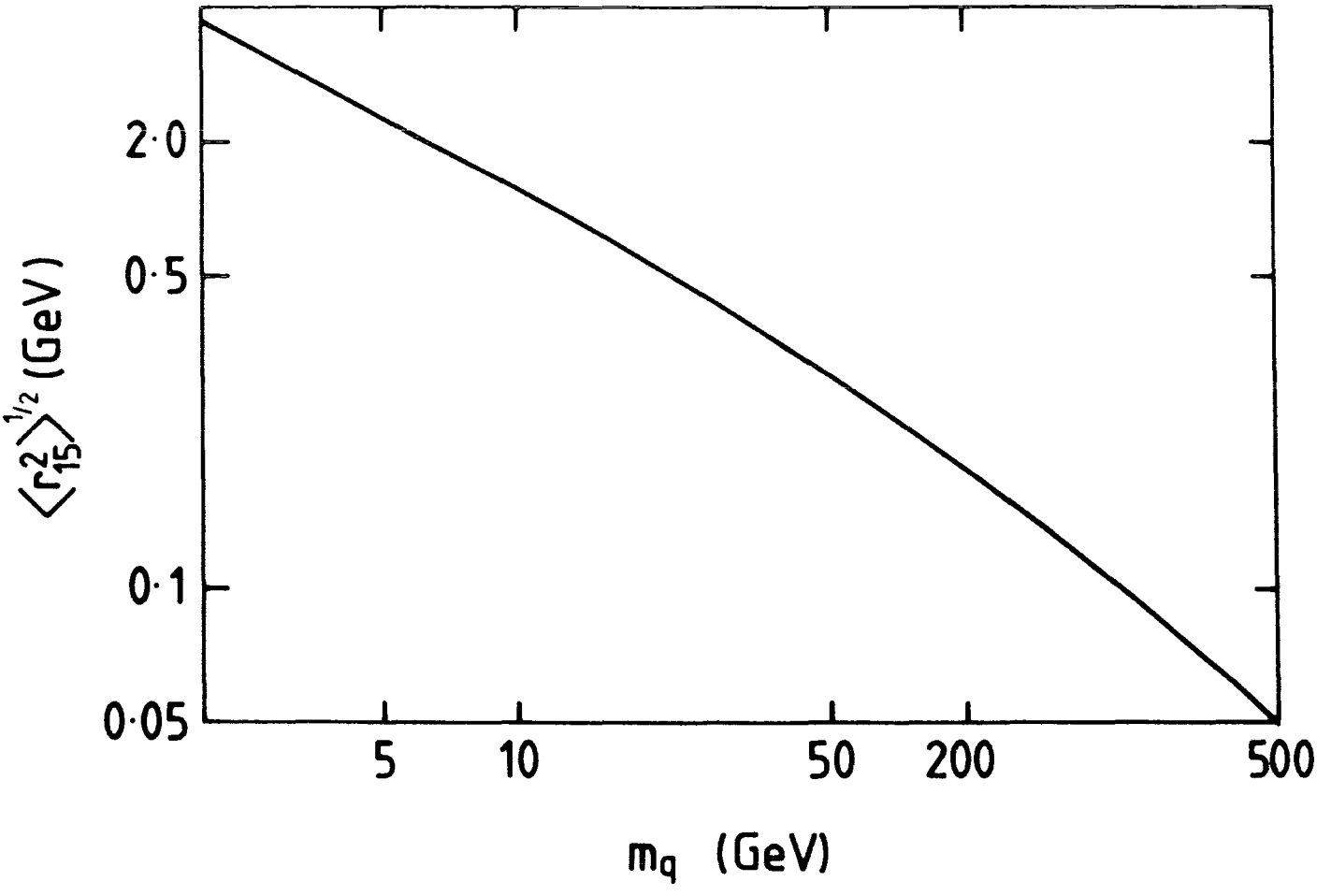

Fig 2.6 : The mean square radius of the 1S state of a quarkonium system versus the quark mass m_q, in the region relevant to the short distance form of the potential.

CHAPTER 3

The Quarkonium Potential and Fits to Charmonium and Bottomonium Data

The QCD perturbative potential given by eq. (2.19) was shown in Chapter 2 to be adequately described by a 4-flavour effective theory with massive charm quark loops, however this potential was only shown to be valid for small quark separations. In Fig 3.1 we show its form in the short distance region, to a maximum value of $r = r_c$ determined by the condition

$$r_c \Lambda = 0.1 \tag{3.1}$$

for various values of $\Lambda^{(4)}_{\overline{MS}}$. For smaller values of $\Lambda = \Lambda^{(4)}_{\overline{MS}}$ the perturbative form is expected to be valid over a larger region of r and vice-versa. The error bars on the $\Lambda = 0.2$ GeV potential, in Fig. 3.1 correspond to the fractional error due to the possible higher order corrections which we estimated and showed in Fig 2.1 as a function of $r\Lambda$. As mentioned in the Introduction, we can only expect charmonium and bottomonium data to probe distances greater than 0.5 Gev^{-1} (0.1fm). If this data is to put any constraint of the perturbative potential there must be some degree of overlap between the regions constrained by QCD and that by data. With this in mind, we would only expect charmonium and bottomonium to be sensitive to values of Λ less than about 0.2 GeV.

Our perturbative quarkonium potential is only relevant to the short distance region so we consider next how to incorporate this into a phenomenological-potential which covers the entire interval $o<r<\infty$ without losing the perturbative behaviour at small r.

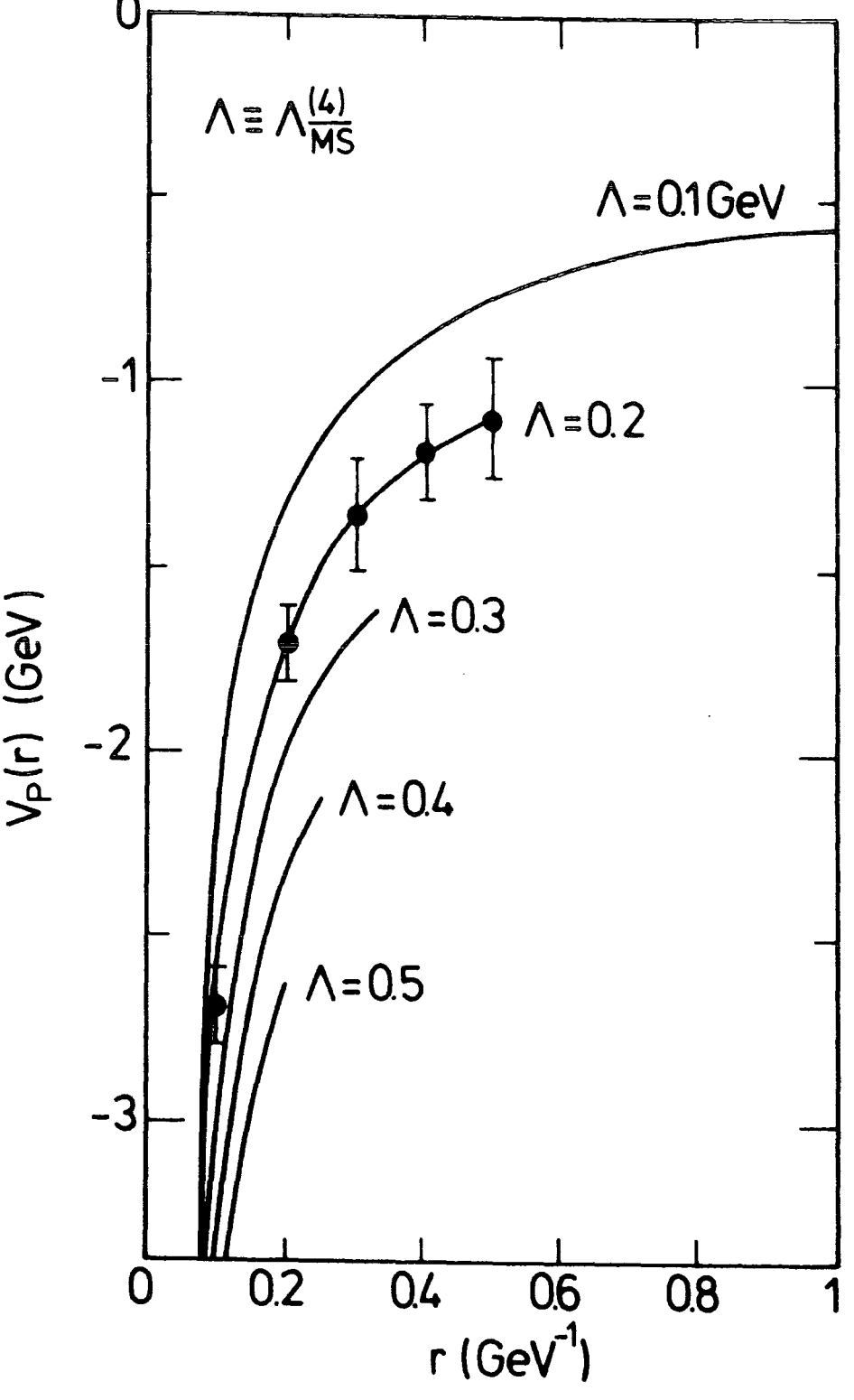

Fig 3.1 : The perturbative potential $V_p(r)$ for various values of $\Lambda = \Lambda^{(4)}_{\overline{MS}}$ in the region of $r\Lambda \leq 0.1$ where it is expected to be valid. The uncertainty ΔV_p, given by eq. (2.21) is also shown for the $\Lambda = 0.2$ GeV potential.

3.1 The Quarkonium Potential

We seek a phenomenological potential which embodies the short distance perturbative behaviour (such that it lies within the perturbative error corridor for $r\Lambda < 0.1$) and yet has a sufficiently flexible form so that its behaviour in the region $r\Lambda > 0.1$ does not constrain the value of Λ strongly. Both these conditions are crucial for a meaningful determination of Λ †. We follow Ref. 15 and use a parameteric form as follows

$$V(r) = V_S(r) + V_I(r) + V_L(r) \qquad (3.2)$$

We shall describe each element of the full quarkonium potential below.

1. $V_L(r)$ is the dominant piece at large distances and is responsible for the confining nature of the potential. It is usual to assume linear confinement

$$V_L(r) = ar \qquad (3.3)$$

where a is the slope and is related to the Regge slope by $a = (2\pi\alpha')^{-1}$. It has been shown that [36] linear confinement is the strongest allowed on grounds of the potential must be a monotonically increasing, concave function of the separation r. In fact, later in Chapter 4 we consider fitting with $r^{\frac{1}{2}}$ confinement, and its effect on the determination of Λ .

---

† For example the Λ parameter in the phenomenologically successful potential due to Richardson [35] is unrelated to our $\Lambda_{\overline{MS}}^{(4)}$ since its value is determined by the shape of the potential in the intermediate region where the perturbation expansion is not expected to work well.

2. The 'intermediate' component $V_I(r)$ is included solely to give sufficient flexibility at intermediate values of r, to be able to fit the quarkonia data, as well as ensuring that $V(r)$ approaches the perturbative form at short distances and retains the confining behaviour imposed by the large distance $V_L(r)$ term. We take

$$V_I(r) = r(c_1 + c_2 r) \exp(-r/r_o) \tag{3.4}$$

where c_1, c_2 and r_o are free parameters to be determined by fitting to the data. However, we also investigate to see whether our results dependent upon this specific parametric form by repeating the analysis including a term $c_3 r^2$ in the expansion of eq. (3.4).

3. The perturbative potential $V_p(r)$ given by eq. (2.19) has a singularity (Landau ghost) at

$$\mu_1 = \Lambda\left(\frac{b_o^2}{2b_1}\right)^{b_1/b_o^2} , \tag{3.5}$$

where the next-to-leading order running coupling constant $\alpha_s(\mu)$ as defined by eq. (2.12) or eq. (2.23), blows up. To obtain the short distance component of the full potential V_s, we regularise the perturbative potential V_p by a shift in the argument of α_s as follows

$$V_S(r) = -\frac{C_F}{r}\,\alpha_s(\tilde{\mu}_1)_{\overline{MS}} \tag{3.6a}$$

with

$$\tilde{\mu}_1 = \mu_1 + \Lambda(b_o^2/2b_1)^{b_1/b_o^2} , \tag{3.6b}$$

where the functional form of $\alpha_s(\mu)_{\overline{MS}}$ is still defined by eq. (2.12) or eq. (2.23). The shift $\mu_1 \to \tilde{\mu}_1$ has the effect of removing the singularity to infinite quark separation so that V_s remains finite and approaches zero at large distances.

In Fig. 3.2, we plot a typical quarkonium potential and separate out the individual components for $\Lambda = 0.2$ GeV, and also plot the perturbative potential. The singularity can be clearly seen and occurs at $r\Lambda \simeq 0.3$.

In summary, all three components of the phenomenological quarkonium potential eq. (3.2) are regular in the entire interval $0 < r < \infty$. V_s dominates at short, and V_L at large, distances and all three components are important in the intermediate region probed by charmonium and bottomonium spectroscopy. The potential depends on 5 parameters, Λ in V_s, a in V_L and c_1, c_2, r_o in V_I. These parameters together with the heavy quark masses † which set the scale of their respective heavy quarkonium spectrum, are to be determined by fitting to the available (and forthcoming) data.

For a meaningful determination of $\Lambda = \Lambda^{(4)}_{\overline{MS}}$ the quarkonium potential V(r) is required to reproduce its perturbative form $V_p(r)$, in the region where the perturbative expansion is expected to be valid, say $r < r_c$, where we define r_c by eq. (3.1). Deviations can occur in this region due to the $V_I + V_L$ component and due to the regularisation of V_p to form V_s (See Fig 3.2). In Chapter 2 we estimated the error $\Delta V_p(r)$ in $V_p(r)$ which may be expected from higher order corrections, eq. (2.21) with K=1.

---

† As discussed in Chapter 2, only the charmed quark mass is needed for the loop corrections to $V_p(r)$. The sensitivity of the spectrum to the actual value used in the loop corrections is found to be very weak and we fix it to be 1.5 GeV independent of the value of m_c determined by the fit to the charmonium data.

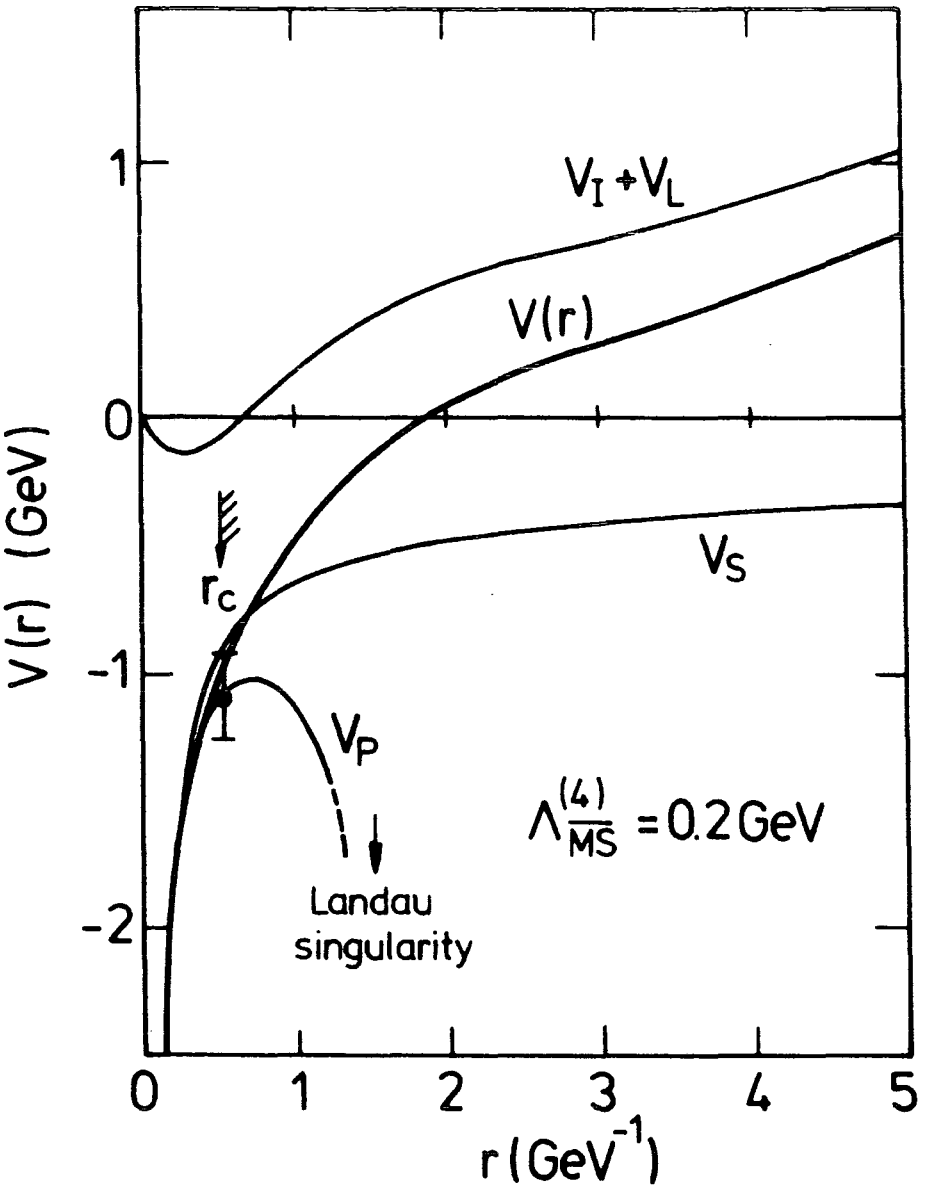

Fig 3.2 : A typical quarkonium potential, V(r) and its components for $\Lambda = 0.2$ GeV : $V(r) = V_S + V_I + V_L$. We require V(r) to lie within an error corridor about the perturbative potential $V_p(r)$ in the region of $r \leq r_c$ (with $r_c \Lambda = 0.1$). The error defined by eq. (2.21) is shown at $r = r_c$.

Thus for any given phenomenological potential V(r), a quantitative measure of its validity in the short distance region can be taken to be

$$\chi_V^2 = \sum_{n=1}^{10} |V(r_n) - V_p(r_n)|^2 / |\Delta V_p(r_n)|^2 \qquad (3.7)$$

with $r_n = nr_c/10$. When considering the value of χ_V^2 we should note that it is proportional to K^{-2} and that we have arbitrarily set K of eq. (2.21) equal to unity.

Before we consider confronting data with our model of the quarkonium potential, two final comments about its form are in order. Since we require our potential to have the short-distance perturbative form, we do not allow an overall constant term in the potential. It is known [14, 15] that the major effect of an overall shift in the potential can be compensated for by a change in the quark mass. Since the heavy quark masses (m_c, m_b and m_t) are taken as free parameters, the effect of a constant term can be regarded as a trivial shift of the quark masses. However, the constant term V_o does affect the level spacings so we need to investigate its inclusion in our potential eq. (3.2). We show later in this Chapter that small values of V_o are preferred. We shall also briefly discuss the correlation between the slope, a, of the long distance linear confining part of the potential ($V_L = ar$) and the value of V_o. In Chapter 4 we also consider if the possibility of determining Λ from toponium data is sensitive to the inclusion of V_o.

The second remark concerns a general property of the quarkonium potential. It has been shown [36] that the potential must be a monotonically increasing, concave function of the separation r. That is:

$$\frac{dV}{dr} > 0 \quad \text{and} \quad \frac{d^2V}{dr^2} \leq 0 \ . \tag{3.8}$$

We do not impose these constraints on our parametrization of the potential but check, a posterori, that the potential resulting from a fit to quarkonia data has these properties. We found that the first condition is always satisfied by a given best fit parameter set, however the second condition was only occasionally violated slightly and then only in fits to both charmonium and bottomonium data for the smallest values of $\Lambda \sim 0.1$ GeV and at large values of r ($r \sim 3.5\ \text{GeV}^{-1}$) and is entirely due to the intermediate part of the potential $V_I(r)$. We should not worry too greatly over this violation as at these small values of Λ the overall fit to data is bad and the parameters c_1, c_2, and r_o of V_I are having to do a lot more work to produce any sort of fit resulting in unphysical behaviour at the large distance end where the effects of V_I are small anyway.

In the next section we shall consider the charmonium and bottomonium data and the structure of the fits using our quarkonium potential of eq. (3.2).

3.2 Description of Charmonium and Bottomonium Data

Only toponium will be heavy enough a system to probe the short distance perturbative behaviour of the potential and we do not expect charmonium or even bottomonium data to put strong constraints on the value of Λ. Rather we use the data to obtain satisfactory phenomenological potentials at various values of Λ with which to confront toponium data when it becomes available.

The fine and hyperfine splittings of toponium states were estimated in Section 1.9 of Chapter 1 are shown to be of order 10 MeV [14] and as such are beyond to resolution of presently foreseeable experiments. We therefore perform an analysis using spin-averaged quarkonium levels, avoiding the added complications of the Lorentz-transformation character of the potential.

The charmonium and bottomonium data [37] set that we use is shown in Table 3.1 where we only list the spin averaged result. There are a few comments we should make about this data set before proceeding. We do not include the 2S charmonium level in the fit due to its proximity to the open flavour threshold and due to mixing effects resulting in it having a fairly large width. The P level is calculated as the spin averaged centre-of-gravity of the three ^3P_J levels and we neglect possible hyperfine splitting from the unobserved $^1P_1$ level. It is commonly assumed that the hyperfine interaction is predominantly of short range, so its effect on P and higher waves is small and as the observed triplet states are weighted three times heavier than the singlet.

$$\text{c. of g.} \equiv m_{1P} + m_H/3 \tag{3.9a}$$

$$^1P_1 \equiv m_{1P} - 3m_H/4 \tag{3.9b}$$

where m_{1P} is the true centre of gravity and m_H is the hyperfine force, then it seems justified to ignore these effects although we take the error to be 10MeV on this state and keep in mind the general tendency to cause the true centre of gravity to be less than that of the ^3P_J levels. In the bottomonium spectrum only the triplet S levels have been observed and the hyperfine splittings for $^3S - ^1S$ are required to obtain the centre-of-gravity for these three levels. Theoretical predictions on the Υ-η_b mass difference are spread

between 30 and 100 MeV [12], however most refined QCD estimates favour lower values based again on the hyperfine force being short range and essentially dependent on the value of the wavefunction at the origin. We use the following predictions

$$m(T) - m(\eta_b) = 32,16,11 \text{ MeV} \tag{3.10}$$

for the 1S, 2S, 3S levels respectively, to determine values for the centre-of-gravity. Again we neglect P wave hyperfine splittings and simply use the weighted average of the observed three ^3P_J levels. The observed ratios of the leptonic widths are included in the fits by using

$$\frac{\Gamma_{ee}(nS)}{\Gamma_{ee}(1S)} = \left(\frac{m(1S)\ R_{nS}(0)}{m(nS)\ R_{1S}(0)} \right)^2 \tag{3.11}$$

where $R_{ns}(0)$ is the value of the n-S wave radial wavefunction at the origin. We choose to fit to ratios of leptonic widths rather than to the absolute widths since the latter have large first order QCD corrections [38]

$$\Gamma_{ee}(nS) = \frac{4\alpha^2 e_q^2}{m(nS)^2} |R_{nS}(0)|^2 \left[1 - \frac{16\alpha_s}{3\pi} \right], \tag{3.12}$$

which are essentially cancelled in the ratio. However, for each fit we present Γ_{ee} calculated from the formula (3.12) by using $\alpha_s(2m_q)_{\overline{MS}}$.

The energy level spectrum for both charmonium and bottomonium are normalised with respect to the lowest S state. The parameters m_c and m_b ensure that the lowest level is then exactly reproduced by the potential in the fitting procedure.

For various fixed values of $\Lambda \equiv \Lambda^{(4)}_{\overline{MS}}$ we vary the remaining 4 parameters of the potential (given by eq. (3.3) and eq. (3.4) and the external heavy quark masses to obtain the best χ^2 fit to the quarkonia data, simultaneously requiring the potential to approximate

its perturbative short distance form by including eq. (3.7) in χ^2.

$$\chi^2 = \chi^2_{data} + \chi^2_V \qquad (3.13)$$

As V(r) is varied to obtain the optimum fit, we need to repeatedly solve the radial Schrodinger equation, eq. (1.33), to find its energy levels and wavefunctions corresponding to the observed charmonium and bottomonium states. We use the matrix inversion method of Ref.[39], described in Appendix B. Here the Schrodinger equation is reduced to a matrix equation, using the finite difference approximation for the derivatives, and solved to obtain eigenvalues and eigenvectors corresponding to energy levels and wavefunctions respectively. We test the method for efficiency and accuracy using both the Coulomb and 3-dimensional oscillator potentials, as described in Appendix B.

3.3 Fitting to Charmonium and Bottomonium Data

Using the above data and fitting procedure we consider two series of fits. Firstly we fit to a combined $c\bar{c}$ and $b\bar{b}$ data and then to the $b\bar{b}$ alone. The detailed results to $\Lambda = 0.2$ and $\Lambda = 0.4$ GeV are given in Table 3.1 and in Fig. 3.3. We show χ^2 as a function of Λ and also plot the components of the total χ^2 coming from the quarkonia data and from the short distance perturbative region. We see that for both data sets there is a marked increase in χ^2, particularly in χ^2_V, for $\Lambda \lesssim 0.15$ GeV, as in this region of Λ it becomes increasingly difficult to obtain a good approximation to the perturbative form over its region of validity which due to the smallness of Λ extends well into the region determined by the data. This puts on a quantitative footing a result originally given by Buchmuller and Tye [14], namely that low values of Λ are ruled out due to the conflict between the slope of the perturbative potential and the one required by the data in the 0.1-1fm (0.5-5 GeV^{-1}) region.

	Data	$c\bar{c}$ + $b\bar{b}$ data fitted				Only $b\bar{b}$ data fitted			
		Λ=0.2	χ^2	Λ=0.4	χ^2	Λ=0.2	χ^2	Λ=0.4	χ^2
$c\bar{c}$ data:									
m(1S)	3068 ± 2	3068	0	3068	0				
m(2S)-m(1S)*	595 ± 2	609	-	596	-				
m(1P)-m(1S)	457 ± 10	426	9.6	423	11.3				
Γ_2/Γ_1	0.43 ± 0.06	0.49	1.1	0.47	0.3				
Γ_1*	4.75 ± 0.51	4.35	-	4.81	-				
$b\bar{b}$ data:									
m(1S)	9452 ± 2.5	9452	0	9452	0	9452	0	9452	0
m(2S)-m(1S)	567 ± 3	571	1.9	568	0.1	569	0.7	566	0.0
m(3S)-m(1S)	900 ± 2.5	902	0.8	903	1.6	902	0.9	902	0.5
m(1P)-m(1S)	448 ± 2.5	446	0.8	447	0.3	446	0.3	447	0.1
m(2P)-m(1S)	809 ± 6	790	10.3	795	5.4	790	10.4	797	3.1
Γ_2/Γ_1	0.44 ± 0.03	0.39	3.1	0.39	2.4	0.38	3.7	0.39	1.9
Γ_3/Γ_1	0.33 ± 0.03	0.32	0.1	0.31	0.5	0.31	0.2	0.30	1.3
Γ_1*	1.22 ± 0.05	1.05	-	1.13	-	1.07	-	1.17	-
χ^2_{data}			27.8		21.9		16.2		6.9
χ^2_V of Eq. (3.8)			1.7		1.2		2.4		0.2
parameter values	m_c (GeV)	1.36		1.58		-		-	
	m_b (GeV)	4.79		4.99		4.82		5.04	
	a (GeV^2)	0.22		0.18		0.21		0.16	
	c_1	-1.12		-1.35		-1.55		-2.54	
	c_2	1.19		1.15		1.40		0.92	
	r_o (GeV^{-1})	0.70		0.57		0.63		0.36	

Table 3.1 : The optimum fits to quarkonia data (and the perturbative potential) for $\Lambda = \Lambda^{(4)}_{\overline{MS}}$ = 0.2 and 0.4 GeV. The masses m(nl) are given in MeV and leptonic widths, $\Gamma_n = \Gamma_{ee}(nS)$ in keV. The data marked by * are not used in the fit.

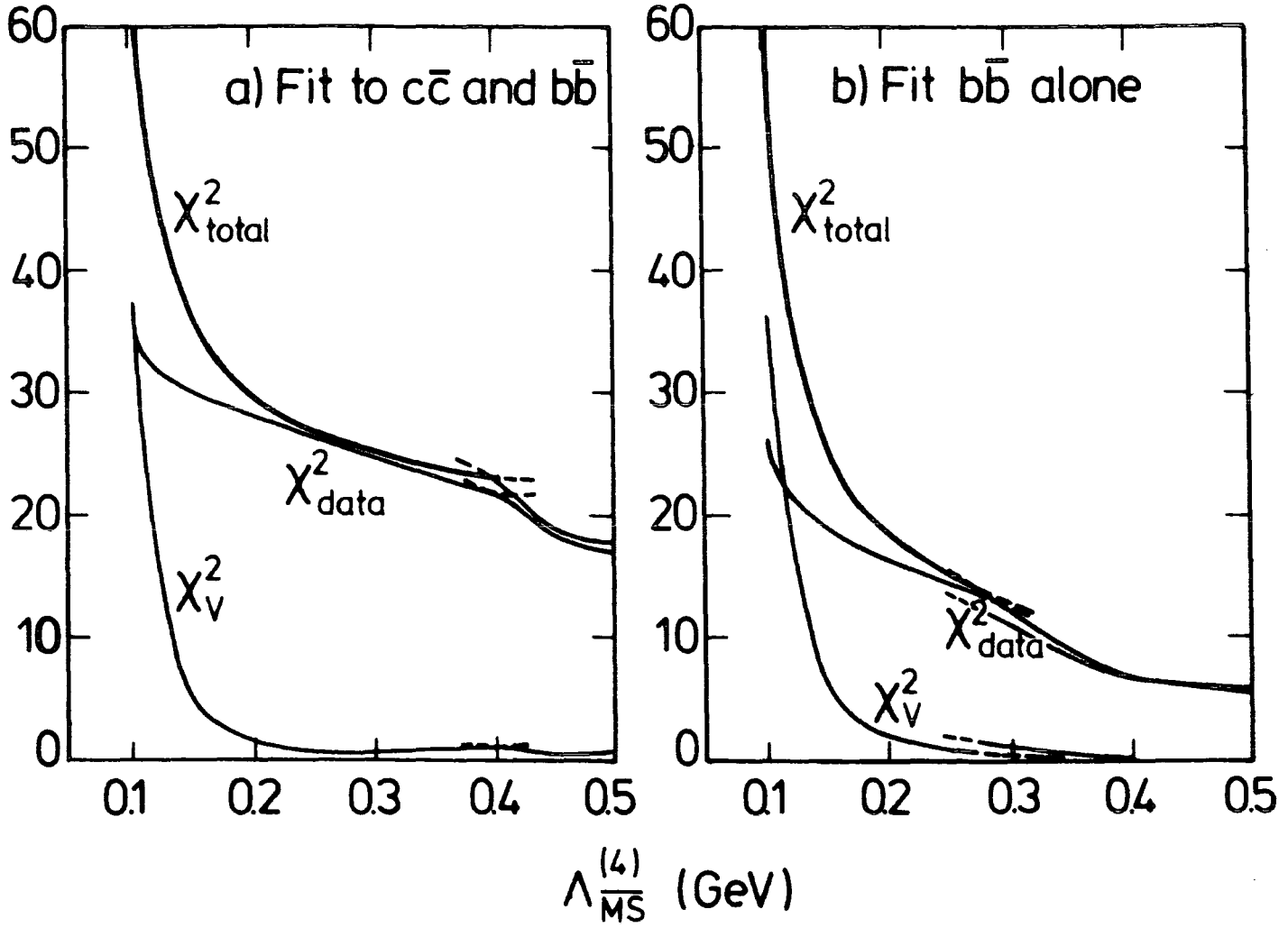

Fig 3.3 : χ^2 as a function of Λ obtained by fitting (a) the $c\bar{c}$ and $b\bar{b}$ quarkonia data, and (b) the $b\bar{b}$ data alone. The total χ^2 includes a component χ^2_V (given by eq. (3.7)) which is a measure of how well the potential reproduces the perturbative potential in the short-distance region. Note that the optimum solution changes discontinuously from one family of solutions of parameters (c_1, c_2, r_o, a, m_q) to another at a certain value of Λ.

As Λ increases from 0.15 GeV, the experimentally constrained region of the potential separates from the perturbative region and not surprisingly, we see χ^2_V as defined by eq. (3.7) plays a negligible role in the fit. The component of χ^2 from the quarkonia data, χ^2_{data}, is essentially independent of Λ, the slight decrease being due to the fact that the 2P bb state becomes better fitted for large values of Λ. The discontinuities in Fig 3.3 are due to the parametric form used for V_I, eq. (3.4), and is a result of a switch from one family of solutions to another, in order to follow the contour of lowest values of χ^2. In following a particular family of solutions, sudden jumps in the parameter values occur at the discontinuities, and indicates that better fits to the data can be produced for a different parameter family. We have repeated the fits using a extra parameter, c_3 in V_I

$$V_I(r) = r(c_1 + c_2 r + c_3 r^2)\exp(-r/r_o) \qquad (3.14)$$

and it is found that the χ^2 profile is smoothed out, but the discontinuity structure is still present. We find that many more fits must be performed in order to determine the different families of solutions and the position of the discontinuities due to the introduction of this extra parameter. The structure of the fit is unchanged and we conclude that there is little sensitivity to the parametric form of the intermediate potential that we have used, either in eq. (3.4) or eq. (3.14). Thus apart from the constraint $\Lambda \gtrsim 0.15$ GeV, we conclude that Λ is not determined by $b\bar{b}$ and $c\bar{c}$ data†.

---

† The rise in χ^2 at larger Λ shown in the fit of Ref [15] is attributed to the inclusion of the observed leptonic width of the $b\bar{b}$ 1S state in the fit and in particular to fitting it with eq. (3.12) without the first-order QCD correction.

3.4 Other Quarkonium Potentials

In this Section we consider some of the other phenomenological quarkonium potentials that have been proposed to describe the $c\bar{c}$ and $b\bar{b}$ data. To obtain a consistent comparison, we use each of the potential forms in turn to fit to the quarkonia data listed in Table 3.1.

3.4.1 The Martin Potential [40]

This potential was originally motivated by the apparent logarithmic behaviour expected in the region sensitive to the data. Such potential behaviour predicts that the level spacings of a $q\bar{q}$ system are strictly independent [41] of the mass of the quark and is consistent with the apparent equality,

$$m(T') - m(T) = m(\psi') - m(\psi) \simeq 0.6 \quad \text{GeV} \tag{3.15}$$

The form of the potential is taken to be

$$V(r) = A + Br^{\nu} \tag{3.16}$$

and the parameter ν is small such that the r-dependence is essentially logarithmic,

$$V(r) \simeq \nu \, \ell nr \tag{3.17}$$

The optimum fit is shown in Table 3.2 and corresponds to the parameter values

$$A = -6.00, \quad B = 5.78, \quad \nu = 0.118$$

$$m_c = 1.43, \quad m_b = 4.83 \quad \text{in GeV units.} \tag{3.18}$$

As this potential is purely phenomenological we cannot compare its short distance behaviour with that expected from perturbative QCD, however, it helps to identify the region sensitive to $c\bar{c}$ and $b\bar{b}$ data. We see from Table 3.2 that it does not achieve a satisfactory description of all the $b\bar{b}$ data also.

3.4.2 The Richardson Potential [35]

Richardson proposed an economical potential which depends only on a single parameter Λ_R, and is constrained by asymptotic freedom, in the guise of single dressed gluon exchange at short distances and linear quark confinement at large distances. In momentum space the potential takes the form

$$\tilde{V}(\vec{q}^2) = -\frac{4}{3}\frac{12\pi}{33-2n_f}\frac{1}{\vec{q}^2}\frac{1}{\ln(1+\vec{q}^2/\Lambda_R^2)} \cdot \qquad (n_f = 4) \qquad (3.19)$$

With this form we obtain the excellent fit to the quarkonia data shown in Table 3.2 for the parameter values,

$$\Lambda_R = 0.375 \text{ GeV}, \quad m_c = 1.50 \text{ GeV}, \quad m_b = 4.91 \text{ GeV} . \qquad (3.20)$$

However, this potential is not constructed to reproduce the two-loop perturbative form and hence the parameter has little to do with the perturbative QCD scale parameter $\Lambda = \Lambda_{\overline{MS}}^{(4)}$, which determines the short distance behaviour and which we are ultimately trying to measure. Indeed, the value of Λ_R is determined from the data by the intermediate and long-range behaviour of the potential and not by its short distance behaviour. However, it is worth noting that this one-parameter potential form gives an exceptionally good fit to the $c\bar{c}$ and $b\bar{b}$ data (See Table 3.2).

3.4.3 The Kühn-Ono Potential [42]

A potential based on the second-order perturbative form in the massless 4-flavour effective theory was considered in Ref. [42];

$$V(r) = -\frac{16\pi}{25}\frac{1}{rf(r)}\left[1 + \frac{2\gamma_E + 53/75}{f(r)} - \frac{462\ \ln f(r)}{625 f(r)}\right] \qquad (3.21a)$$

with $\qquad + a\sqrt{r} + c$

$$f(r) \equiv \ln[1/(\Lambda r)^2 + b] , \qquad (3.21b)$$

Where the parameter b is introduced to avoid the Landau singularity. Here $\Lambda \equiv \Lambda'^{(n_f)}_{\overline{MS}}$ defined in eq. (2.24) and is very closely related to our QCD parameter $\Lambda^{(4)}_{\overline{MS}}$ which is defined in eq. (2.12). In eq. (3.21) massless charm quark loops are considered which, as discussed in Chapter 2, cause a downward shift of above 20 MeV in the value of Λ when fitted to the same data. The optimum fit to the data using the potential of eq. (3.21) is shown in Table 3.2 for Λ = 0.2 and for Λ = 0.4 GeV and the corresponding parameter values are given in Table 3.3. We see that the excellent descriptions of the data can be found, provided that the regularisation parameter b is allowed to take arbitrary values†. The approach of the Kühn-Ono potential to the perturbative potential at short distances is relatively slow due to the large value of the regularisation parameter b and also to the presence of the constant term, c, in the potential. The χ^2_V values are shown in Table 3.2 and, though large, are acceptable. However, as Λ is decreased below 0.15 GeV, the value of χ^2_V increases rapidly, as in Fig 3.3, confirming once again that the $c\bar{c}$ and $b\bar{b}$ data cannot accommodate a short distance potential with $\Lambda \lesssim 0.15$ GeV.

All the above potentials are compared in Fig 3.4. As expected they have a common slope in the region sensitive to the $c\bar{c}$ and $b\bar{b}$ data, $0.5 < r < 5\ \text{GeV}^{-1}$. At short distances both our potential and the Kühn-Ono potential behave roughly

---

† Ref [42] advocates a value of b = 20 and fixed. We find with b = 20 that χ^2_{data} = 84.3 for Λ = 0.2 GeV and χ^2_{data} = 630 for Λ = 0.4 GeV.

		Martin		Richardson		Kühn-Ono, Λ=0.2		Kühn-Ono, Λ=0.4	
$c\bar{c}$ data:			χ^2		χ^2		χ^2		χ^2
m(1S)	3068 ± 2	3068	0	3068	0	3068	0	3068	0
m(2S)-m(1S)*	595 ± 2	615	-	588	-	596	-	593	-
m(1P)-m(1S)	457 ± 10	441	1.4	423	11.5	429	7.7	427	9.1
Γ_2/Γ_1	0.43 ± 0.06	0.39	0.5	0.44	0.0	0.42	0.1	0.42	0.0
Γ_1*	4.75 ± 0.51	4.34	-	4.63	-	3.65	-	3.94	-
$b\bar{b}$ data:									
m(1S)	9452 ± 2.5	9452	0	9452	0	9452	0	9452	0
m(2S)-m(1S)	567 ± 3	575	7.6	569	0.6	572	2.9	570	0.8
m(3S)-m(1S)	900 ± 2.5	913	28.2	899	0.0	901	0.3	901	0.2
m(1P)-m(1S)	448 ± 2.5	413	190.0	451	2.1	444	2.9	446	0.6
m(2P)-m(1S)	809 ± 6	800	2.3	805	0.4	804	0.7	806	0.3
Γ_2/Γ_1	0.44 ± 0.03	0.50	4.4	0.41	1.1	0.43	0.2	0.42	0.2
Γ_3/Γ_1	0.33 ± 0.03	0.34	0.1	0.28	2.2	0.29	1.7	0.29	1.7
Γ_1*	1.22 ± 0.05	0.69	-	1.32	-	1.12	-	1.22	-
χ^2_{data}			235		17.9		16.4		13.0
χ^2_V			-		-		25.9		22.4

Table 3.2 : **The optimum fits to the quarkonia data using various potential forms. The masses are given in MeV and the leptonic widths, $\Gamma_n = \Gamma_{ee}(nS)$ in keV. The data marked by * are not used in the fits.**

Λ (GeV)	a $(\text{GeV})^{\frac{3}{2}}$	b	c (GeV)	m_c (GeV)	m_b (GeV)
0.2	0.67	238	-0.41	1.22	4.66
0.4	0.70	499	-0.81	1.41	4.83

Table 3.3 : The parameter values corresponding to the fits shown in Table 3.2 for the Kühn-Ono potential form of eq. (3.21).

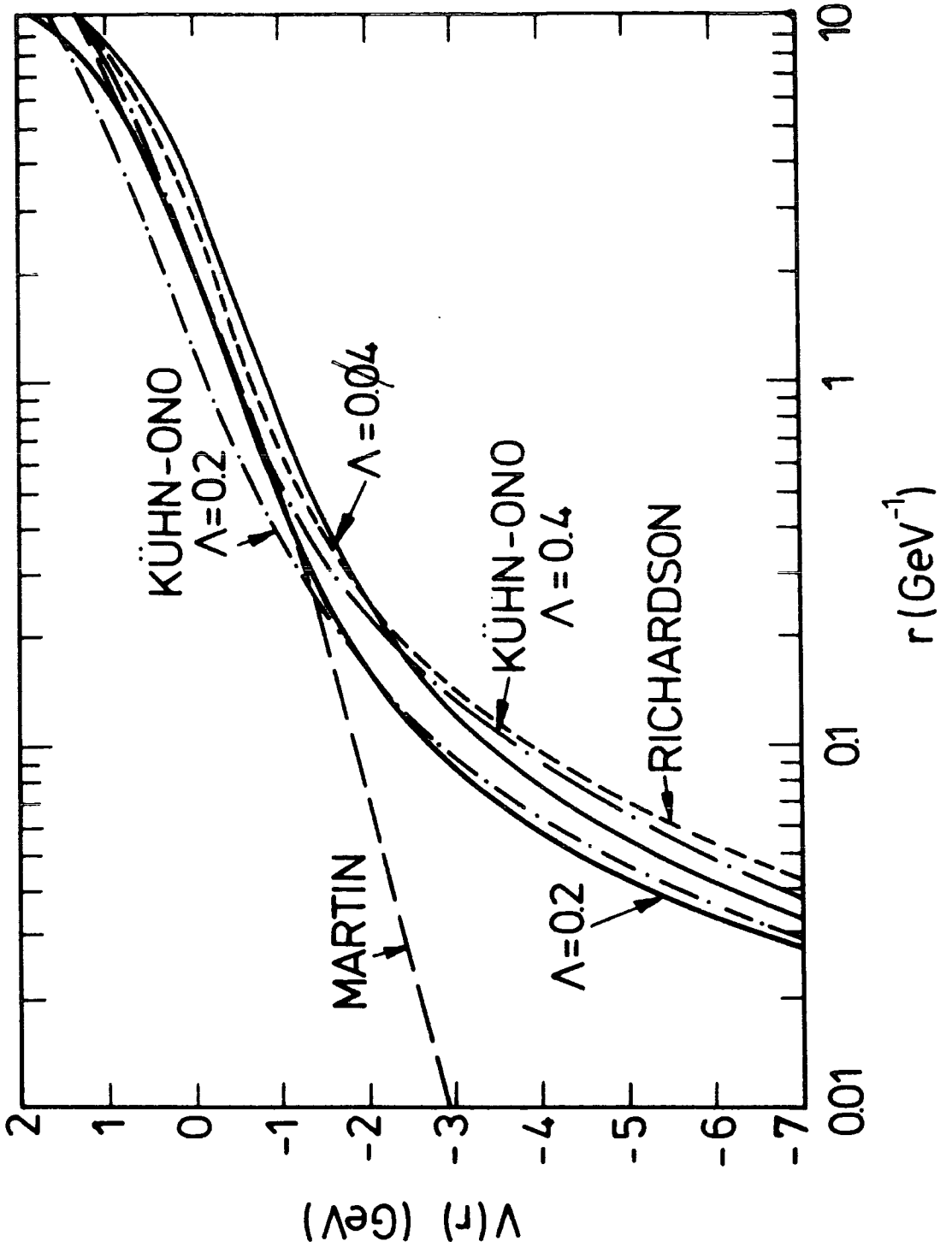

Fig 3.4 : Quarkonia potentials, obtained by fitting various phenomenological forms [given by eqs. (3.16), (3.19) and (3.21)] to the $c\bar{c}$ and $b\bar{b}$ data of Table 3.1, compared with the potential of eq. (3.2) for two representative Λ values.

as the two-loop perturbative potential. The Richardson potential with $\Lambda_R = 0.375$ GeV gives the most singular behaviour at short distances, but it is not too different from the two loop potential with $\Lambda_{\overline{MS}}^{(4)} = 0.5$ GeV around $r = 0.1$ GeV^{-1}. At large distances ($r \gtrsim 5$ GeV^{-1}), the linearly rising behaviour of our potential and that of Richardson is clearly seen. We consider next the inclusion of a constant term V_o in the potential of eq. (3.2).

3.5 Including A Constant Term In The Quarkonium Potential

Using a fixed value of $\Lambda = 0.2$ GeV, we consider the quantitative effects of a constant term in the quarkonium potential, by repeating the fits to $c\bar{c}$ and $b\bar{b}$ data, the results of which are shown in Table 3.4. The procedure was to fix the parameter 'a' at a specific value and allow the other parameters (c_1, c_2, r_o, m_c, m_b, V_o) to vary and reach the minimum in χ^2, then to repeat the analysis for other values of 'a'. We see a definite correlation between the slope, a, and the value of V_o. Acceptable fits only occur for slopes $a \simeq 0.2$ GeV^2 and values of V_o around zero.

The parameter a describes the expected QCD structure of the potential at large quark separations, as seen in Section 1.8 and Fig 1.8b, and characterises a linear energy density between the quark and antiquark. A qualitative argument in favour of values of $a \simeq 0.2$ GeV^2 comes from the experimental relation between the mass M and orbital angular momentum L of systems consisting of light quarks

$$L = \text{const.} + \alpha' M^2 \qquad (3.22)$$

where the Regge slope α' appears to be

$$\alpha' \simeq 0.8 - 0.9 \ \text{GeV}^{-2} \qquad (3.23)$$

a (GeV²)	V_o GeV	χ^2
0.35	-0.41	98
0.33	-0.40	74
0.31	-0.35	54
0.29	-0.26	41
0.27	-0.20	34
0.25	-0.10	33
0.23	-0.04	30
0.21	0	29
0.19	0.11	27
0.17	0.19	24
0.15	0.22	46
0.13	0.23	92

Table 3.4 : **The optimum fits to $c\bar{c}$ and $b\bar{b}$ data for $\Lambda = 0.2$ for different fixed values of the slope, a, defined by $V_L = ar$, but with a constant term V_o included in the potential as a free parameter.**

in a wide variety of circumstances. To obtain [43] a connection between α' and 'a' we imagine two massless quarks to be connected by a 'string' of energy density 'a' per unit length. For states of zero angular momentum the string is stationary, however higher states correspond to rotations of the string about its centre with the ends moving at the velocity of light. Each point along the string then has a local velocity determined by its distance from the centre of the string. Relating the orbital angular momentum and mass of the string, we find $L = M^2/(2\pi a)$ or,

$$a = 1/2\pi\alpha' \simeq 0.18 - 0.20 \quad GeV^2 \tag{3.24}$$

consistent with values obtained in fits to quarkonia data. Indeed, from the phenomenological potential of the Cornell Group [7]

$$V(r) = -\frac{K}{r} + ar \tag{3.25}$$

the best fit ($\chi^2_{data} = 65.3$) to the combine $c\bar{c}$ and $b\bar{b}$ data has $K = 0.47$, $a = 0.19$ GeV, $m_c = 1.32$ GeV and $m_b = 4.75$ GeV. The success of the Buchmuller - Grunberg - Tye potential [14] can also be attributed to its large-distance behaviour being determined by the Regge-slope. If, for instance, one chooses a larger value of a ($a > 0.2$ GeV^2) then a negative V_o is required in an attempt to compensate for the rapid rise of the stored energy as the quark separation increases through the region sensitive to the $c\bar{c}$ and $b\bar{b}$ data. We are lead to conclude here that small values, consistent with zero, of V_o are preferred by the data.

CHAPTER 4

Toponium

Toponium, in analogy with charmonium and bottomonium, is the name given to the spectroscopy of particles containing t and $\bar{t}$ quarks bound together, but as the top quark is very much heavier than either that of the charm or bottom quarks, the toponium spectrum is expected to be much richer than either those of charmonium or bottomonium. However, as the top quark has not yet been definitely observed any discussion of toponium must be purely theoretical.

For any general potential the WKB approximation [44] can be used to show that the number of narrow toponium S states below the threshold for pair production of $T(t\bar{q})$ mesons is [45, 13]

$$n \simeq 3.8 \left(\frac{m_t}{m_b}\right)^{\frac{1}{2}} . \qquad (4.1)$$

Taking $m_t = 40$ GeV we anticipate about 10 narrow toponium S states.

Our main objective in this Chapter is to see the additional constraints that toponium data (when they become available) can impose on the short distance behaviour of the potential, and specifically to see how accurately the value of $\Lambda \equiv \Lambda^{(4)}_{\overline{MS}}$ can be determined. With this in mind we shall first consider the toponium predictions using the potentials discussed in Chapter 3.

4.1 Toponium Predictions

The predictions for the S states of the toponium spectrum are shown in Table 4.1 for the quarkonium potentials with $\Lambda = 0.2$ and $\Lambda = 0.4$ GeV that were determined by the fit to the $c\bar{c}$ and $b\bar{b}$ data listed in Table 3.1. For comparison we also show the predictions of the 'Martin' and 'Richardson' potentials of eq. (3.16) and eq. (3.19) and give value of $\langle r^2 \rangle^{\frac{1}{2}}$ for each state which indicates the region of the potential probed by that state. We see that the level spacings of the higher radial excitations (n>3) have little dependence on the choice of potential since they are sensitive to the region of the potential already constrained by the $c\bar{c}$ and $b\bar{b}$ data. The observation of these higher excited states is still important in order to check the flavour independence of the potential, however the decreasing separation between the higher excited states will make them much more difficult to resolve experimentally [13, 46].

For a toponium system of mass $m_{1S} = 80$ GeV, it seems that the data which is most sensitive to the form of the short distance potential are the lowest lying states, namely the 1S, 2S and 1P levels. It is indeed fortunate that it is precisely these states that are easiest to measure [13], (provided the toponium mass is less than about 80 GeV). Other quantities in the spectrum which may be sensitive to the short distance behaviour are the leptonic widths given by eq. (3.12) and the ratio of widths eq. (3.11), and in Table 4.2 we show toponium predictions for five different values of $\Lambda = \Lambda_{\overline{MS}}^{(4)}$ using three possible toponium masses, m(1S) = 60, 80 and 100 GeV. We see that the predictions exhibit a strong Λ dependence. In Table 4.2 and in the following, $\Gamma_n^{(0)}$ stands for the 'virtual photon contribution' to the leptonic width of the triplet nS states

m(1S) GeV	Λ GeV	Mass differences in MeV				$\Gamma_1^{(0)}$ keV	$\frac{\Gamma_2^{(0)}}{\Gamma_1^{(0)}}$	$\frac{\Gamma_3^{(0)}}{\Gamma_1^{(0)}}$
		2S-1S	3S-1S	1P-1S	2P-1S			
60	0.1	603	945	458	853	2.58	0.53	0.32
	0.2	652	997	517	913	3.35	0.46	0.27
	0.3	679	1025	550	945	3.82	0.43	0.24
	0.4	707	1051	582	975	4.26	0.40	0.22
	0.5	752	1090	627	1017	4.73	0.37	0.20
80	0.1	603	954	473	863	2.65	0.50	0.32
	0.2	670	1028	548	945	3.54	0.42	0.26
	0.3	708	1069	590	990	4.09	0.40	0.23
	0.4	746	1108	630	1033	4.60	0.37	0.21
	0.5	802	1162	681	1090	5.08	0.35	0.19
100	0.1	610	964	492	877	2.79	0.46	0.30
	0.2	694	1059	583	978	3.78	0.39	0.24
	0.3	741	1112	633	1034	4.40	0.36	0.22
	0.4	787	1163	680	1088	4.96	0.34	0.20
	0.5	851	1229	735	1158	5.45	0.34	0.18

Table 4.2 : **Predictions for the properties of toponium that are most sensitive to the value of $\Lambda = \Lambda_{\overline{MS}}^{(4)}$ shown for various values of the toponium mass, m(1S), and various values of Λ . The potential is obtained by fitting to the $c\bar{c}$ and $b\bar{b}$ data as in Table 3.1.**

n	$\langle r^2 \rangle_{nS}^{\frac{1}{2}}$	$E_{n+1}-E_n$ in MeV			
	$(GeV)^{-1}$	Λ=0.2	Λ=0.4	Richardson	Martin
1	0.35	670	746	987	505
2	0.82	358	363	372	298
3	1.32	224	221	228	215
4	1.89	157	161	170	170
5	2.43	130	135	140	141
6	2.88	118	121	120	121
7	3.23	111	111	108	106
8	3.71	105	104	98	95
9	3.88	100	98	91	85
10	4.16				

Table 4.1 : Predictions for the toponium S states obtained using potentials that describe $c\bar{c}$ and $b\bar{b}$ data. We have taken m(1S) = 80 GeV.

$$\Gamma_n^{(0)} = \Gamma(nS \to \gamma^* \to e^+e^-) \qquad (4.2)$$

including first order QCD corrections given in eq. (3.12). The true leptonic width, including the effects of the Z boson contributions, is then trivially obtained from $\Gamma_n^{(0)}$ once the Z boson mass and couplings are accurately measured [13]. From Table 4.2 we see, as Λ grows from 0.1 to 0.5 GeV, that both the 2S-1S and 1P-1S mass differences increase, and that $\Gamma_1^{(0)}$ grows, whereas the ratios $\Gamma_2^{(0)}/\Gamma_1^{(0)}$ and $\Gamma_3^{(0)}/\Gamma_1^{(0)}$ decrease.

In Figs 4.1, 4.2, 4.3 we show the predictions for m(2S) - m(1S), $\Gamma_1^{(0)}$ and $\Gamma_2^{(0)}/\Gamma_1^{(0)}$ respectively, over a wide range of m(1S) values, that were obtained from our potential with Λ = 0.2 and Λ = 0.4 GeV, together with those we have obtained using the 'Martin' and 'Richardson' potentials, in Chapter 3. It should be noted that the $\psi' - J/\psi$ mass difference shown in Fig 4.1 and the J/ψ and Υ leptonic width data shown in Fig 4.2 were not included in the fits as explained in Chapter 3. Nevertheless, all the potentials give satisfactory descriptions of the $c\bar{c}$ and $b\bar{b}$ data with the exception of the large discrepancy in the Υ leptonic width predicted by the Martin-type potential (see Fig 4.2), although this should not be too worrying as the overall fit to the Martin potential is bad for $b\bar{b}$ as seen in Table 3.2.

For higher mass quarkonium states we see from the figures that the predictions of the different potential models are very clearly distinguished. The Richardson potential predicts a rapid growth

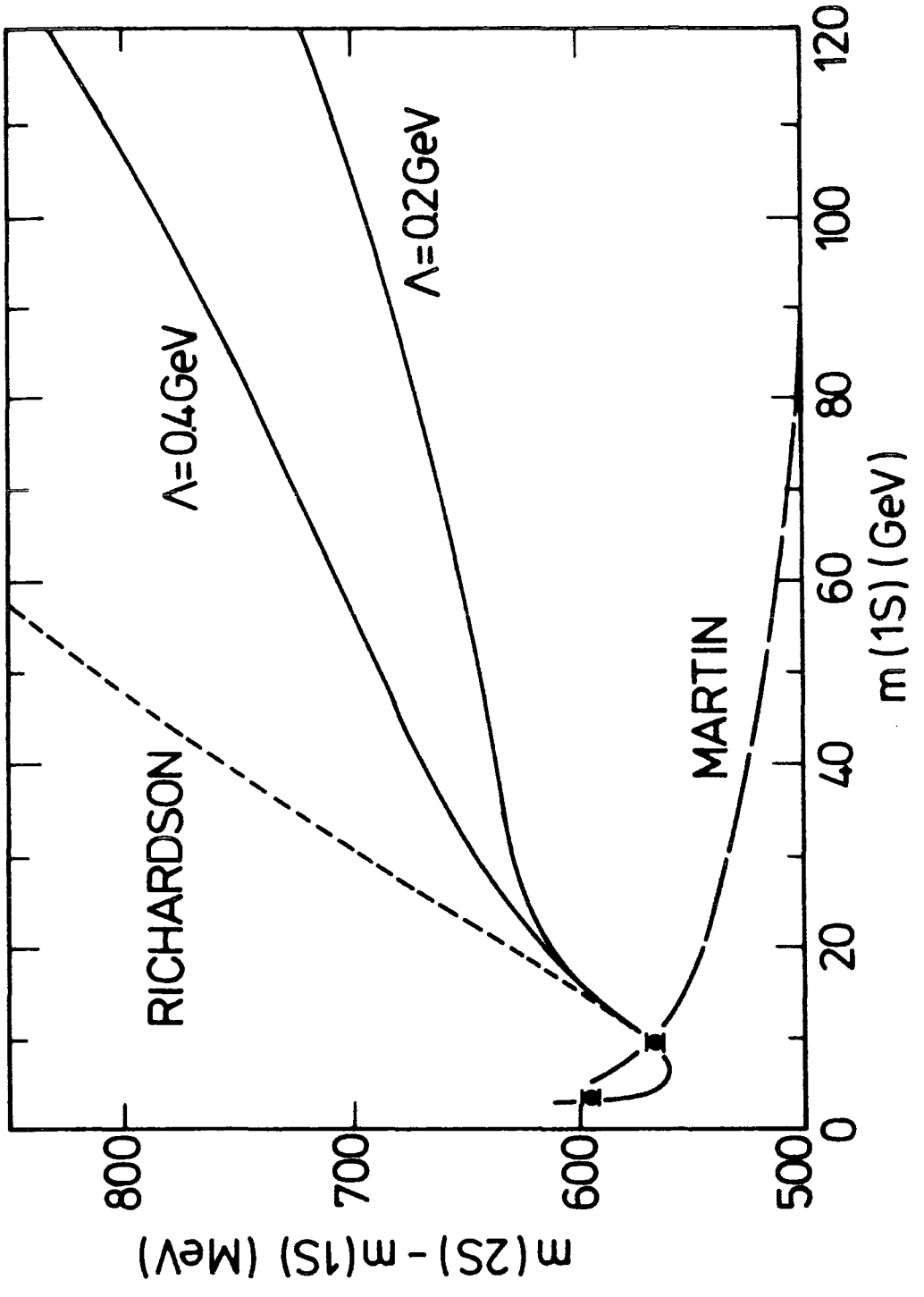

Fig 4.1 : The predictions of the 2S-1S mass difference for $\Lambda = 0.2$ and $\Lambda = 0.4$ GeV (solid lines), compared to that of the Martin and Richardson potentials as a function of the toponium mass. The $\psi' - J/\psi$ and $\Upsilon' - \Upsilon$ mass differences are also shown. The former has not been used in the fit.

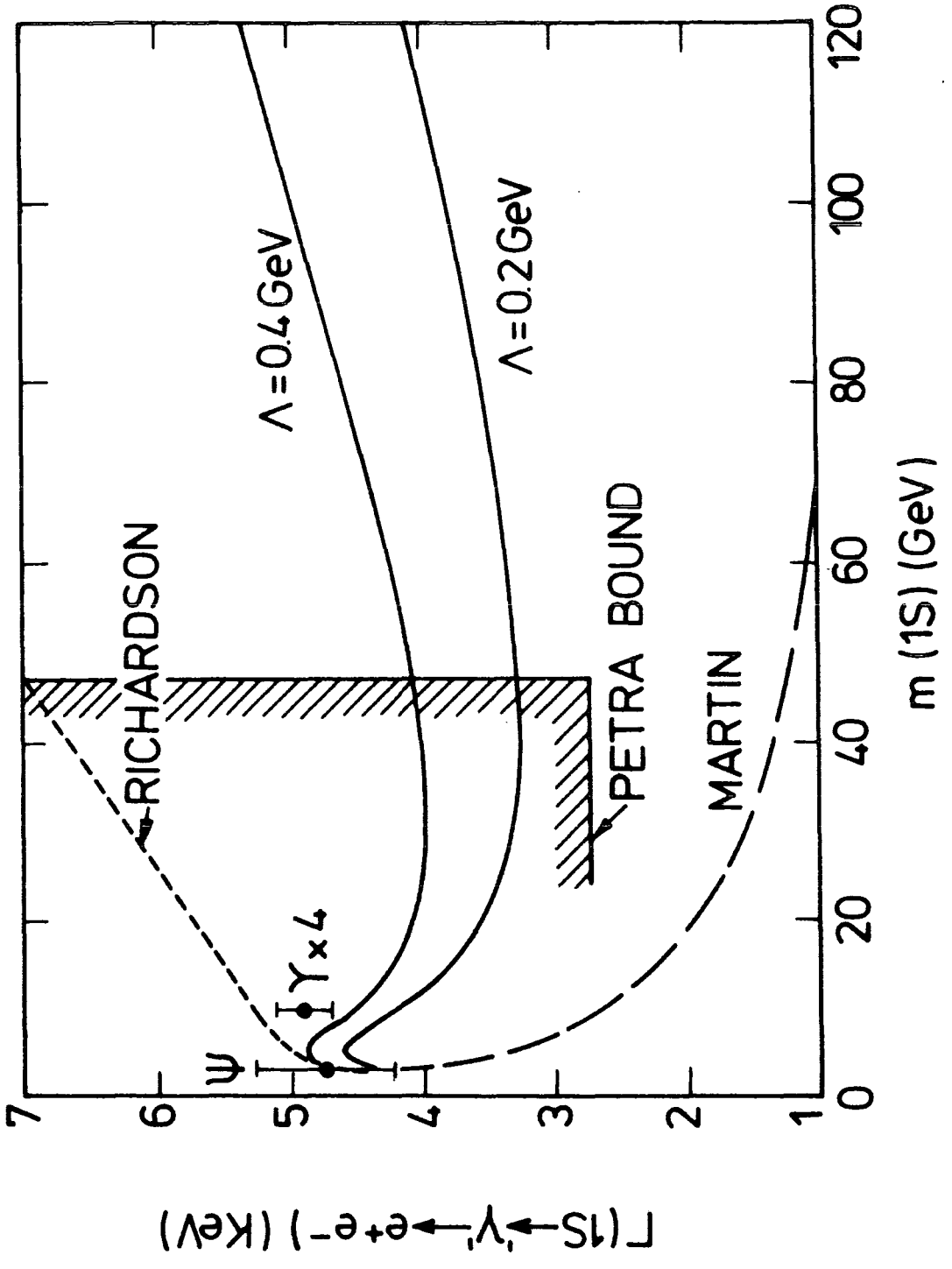

Fig 4.2 : The leptonic width $\Gamma(\theta \to `\gamma' \to e^+e^-)$ as a function of the toponium (θ) mass. Γ_{ee} is given by eq. (4.2); the contribution of the virtual Z is omitted. The observed ψ and Υ leptonic widths are also shown, the latter multiplied by 4. These data have not been used in the fits.

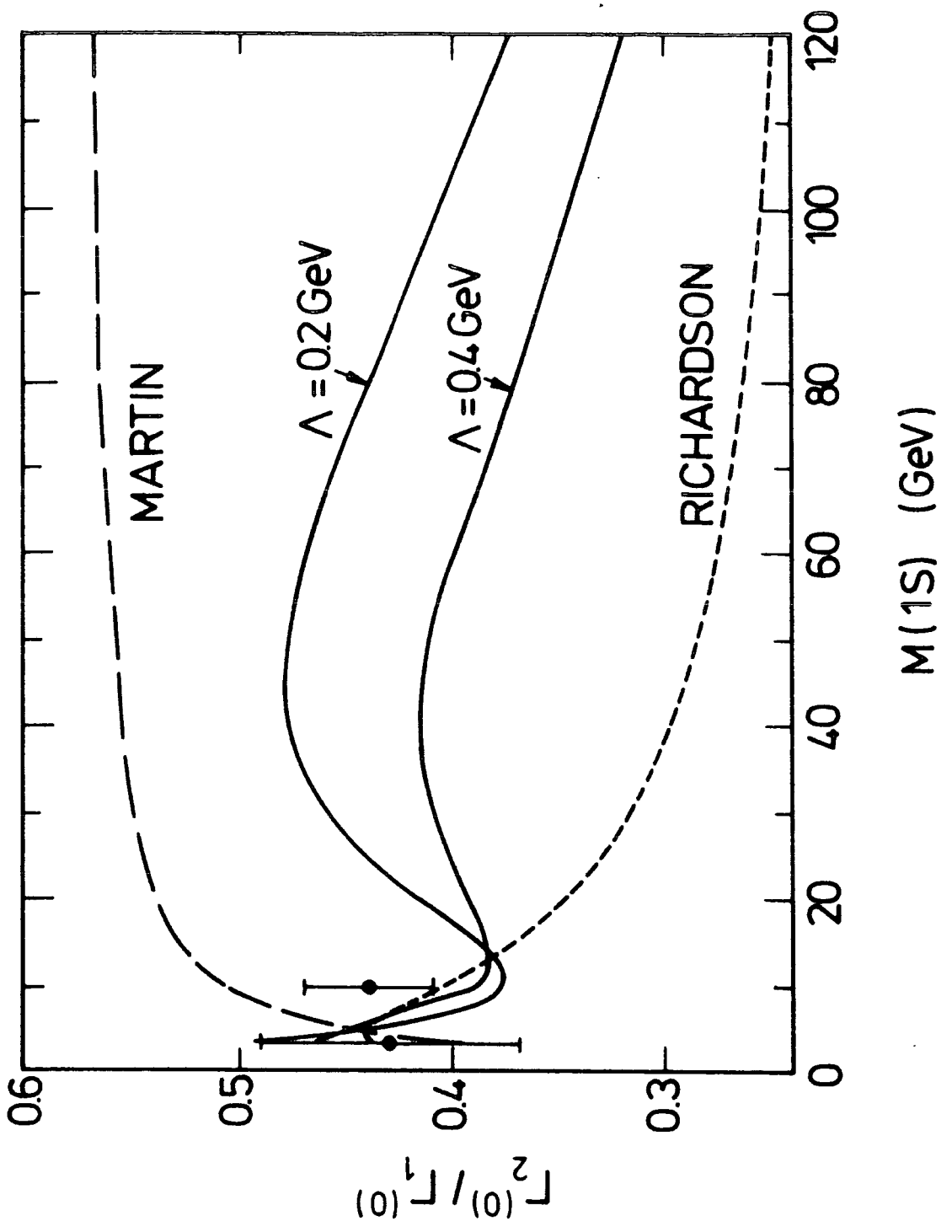

Fig 4.3 : The ratio of the toponium 2S to 1S leptonic widths as a function of the toponium mass; the ratio is expected to be essentially free from uncertainties due to QCD corrections. The ratios obtained from $c\bar{c}$ and $b\bar{b}$ data are also shown.

of the 2S-1S mass difference and of the leptonic width with increasing quarkonium mass, whereas the Martin potential predicts a decrease of these quantities. The potentials whose short distance behaviour is controlled by two-loop perturbative QCD give intermediate predictions, reflecting a milder short-distance behaviour as compared to that of Richardson's potential but more singular than the Martin form (see Fig 3.4).

A further point to notice in the predictions for toponium is that the curves in Fig 4.2 for the leptonic widths include the first order QCD correction factor of $(1 - 16\alpha_s/3\pi)$, in eq. (3.12). This large correction (about 27% for $\Gamma_{ee}(T)$) means the leptonic width predictions may be unreliable. For instance, by simply replacing the corrections factor by the positive-definite term $(1 + 16\alpha_s/3\pi)^{-1}$ makes the $\Lambda = 0.4$ GeV prediction for $\Gamma_1^{(0)}$ agree with the $T \to e^+e^-$ data (see Fig 4.2). Such ambiguities in $\Gamma_i^{(0)}$ are largely cancelled in the ratio of branching fractions shown in Fig 4.3 and so Γ_2/Γ_1 rather than Γ_1 should be used to probe the short distance part of the potential and hence to determine Λ

We consider next the extent to which the prospective toponium measurements will be able to determine the QCD parameter Λ .

4.2 Determination of Λ

Our aim is to determine the constraints imposed on the short distance region of the potential and for this purpose we assume a toponium mass of m(1S) = 80 GeV, and include 'dummy' toponium data in the fit which could be obtained at the forthcoming e^+e^- coiliders. To be precise the toponium 'data' are taken to be the values predicted by our potential, shown in Section 4.1, but with statistical errors

corresponding to those expected to be achieved at LEP, as estimated by the LEP study group [13]. We consider two sets of toponium 'data' to be included in the fits. These are the central values predicted by our $\Lambda = 0.2$ and $\Lambda = 0.4$ GeV potentials given in Table 3.1.

For $\Lambda = 0.2$ GeV we have

$$m(2S) - m(1S) = 670 \pm 20 \text{ MeV} \tag{4.3a}$$

$$\Gamma_2^{(0)}/\Gamma_1^{(0)} = 0.42 \pm 0.06 \tag{4.3b}$$

and for $\Lambda = 0.4$ GeV

$$m(2S) - m(1S) = 746 \pm 20 \text{ MeV} \tag{4.4a}$$

$$\Gamma_2^{(0)}/\Gamma_1^{(0)} = 0.37 \pm 0.06 \ . \tag{4.4b}$$

Here we have taken a 20 MeV error† on the mass difference and a 15% error on the ratio of leptonic widths as anticipated [13] to be relevant to the forthcoming experiments. The absolute measurement of the mass may have a systematic error of about 100 MeV but fortunately this is not relevant to the measurement of the mass difference. To determine Λ we then combine the toponium 'data' of eq. (4.3) and eq. (4.4) with the $c\bar{c}$ and $b\bar{b}$ data listed in Table 3.1, and perform a fit to the combined data as a function of Λ in exactly the same way as explained in Chapter 3, including also a fit to the perturbative potential over its region of validity, (see eq. (3.7)). The top quark mass is fixed in the fit by requiring m(1S) = 80 GeV. The resulting fits due to the inclusion of the toponium 'data' of eq. (4.3) and eq. (4.4), are shown by the dashed curves in Fig 4.4. The solid curve, upon which the dashed curves are superimposed, corresponds to that of Fig 3.3a resulting from a fit to $c\bar{c}$ and $b\bar{b}$ data alone.

---

† The expected experimental accuracy assumes a luminosity of 0.4 pb^{-1} at nine different energies in the resonance region, see Ref [13].

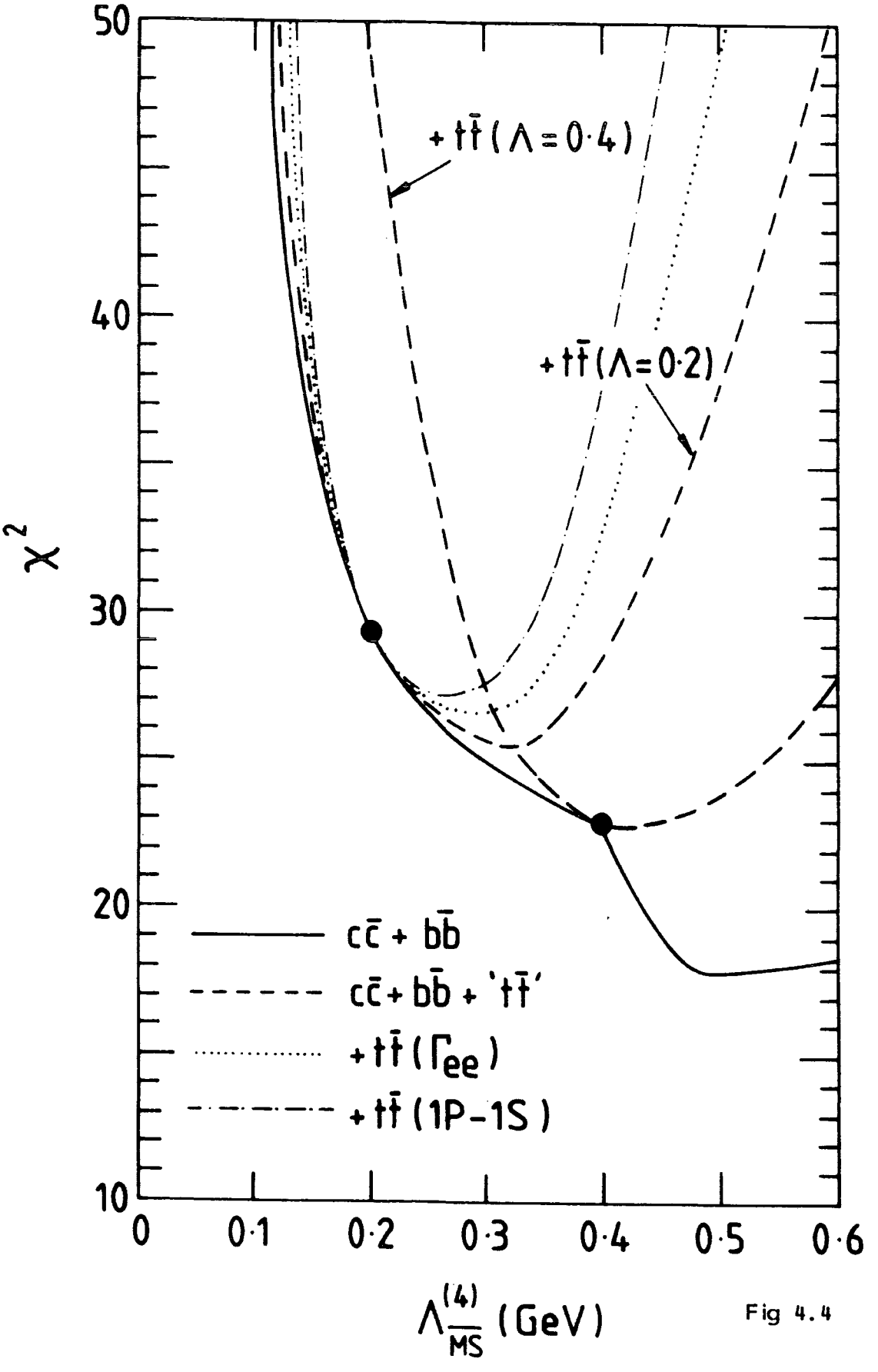
50
40
30
20
10
χ^2
+ $t\bar{t}$ (Λ = 0·4)
+ $t\bar{t}$ (Λ = 0·2)
$c\bar{c}$ + $b\bar{b}$
$c\bar{c}$ + $b\bar{b}$ + '$t\bar{t}$'
+ $t\bar{t}$ (Γ_{ee})
+ $t\bar{t}$ (1P-1S)
0
0·1
0·2
0·3
0·4
0·5
0·6
$\Lambda^{(4)}_{\overline{MS}}$ (GeV)

Fig 4.4

Fig 4.4 : The effect of including toponium 'data' in the fit to determine Λ. The continuous curve is the χ^2 profile obtained by fitting to $c\bar{c}$ and $b\bar{b}$ as presented in Fig 3.3a. The dashed curves show the effect of including the toponium 'data' of either eq. (4.3) or eq. (4.4). These 'data' are the predictions of our Λ = 0.2 and Λ = 0.4 GeV potentials and so give zero additional χ^2 contributions at these values (as indicated by the solid dots). The dotted curve shows the effect of including $\Gamma_1^{(0)}$ = 3.54 ± 0.35 KeV in the fit rather than the ratio of (4.3b). The dot-dashed curve shows the improvement obtained by including, in addition, the 1P-1S mass difference of 548 ± 20 MeV.

We notice that the dashed curves meet the solid curve at $\Lambda = 0.2$ GeV and $\Lambda = 0.4$ GeV, corresponding to the points where the toponium 'data' predictions of eq. (4.3) and eq. (4.4) are made. As noted in Chapter 3, the solid curve in Fig 4.4 has a discontinuity, close to $\Lambda = 0.4$ GeV, due to a switch from one family of solutions to another, by following the contour of lowest values of χ^2 . It is perhaps unfortunate that we have chosen to make a toponium prediction so close to the discontinuity at $\Lambda = 0.4$ GeV, and not in a more continuous part of the curve where only a single family of solutions is present. However, as the two dashed curves are essentially identical we conclude that there is little sensitivity to the change in the family of solutions introduced by passing through the discontinuity. Indeed we found that only a single family of solutions is necessary for the dashed curves, until the χ^2 value becomes very much larger than those at the minima. For these very large values of χ^2 many families of solutions seem to be present and essentially indistinguishable.

If one allows χ^2 values up to $\chi^2_{min} + 3$ then we see that these toponium data should be able to determine $\Lambda \equiv \Lambda^{(4)}_{\overline{MS}}$ to an accuracy of just less than $\pm$ 100 MeV, and we find that it is essentially the mass difference 'data' which determines Λ , while the ratio of leptonic widths gives only a weak constraint on its value. These conclusions can be anticipated from Figs 4.1 and 4.3 due to the fairly large errors in the 'data' of eq. (4.3b) and eq. (4.4b) covering a wide region of predictions. However, the expected accuracy [13] of the 'data' for $\Gamma_1^{(0)}$ is 10% and from Fig 4.2 we see that the width is more sensitive to Λ than the ratio.

Indeed, if instead of using the ratio of leptonic widths we use the absolute value $\Gamma_1^{(0)}$ with this error in the fit, and the mass difference, and if the prediction eq. (3.12) can be taken at face value, then the χ^2 versus Λ profile is shown by the dotted curve in Fig 4.4 and we see Λ is determined to within ± 85 MeV using the above criterion. However from eq. (3.12) we note that the first-order QCD corrections to the leptonic width are $-16\alpha_s/3\pi$ relative to unity and so we can expect higher-order corrections of order $(16\alpha_s/3\pi)^2$ which at the scale of toponium mass are of the order 4%. It is clearly important to reduce the theoretical uncertainty in eq. (3.12) so that the measurement of $\Gamma_1^{(0)}$ can be reliably incorporated into the fit and hence the determination of Λ can be improved.

We also studied the possible improvement in the determination of Λ if the 1P toponium state was observed, for example via,

$$2S \rightarrow 1P + \gamma \rightarrow 1S + \gamma + \gamma \qquad (4.5)$$

Fitting now to the 2S-1S and 1P-1S mass differences both with an error of ± 20 MeV and to the absolute leptonic width $\Gamma_1^{(0)}$ results in a χ^2 versus Λ profile shown by the dot-dashed curve in Fig 4.4, and leading to a determination of Λ to within about ± 75 MeV. Summarising these results for toponium data at Λ = 0.2 we have

$$c\bar{c} + b\bar{b} + t\bar{t}(1) - \Lambda \pm 100 \text{ MeV} \qquad (4.6a)$$
$$c\bar{c} + b\bar{b} + t\bar{t}(2) - \Lambda \pm 85 \text{ MeV} \qquad (4.6b)$$
$$c\bar{c} + b\bar{b} + t\bar{t}(3) - \Lambda \pm 75 \text{ MeV} \qquad (4.6c)$$

where $t\bar{t}$ data set 1 contains 2S-1S, $\Gamma_2^{(0)}/\Gamma_1^{(0)}$,
$t\bar{t}$ data set 2 contains 2S-1S, $\Gamma_1^{(0)}$,
$t\bar{t}$ data set 3 contains 2S-1S, 1P-1S, $\Gamma_1^{(0)}$.

We studied the dependence of our determination of Λ to relativistic corrections by repeating the above procedure of fits omitting $c\bar{c}$ data. We include additional toponium 'data', predicted from the Λ = 0.2 GeV best fit potential to $b\bar{b}$ data alone of Table 3.1, and

fit to only $b\bar{b}$ and $t\bar{t}$ 'data'. The $t\bar{t}$ 'data' used in the fits are:

$$m_{2S} - m_{1S} = 669 \pm 20 \quad \text{MeV} \tag{4.7a}$$

$$\Gamma_2^{(0)}/\Gamma_1^{(0)} = 0.44 \pm 0.07 \tag{4.7b}$$

$$\Gamma_1^{(0)} = 3.44 \pm 0.34 \tag{4.7c}$$

$$m_{1P} - m_{1S} = 542 \pm 20 \quad \text{MeV} \tag{4.7d}$$

The results of these fits are shown in Fig 4.5 and are found to give almost identical results to those of eqs. (4.6), indicating that such corrections are small. The $t\bar{t}$ 'data' curves in Fig 4.5 are superimposed on that of Fig 3.3b, which corresponds to the fit to $b\bar{b}$ data alone.

We have also checked to see whether the determination of Λ is biased by the parametric form used in the intermediate part of the potential. First we fitted the data of eq. (4.6a) by adding one more parameter c_3, into eq. (3.14) and found essentially the same χ^2 versus Λ profile as that shown in Fig 4.4. Next we studied the effect of including an overall constant term V_o in the potential. Repeating the fit to $c\bar{c}$ and $b\bar{b}$ data with V_o, we make $t\bar{t}$ predictions from the optimum fit. We then repeat this analysis changing the long distance confining potential from the linear form $V_L = ar$ to the form $V_L = a\sqrt{r}$. The results are summarised in Table 4.3 which shows four different fits to the $c\bar{c}$ and $b\bar{b}$ data using the two different forms of V_L. We see that the $t\bar{t}$ predictions are dependent on the choice of parametrization to varying extents. Firstly we notice from the value of χ_V^2 that a quarkonium potential with a square root confining part is unable to adequately approximate to the perturbative form in the short distance region, although including a constant term V_o does make a significant improvement.

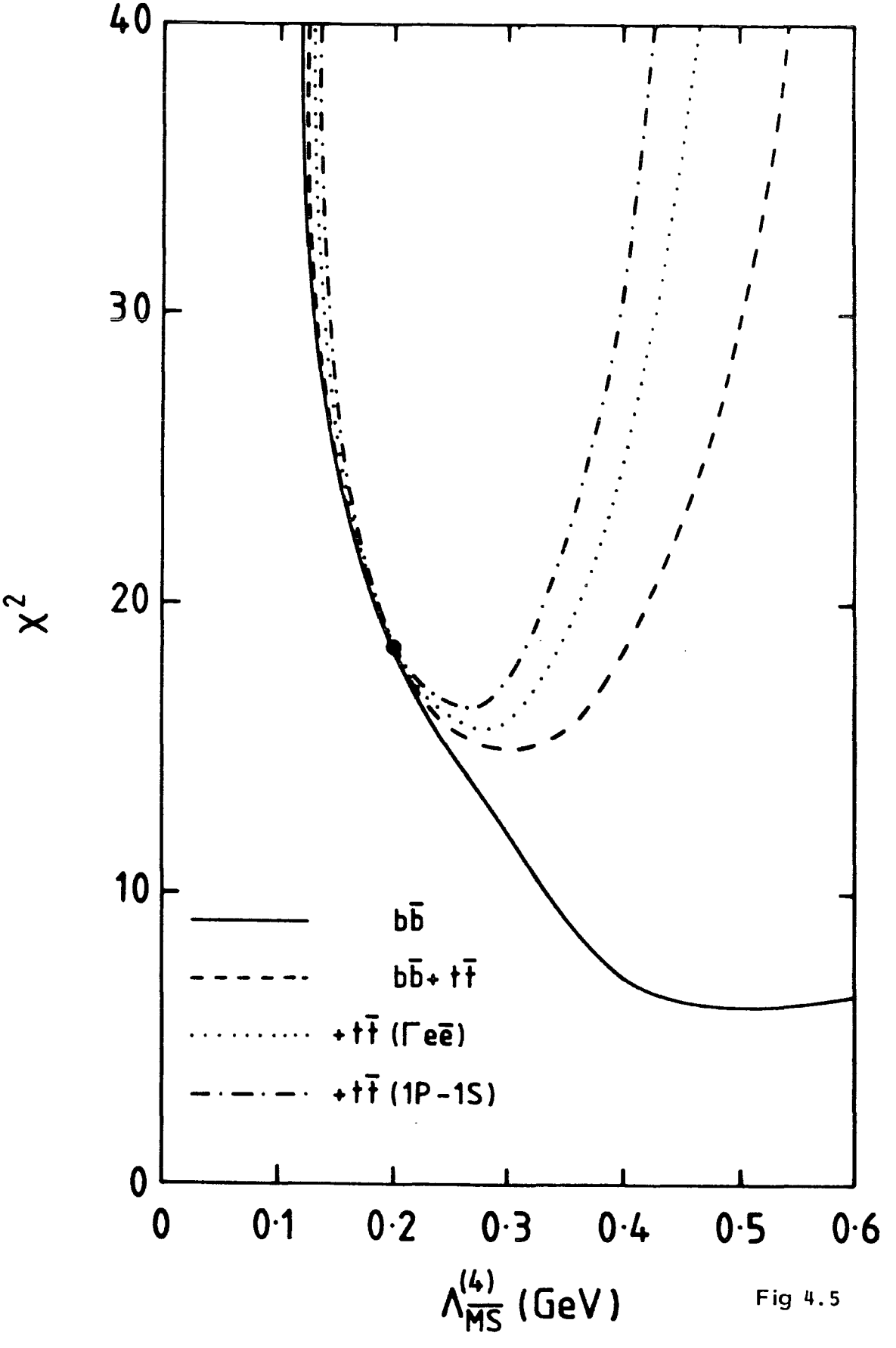
40
30
20
10
0
χ^2
0
0·1
0·2
0·3
0·4
0·5
0·6
$\Lambda^{(4)}_{\overline{MS}}$ (GeV)
$b\bar{b}$
$b\bar{b}+t\bar{t}$
$+t\bar{t}$ ($\Gamma e\bar{e}$)
$+t\bar{t}$ (1P-1S)

Fig 4.5

Fig 4.5 : The effect of including toponium 'data' in the fit to determine Λ and at the same time omitting any relativisitic dependence by fitting only to $b\bar{b}$ and $t\bar{t}$ 'data'. The continuous curve is the χ^2 profile obtained by fitting to $b\bar{b}$ data alone as presented in Fig 3.3b. The dashed curve shows the effect of including the toponium 'data' of eq. (4.7a) and eq. (4.7b), the dotted curve includes the 'data' of eq. (4.7a) and eq. (4.7c) while the dot-dashed includes the 'data' of eqs. (4.7a), (4.7c) and (4.7d). All 'data' values are predictions from the Λ = 0.2 GeV potential for $b\bar{b}$ data alone.

V_L	a GeV units	V_o GeV	χ^2_{data}	χ^2_V	Mass diff. (MeV)		$\Gamma_1^{(0)}$ keV	$\frac{\Gamma_2^{(0)}}{\Gamma_1^{(0)}}$
					2S-1S	1P-1S		
ar	0.22	-	27.8	1.7	670	548	3.54	0.42
ar	0.18	0.22	21.1	2.2	692	548	3.26	0.46
$a\sqrt{r}$	0.65	-	12.6	25.7	880	725	4.64	0.36
$a\sqrt{r}$	0.65	-0.22	14.8	9.6	780	646	4.27	0.38

Table 4.3 : **Fits to the $c\bar{c}$ and $b\bar{b}$ data and the perturbative potential for $\Lambda = 0.2$ GeV using two different forms of the confining potential V_L, in each case for $V_o = 0$ and for the value of V_o which gives the optimum fit. The other parameters (a, c_1, c_2, r_o, m_c, m_b) are also varied to their optimum values. The predictions for the mass differences and leptonic widths of the low lying toponium levels are also shown for m(1S) = 80 GeV.**

The reason is that a confining term $V_L = a\sqrt{r}$ gives an appreciable contribution to the intermediate and short distance regions with the consequence that the low lying toponium levels are very sensitive to the introduction of V_o. Indeed we conclude that toponium data could not reliably determine Λ if the quarkonium potential incorporates a $V_L = a\sqrt{r}$ component.

We believe that the linear confining form $V_L = ar$ is appropriate, not only because it has less influence on the short distance and intermediate form of the potential, but also because it is consistent with the expectations of the string model, which we derived in the Section 3.5. We also note that there is much less sensitivity to the introduction of V_o if the linear confining term is used. Repeating the combined fit to the data of eq. (4.6a) shown as the dashed curve of Fig 4.4 for $V_o = 0$, but now leaving V_o as a free parameter we found very similar χ^2 profiles with minima at the same values of Λ We conclude the determination of Λ is not influenced by the parametric form of the intermediate potential or whether V_o is included provided long distance linear confinement $V_L = ar$ is used.

CHAPTER 5

Quarkonium Decays

In the previous chapters we have analysed how QCD constrains the quarkonium potential in its short-distance regime, and by fitting to the available $c\bar{c}$ and $b\bar{b}$ data, as well as demanding the perturbative form, we obtained satisfactory potentials for a variety of values of $\Lambda \equiv \Lambda^{(4)}_{\overline{MS}}$. We also discussed how toponium data, when eventually available, will be able to distinguish between the wide variety of phenomenologically successful potentials and should indeed be able to determine the value of Λ , due to the enormous variety of predictions made for physically measurable quantities of a heavy quarkonium system. However, all potentials considered, produce essentially equally good fits to the $c\bar{c}$ and $b\bar{b}$ data and, as can be seen in Fig 3.4, have a common slope in the region $0.5 < r < 5\ \text{GeV}^{-1}$. We should therefore expect that predictions made for physical quantities in the $c\bar{c}$ and $b\bar{b}$ system should be reasonably independent of the potential and compare favourably against experiment. Specifically in this Chapter, we discuss hadronic decay widths of S and P wave states in the $c\bar{c}$ and $b\bar{b}$ spectrum in the light of recent measurements. Predictions for these quantities were among the earliest made for QCD [47, 48] however, for several of the states no accurate experimental evidence has been available to test them, until recently.

5.1 Charmonium S-Wave Decays

We shall consider the lowest S wave multiplet of charmonium (ψ, η_c) and the production of non-charmed hadrons as a result of their decay.

The decay, $\psi \rightarrow$ hadrons, has been carefully studied and agrees well with experimental values for $\alpha_s \simeq 0.2$. The mechanism proposed in QCD for such a decay is depicted in Fig 1.5a where the $c\bar{c}$ pair first annihilate to produce gluons, the gluons then produce light quarks and antiquarks which in turn fragment into the familiar hadrons. The decay must proceed in this way as it is energetically impossible for these low lying bound states of $c\bar{c}$ to form charmed mesons by the creation of a light $q\bar{q}$ pair.

If the coupling constant α_s is small then lowest order perturbation theory should suffice. In this approximation it is supposed that the gluons are quasi-free, i.e. that no three gluon vertices are present, then the ψ decays into three gluons while the singlet, η_c decays into two. The decay widths are [48]

$$\Gamma(\psi \rightarrow 3g) = \frac{40}{81\pi}(\pi^2 - 9)\frac{\alpha_s^3}{M^2}\left|R_s(0)\right|^2 \qquad (5.1)$$

$$\Gamma(\eta_c \rightarrow 2g) = \frac{8}{3}\frac{\alpha_s^2}{M^2}\left|R_s(0)\right|^2 \qquad (5.2)$$

Where $R_s(0)$ is the value of the radial wavefunction at the origin and M is the mass of the state in each case. The wave-function dependence of these equations can be cancelled by expressing one width in terms of the other

$$\Gamma(\eta_c \rightarrow 2g) \simeq 97.5\ (\frac{0.2}{\alpha_s})\ \Gamma(\psi \rightarrow 3g) \qquad (5.3)$$

The ψ width [49] is about 45 KeV and for $\alpha_s \simeq 0.2$, we have reasonable agreement with the Crystal Ball value [50] of $\Gamma(\eta_c \rightarrow$ all) = 11.5 (+4.5,-4.0) MeV. In writing eq. (5.3) possible wavefunction distortion due to initial gluon exchanges as well as relativistic corrections cancel.

However, by calculating these wavefunctions using the potentials discussed in earlier chapters, these effects can be investigated. In Table 5.1 we list the resulting numerical solutions for the wave-function at the origin for a variety of potentials, and in Fig 5.1 we show the pseudoscalar, η_c hadronic width in lowest order as a function of α_s from eq. (5.2). We observe that a choice of $\alpha_s \simeq 0.2$ accounts for the experimental width, although the uncertainty is large. Values of $\alpha_s \simeq 0.2$ are also consistent with those obtained [51] from three-gluon jet and deep inelastic analyses as well as seen in the perturbative potential of Chapter 2. Predictions from all the potentials are fairly similar and our first conclusion is that from a phenomenological standpoint the lowest-order result describing hadronic decays of charmonium S waves is satisfactory, at least within a factor of 2. Wavefunction distortion, relativistic wave-function corrections and ultraviolet renormalisation effects do not seem to be large. However, a quite different result is found for P wave charmonium decays.

5.2 Charmonium P-Wave Decays

Due to hyperfine splitting the 1P level of charmonium is composed of the 3 levels. χ_J with J = 0,1,2 shown in Fig 1.6a. We consider the states χ_0, χ_2 which to first order both decay into two gluons. The widths are given by [48, 59].

$$\Gamma(\chi_2 \to 2g) = \frac{128}{5} \frac{\alpha_s^2}{M^4} \left| R_p'(0) \right|^2 \qquad (5.4)$$

$$\Gamma(\chi_0 \to 2g) = \frac{15}{4} \Gamma(\chi_2 \to 2g) \qquad (5.5)$$

where $R_p'(0)$ is the derivative of the P wave radial wavefunction at the origin. In eq. (5.5), the wavefunctions and their distortions cancel out, and including one loop corrections, eq.(5.5) becomes [52]

Potential	Λ=0.2	Λ=0.4	Martin	Richardson
Charm				
$\lvert R_S(0)\rvert^2$ (GeV^3)	0.698	0.90	0.88	0.857
$\lvert R'_P(0)\rvert^2$ (Gev^5)	0.065	0.092	0.11	0.081
$\langle R_S \lvert r \rvert R_P\rangle^2$(GeV^5)	4.844	4.172	3.76	4.385
Bottom				
$\lvert R_S(0)\rvert^2$ (GeV^3)	5.447	6.273	3.99	7.267
$\lvert R'_P(0)\rvert^2$ (GeV^5)	1.511	1.665	1.34	1.652
$\langle R_S \lvert r \rvert R_P\rangle^2$(GeV^5)	1.24	1.177	1.37	1.167

Table 5.1 : Square of the S-wave and derivative of the P-wave radial wave-function at the origin along with transition matrix elements for $\chi_2 \rightarrow (1S)\gamma$. The wave-functions are computed using the potentials in Chapter 3 with parameters chosen according to the best fit to the spin-averaged data.

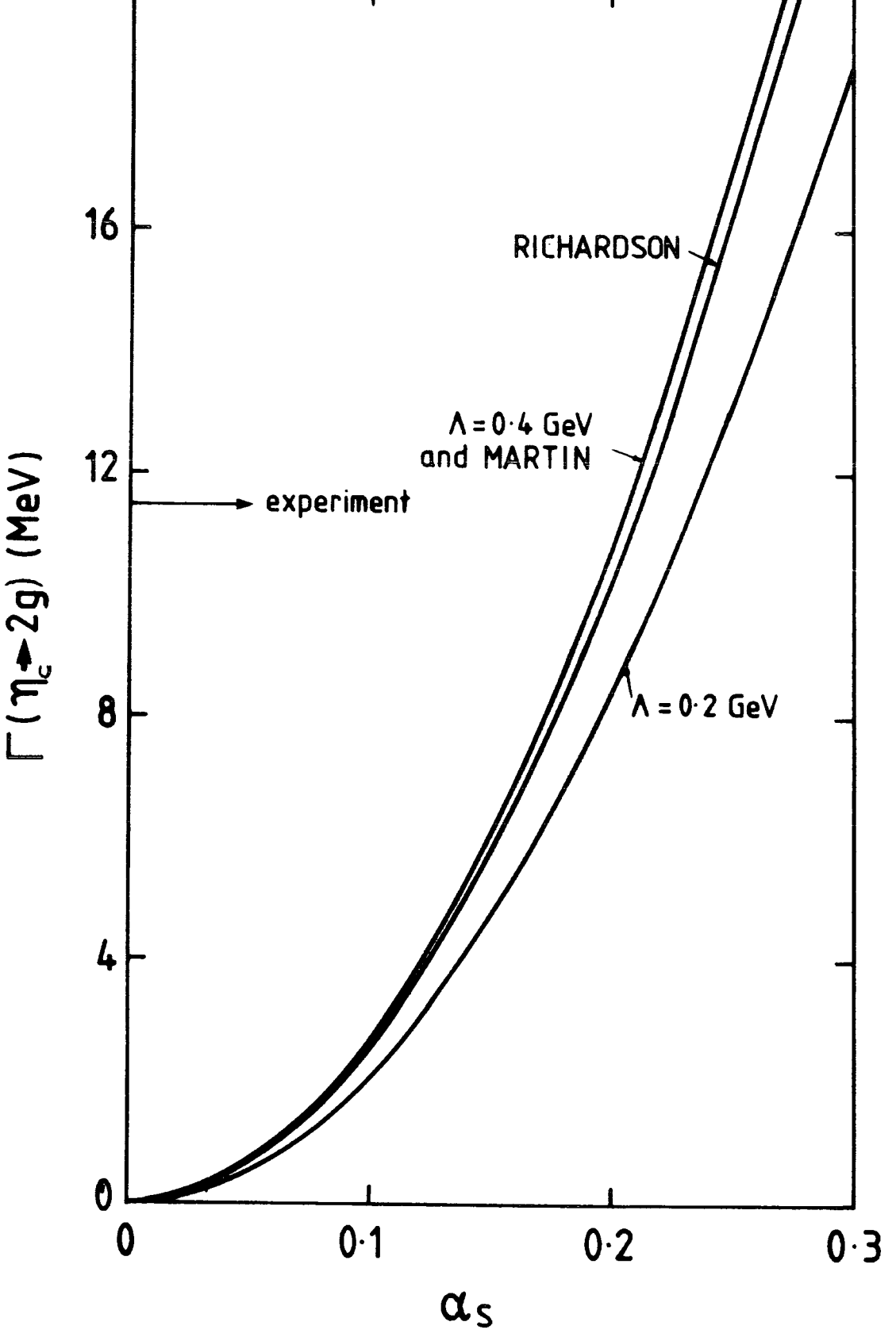

Fig 5.1 : Predictions for the hadronic width of the pseudoscalar as a function of α_s , for several phenomenologically successful potentials. The experimental width is accounted for with values of $\alpha_s \simeq 0.2$.

$$\frac{\Gamma(\chi_0 \to 2g)}{\Gamma(\chi_2 \to 2g)} = \frac{15}{4}\left[1 + \frac{12\alpha_s}{\pi}\right] \simeq 6.6 \qquad (5.6)$$

with $\alpha_s = 0.2$. This ratio can be determined from experimental data with the minimum of theoretical assumptions

$$\frac{\Gamma(\chi_0 \to 2g)}{\Gamma(\chi_2 \to 2g)} \simeq \frac{\Gamma(\chi_0 \to \psi\gamma)}{\Gamma(\chi_2 \to \psi\gamma)} \frac{B(\chi_2 \to \psi\gamma)}{B(\chi_0 \to \psi\gamma)} \frac{1 - B(\chi_0 \to \psi\gamma)}{1 - B(\chi_2 \to \psi\gamma)} \qquad (5.7)$$

The ratio of radiative widths should be [53] nearly the ratio of phase space factors [54] and taking the branching fractions from the Particle Data Group [37] we obtain

$$\frac{\Gamma(\chi_0 \to 2g)}{\Gamma(\chi_2 \to 2g)} \simeq 7.2 \begin{matrix} +3.6 \\ -1.8 \end{matrix} \qquad (5.8)$$

agreeing well with eq. (5.6). Considering the separate p-wave decay rates of eq. (5.4) and eq. (5.5) we show in Fig 5.2 predictions for the lowest order χ_2 hadronic width, using values taken from Table 5.1, as a function of α_s.

There is now considerable experimental evidence for a very broad χ_2. Firstly, from the Crystal Ball [55] radiative decay analysis

$$\Gamma(\chi_2 \to \text{all}) = 2.7 \pm 1.0 \quad \text{MeV} \qquad (5.9)$$

under the assumption that $\Gamma_{tot}(\chi_1) < 0.5$ MeV. Also from the CERN ISR formation experiment [56], (which used an antiproton beam incident on a gas-jet target) a value

$$\Gamma(\chi_2 \to \text{all}) \simeq 3 \quad \text{MeV} \qquad (5.10)$$

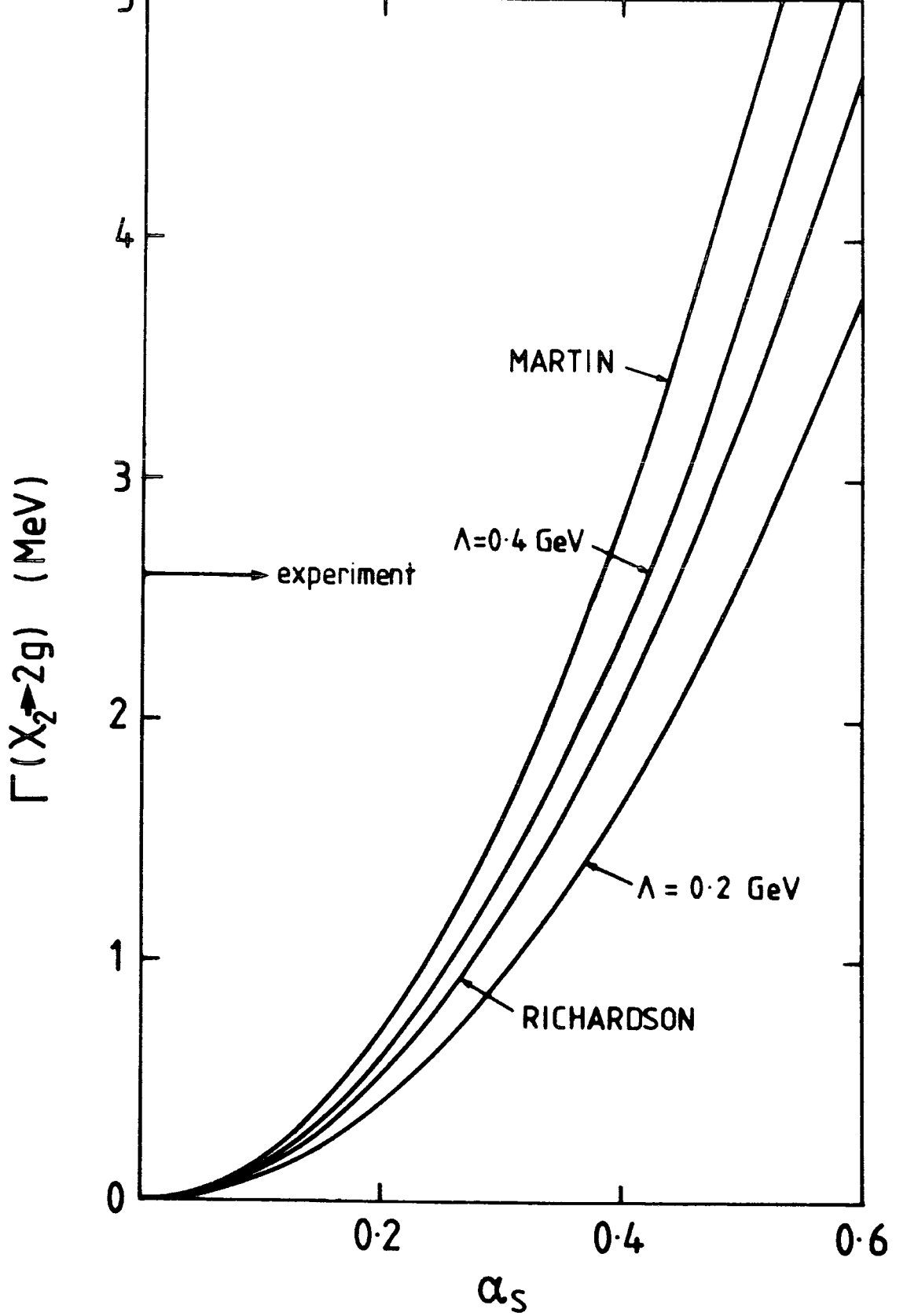

Fig 5.2 : Predictions for the hadronic width of the χ_2 state, as a function of α_s . It is seen that only large $\alpha_s \simeq 0.5$ can possibly account for the large experimental width. More realistic values of $\alpha_s \simeq 0.2$ predict the width to be an order of magnitude smaller than the experimental value.

was directly measured. Finally the branching fraction $B(\chi_2 \to \psi\gamma)$ $= 0.155 \pm 0.018$ together with the computed radiative width[†] $\Gamma(\chi_2 \to \psi\gamma) \simeq 0.59 \pm 0.06$ MeV yield the value

$$\Gamma(\chi_2 \to \text{all}) = 3.8 \pm 0.8 \quad \text{MeV} \tag{5.11}$$

Subtracting the computed radiative width from these determinations [eqs. (5.9), (5.10) and (5.11)] gives the hadronic width

$$\Gamma(\chi_2 \to 2g) \simeq 2.6 \quad \text{MeV} \tag{5.12}$$

Then from Fig 5.2, we observe that only a very large $\alpha_s \simeq 0.5$ could possibly account for the large experimental χ_2 width and that more realistic values of $\alpha_s \simeq 0.2$ predict the width to be an order of magnitude smaller than the experimental value.

The effect of radiative one-loop corrections is to reduce the χ_2 width [57] and cannot explain this discrepancy. Moreover, since the ratio $\Gamma(\chi_0 \to 2g)/\Gamma(\chi_2 \to 2g)$ comes out nearly correct we can infer that there is no special enhancement of the χ_2 width due to interference with possible nearby 2^{++} glueball states etc.

Because of the ratio of χ_0 to χ_2 widths is correctly predicted whereas individual rates are poorly predicted, we are lead to the conclusion that a distortion, or relativistic effect, in the wavefunction is involved

---

[†] The estimate of the radiative width comes from the potentials shown in Table 5.1, where the average value is taken for the four potentials and the uncertainty is reflected in the number quoted for $\Gamma(\chi_2 \to \text{all})$. Relativisitic corrections are expected to be small in calculating this transition rate [53] since both the wavefunctions have no nodes.

Before trying to estimate these effects we consider how well the equivalent quantities in the bottomonium spectrum are predicted using the values in Table 5.1.

5.3 Bottomonium P-Wave Decays

We expect that at least relativistic corrections in the $b\bar{b}$ spectrum should be fairly small and that the lowest-order decay widths, eq. (5.4) and eq. (5.5), should be a reasonable approximation. The observed [37] branching ratio of χ_2 is $B(\chi_2 \to T\gamma) = 0.200 \pm 0.044$. Now, reliable theorietical predictions for the radiative decay widths can be obtained by inserting the matrix elements of Table 5.1 into the expression

$$\Gamma(\chi_2 \to (1S)\gamma) = \frac{4\alpha k^3 e_q^2}{9} \langle R_s | r | R_p \rangle^2 \qquad (5.13)$$

where $e_q = -1/3$, is the charge of the quark and k is the photon energy, which neglecting recoil of the 1S state in the decay, is taken as the mass difference between the two states, i.e. k = 455 MeV [37]. Eq. (5.13) then yields $\Gamma(\chi_2 \to T\gamma) = 42 \pm 3$ KeV from which we obtain

$$\Gamma(\chi_2 \to \text{all}) = 210 \pm 50 \text{ keV} \qquad (5.14)$$

subtracting the radiative width gives

$$\Gamma(\chi_2 \to 2g) = 168 \pm 50 \text{ keV} \qquad (5.15)$$

Using the lowest order theoretical predictions for this decay eq. (5.4) and the $\alpha_s = 0.2$, we obtain

$$\Gamma(\chi_2 \to 2g) = \begin{cases} 160 \text{ keV} & (\Lambda=0.2) \\ 176 \text{ keV} & (\Lambda=0.4) \\ 142 \text{ keV} & (\text{Martin}) \\ 175 \text{ keV} & (\text{Richardson}) \end{cases} \qquad (5.16)$$

We see that agreement between (5.15) and (5.16) is quite satisfactory showing that the corrections are indeed small in $b\bar{b}$.

As only the triplet $^3S_1(\Upsilon)$ of the S-wave multiplet in $b\bar{b}$ has been observed, the equation for the pseudoscalar component, η_b, hadronic width eq. (5.2) cannot be tested, although values of $\alpha_s \simeq 0.2$ give good agreement with the triplet three-gluon width of eq. (5.1).

5.4 Branching Ratio Predictions

An alternative way of presenting the χ_2 decay results in charmonium and bottomonium is by a calculation of the observed branching ratios. By doing so we directly compare an experimental value to a quantity depending on the wavefunctions and the strong coupling constant. We express the branching ratio in terms of the radiative decay rate and the decay into 2 gluons

$$B(\chi_2 \to (1S)\gamma) = \frac{\Gamma(\chi_2 \to (1S)\gamma)}{\Gamma(\chi_2 \to (1S)\gamma) + \Gamma(\chi_2 \to 2g)} \qquad (5.17)$$

and use eq. (5.4) and eq. (5.13). To obtain the theoretical prediction we average over the predictions for each potential and take $\alpha_s = 0.2$. We then compare with the value measured for charmonium;

$$\begin{aligned} B(\chi_2 \to \psi\gamma) &= 0.155 \pm 0.018 \quad \text{(experiment)} \\ &\quad 0.52 \pm 0.08 \quad (\text{theory}, \alpha_s = 0.2) \end{aligned} \qquad (5.18)$$

In order to obtain the experimental branching ratio α_s must be taken to be approximately $\alpha_s \simeq 0.5$.

Comparing eq. (5.17) with the value measured for bottomonium, again using $\alpha_s = 0.2$, we obtain

$$\begin{aligned} B(\chi_2 \to \Upsilon\gamma) &= 0.200 \quad 0.044 \quad \text{(experiment)} \\ &\quad 0.206 \quad 0.030 \quad (\text{theory}, \alpha_s = 0.2) \end{aligned} \qquad (5.19)$$

We see here a striking agreement for radiation from the b quark.

We have thus observed that the $\chi_2 \to gg$ decay rates of eq. (5.4) seem to be correctly predicted in the lowest order for a variety of quarkonium potentials if the quarks are very heavy or, in the case of charm, if ratios like χ_0/χ_2 are considered. However, the individual charmed χ_2 decay into two gluons is considerably underestimated, and we are led to conclude that the problem probably lies in corrections of the charmonium wavefunction.

5.5 Wavefunction Corrections

These effects can be considered to be of two types, distortion and relativistic corrections. Wavefunction distortion effects are seen to arise in the complete one-loop-correction result [58] for the χ_2 width where a gluon exchange between the initial c and $\bar{c}$ quarks contributes a large term proportional to the inverse of the quark velocity. Such terms cancel in the ratio $\Gamma(\chi_0)/\Gamma(\chi_2)$, although for the individual widths it is believed that they factorise into the wavefunction normalisation causing changes in the wavefunction.

Relativistic corrections are of two types, spin-dependent resulting in a splitting of the degeneracy in a level, and spin-independent, due to a truncation of the full relativistic Hamiltonian to a non-relativistic form. We shall consider an estimate of these spin-independent corrections. The full Hamiltonian can be written as:

$$f(-\nabla^2)\Psi + V(r)\Psi = M\Psi \tag{5.20}$$

where **relativistically** : $f(-\nabla^2) = 2(-\nabla^2 + m^2)^{\frac{1}{2}}$ (5.21)

non-relativistically: $f(-\nabla^2) = \frac{-\nabla^2}{m} + 2m$ (5.22)

and m is the quark mass. A next-to-leading order expansion of (5.12a) yields

$$f(-\nabla^2) \simeq 2m - \frac{\nabla^2}{m} - \frac{1}{4m}\left(\frac{\nabla^2}{m}\right)^2 \quad \ldots\ldots \tag{5.23}$$

and an estimate of the error in truncating (5.23) to the first term in ∇^2 , is obtained by considering the parameter

$$d = \frac{1}{4m} \frac{\langle (E_{NR} - V(r))^2 \rangle}{\langle E_{NR} - V(r) \rangle} \tag{5.24}$$

where

$$\frac{-\nabla^2}{m} = E_{NR} - V(r) \tag{5.25}$$

The parameter d, depends inversely on the quark mass and we should expect smaller values for heavy systems. In Table 5.2 we show this parameter for a variety of states and as expected only charmonium states should have some relativistic dependence. In an effort to make a quantitative estimate of this effect on the S and P wave functions at the origin we notice that in eq. (5.23) if we include the next-to-leading order term, then we can still use the non-relativistic treatment provided that the quarkonium potential is replaced by the effective potential

$$V_{eff(r)} = V(r) - \frac{(E_{NR} - V(r))^2}{4m_q} \tag{5.26}$$

where E_{NR} is the binding energy of the non-relativistic treatment. Using this effective potential, where V(r) is our quarkonium potential with $\Lambda = 0.2$ and 0.4 GeV, we predict the values of the square of the S-wave and the derivative of the P-wave radial wavefunctions at the origin that are shown in Table 5.3. For $c\bar{c}$, we see that the value of $|R_s(0)|^2$ is increased by about 45% which is still consistent with a value of $\alpha_s \simeq 0.2$ needed in eq. (5.2) to agree with the experimental value. Also $|R'_p(0)|^2$ is increased by 60% offering some hope of improving the agreement between the calculated rate of eq. (5.4) and the experimental value eq. (5.12) for reasonable values of α_s .

State		Expansion Parameter
cc	1S	0.135
	1P	0.102
bb	1S	0.057
	1P	0.028
tt	1S	0.020
	1P	0.005

Table 5.2 : **The relativistic expansion parameter, d, for the lowest S- and P-wave states of heavy quarkonium systems (m_t = 40 GeV). The appropriate value of d, defined in eq. (5.24), is obtained by averaging over the predictions using several different phenomenologically successful potentials.**

Potential	Λ=0.2	Λ=0.4
Charm		
$\lvert R_S(0)\rvert^2$ (GeV^3)	1.02	1.286
$\lvert R'_P(0)\rvert^2$ (GeV^5)	0.106	0.144
Bottom		
$\lvert R_S(0)\rvert^2$ (GeV^3)	6.265	7.355
$\lvert R'_P(0)\rvert^2$ (GeV^5)	1.806	1.991

Table 5.3 : **Square of the S-wave and derivative of the P-wave radial wave-function at the origin using the effective potential eq. (5.26) where V(r) is that of eq. (3.2), with Λ = 0.2 and 0.4 GeV. These values are to be compared with those in the first two columns of Table 5.1.**

In $b\bar{b}$, $|R_s(0)|^2$ and $|R'_p(0)|^2$ are increased only by 16% and 19% respectively which, as expected, are a lot smaller than for $c\bar{c}$ and leave our conclusions unchanged.

CHAPTER 6

Summary and Conclusions

The aim of this work has been to consider the extent to which the presently known, and future, heavy quarkonium spectroscopies test the perturbative QCD prediction for the interquark potential, and specifically to determine constraints imposed by the data on the value of the QCD scale parameter, Λ.

The procedure has been to develop a quarkonium potential which in the short-distance region is constrained by the perturbative behaviour (consistent with the asymptotically free property of QCD), which has long distance linear confinement and which has a flexible form at intermediate distances. Then by fitting to the quarkonia data for various fixed values of Λ, and comparing the resultant potential with that expected from perturbative QCD at short distances, constraints on the value of Λ are determined.

In Chapter 2, we studied the next-to-leading order QCD perturbative prediction for the potential, both in the massless theory and including the effects of heavy quark loops. We found that working in the $\overline{\text{MS}}$ scheme produced logarithmic quark mass divergences which however could be neglected in effective light flavour theories provided we work in regions far away from the divergences. The effects of heavy quark loop effects are best seen working in the MOM renormalisation scheme in which the heavy quarks decouple, and we found that over the entire region of sensitivity to any foreseeable heavy quarkonium system, an effective 4-flavour theory with massive charm quarks gives the best description of the perturbative potential.

A realistic quarkonium potential was developed in Chapter 3 which embodies the short distance perturbative behaviour and yet has sufficient flexibility in the region unconstrained by the perturbative result, to be able to fit the data. Using the framework of non-relativistic quantum mechanics to fit the $c\bar{c}$ and $b\bar{b}$ data, we found that the data do not constrain the value of $\Lambda \equiv \Lambda^{(4)}_{\overline{MS}}$, apart from requiring $\Lambda \gtrsim 150$ MeV. We tested this conclusion by changing the parametric form, at intermediate distances of the potential, and also by including a constant term V_o and found similar results. Indeed small values of V_o consistent with zero were preferred by the data provided a linear confining term was included in the potential.

Predictions for the properties of higher mass quarkonium states are found to be quite sensitive to the value of Λ , and in Chapter 4, we compared predictions for two values of Λ with those obtained from a Richardson - [35] and a Martin - [40] type potential. The predictions that we emphasised are those expected to be measured rather accurately, m(2S)-m(1S) and $\Gamma(2S \to e^+e^-)/\Gamma(1S \to e^+e^-)$, in the forthcoming toponium studies at LEP [13], and elsewhere. Assuming the predictions corresponding to a given value of Λ to be sample 'data', we investigated how well toponium measurements will be able to determine Λ . Using three different data sets listed in eq. (4.6), with statistical errors expected in the forthcoming experiments, we found that at the least we should be able to determine to within ±100 MeV, if Λ is in the region 0.2-0.5 GeV. This constraint on Λ was found by only including the m(2S)-m(1S) mass difference and the ratio of leptonic widths of these states whose value is rather insensitive to the value of Λ. This situation could be improved by replacing the ratio of leptonic widths, with the absolute width $\Gamma(1S \to e^+e^-)$,which is expected to be measured to 10% accuracy. Including this 'data' would enable Λ to be determined to ±85 MeV, however higher-order QCD corrections, indicated

in eq. (3.12) for $\Gamma(1S \to e^+e^-)$, need first to be computed to ensure that the theoretical predictions are reliable. We also considered including P-wave 'data' and found that Λ could be determined to within ±75 MeV, although such data may take a long time to collect experimentally.

We returned to $c\bar{c}$ and $b\bar{b}$ specroscropy in Chapter 5 and analysed the hadronic decays of the lowest S and P wave states using predictions from the potentials that were developed in Chapter 3. The relevant quantities to determine the hadronic decay widths are the values of the radial S-state wavefunctions and derivative of the P-state wavefunction at the origin, as indicated by eqs. (5.1), (5.2) and (5.4). We found, for reasonable values of $\alpha_S \simeq 0.2$, that the lowest-order QCD prediction for the $c\bar{c}$ 1S-singlet hadronic decay, eq. (5.2), accounts well for the experimental value, as seen in Fig 5.1. However, eq. (5.4), for the decay of the χ_2 in $c\bar{c}$ can only account for the experimental result if $\alpha_S \simeq 0.5$, as can be seen from Fig 5.2. As ratios of hadronic widths like χ_0/χ_2, which are independent of wavefunction effects, are correctly predicted we concluded that the problem lies with wavefunction corrections. An estimation of the spin-independent relativistic corrections to the wavefunction indicated an increase in $|R'_p(0)|^2$ of 60%, offering some improvement in the discrepancy between the experimental and theoretical values.

We conclude finally, that in order to probe the perturbative region of the interquark potential, a heavy quark bound state system is required and that the experimental determination of the mass and e^+e^- decay widths of the 1S and 2S resonances of such a system (assuming a mass around 80 GeV) with accuracy anticipated at the forthcoming e^+e^- resonances should enable the QCD scale parameter to be determined to within ±100 MeV.

REFERENCES

(1) Arnison, G. et al., UA1 collab., Phys. Lett. 147B, 493, (1984).

(2) t'Hooft, G., Nucl.Phys. B61, 455, (1973).

(3) Bardeen, W.A. et al., Phys. Rev. D18, 3998, (1978).

(4) Celmaster, W. and R. J. Gonsalves, Phys. Rev. D20, 1420, (1979).

(5) Glashow, S.L., J. Iliopoulos and L. Maiani, Phys. Rev. D2, 1285, (1970).

(6) Zweig, G., CERN Report 8419/Th 412, (1964).

(7) Eichten, E., K. Gottfried, T. Kinoshita, K.D. Lane and T.H. Yan, Phys. Rev. D17, 3090, (1978).

(8) Billoire, A., Phys. Lett. 92B, 343, (1980).

(9) Martin, A., Phys. Lett. 93B, 338, (1980)

(10) Landau and Lifshitz, Quantum Electrodynamics, Pergamon International Library (1979).

(11) Krasemann, H., S.Ono, Nucl.Phys. B154, 283, (1979).

(12) Steiger, A.D., Phys. Lett. 129B, 335, (1983).

(13) W. Buchmuller et al., Physics at LEP, CERN 86-02, Vol.1, p.203

(14) Buchmuller, W., S.-H.H. Tye, Phys. Rev. D24, 132, (1981).
Buchmuller, W., et al., Phys. Rev. Lett., 45, 103 and 587(E), (1980).

(15) Hagiwara, K., S. Jacobs, M.G. Olsson and K.J. Miller, Phys. Lett., 103B, 209, (1983).

(16) Igi, K. and S. Ono, Phys. Rev. D33, 3349, (1986).

(17) L. Susskind, in Weak and Electromagnetic interactions at high energy, Les Houches 1977 p.207.

(18) Gross, D.J. and F. Wilczek, Phys. Rev. Lett. 30, 1343, (1973).

(19) Applequist, T., M. Dine and I.J. Muzimuch, Phys. Lett. 69B, 231, (1977);
Feinberg, F., Phys. Rev. Lett. 39, 316, (1977);
Fischer, W., Nucl. Phys. B129, 157, (1977).

(20) Duke, D.W. and R.G. Roberts, Phys. Rep. 120, 275, (1985).

(21) Hagiwara, K., Supp. Prog. Theor. Phys. 77, 101, (1983).

(22) t'Hooft, G., Nucl. Phys. B72, 461, (1974).

(23) Grunberg, G., Phys. Lett. 95B, 70, (1980); Phys. Lett. 114B, 271, (1982); Phys. Rev. D29, 2315, (1984).

(24) Tarasov, O.U., A.A. Valdmirov and A. Yu. Zharkov, Phys. Lett. 93B, (429), (1980).

(25) Braaten, E. and J.P. Leveille, Phys. Rev. D24, 1369, (1981).

(26) Hagiwara, K., T. Yoshino, Phys. Rev. D26, 2038, (1982).

(27) Hagiwara, K., Phys. Lett. 118B, 141, (1982).

(28) Kinoshita, T., J. Math. Phys. 3, 650 (1962); Lee, T.D. and M. Nauenberg, Phys. Rev. 133, B1549, (1964).

(29) Symanzik, K., Commun. Math. Phys. 34, 7, (1973); Applequist, T. and J. Carazzone, Phys. Rev. D11 2856, (1975).

(30) Weinberg, S., Phys. Lett. 91B, 51, (1980); Ovrut, B. and H.J. Schnitzer, Phys. Rev. D21, 3369, (1980).

(31) Weinberg, S., in ref. 25; Hall, L., Nucl. Phys. B178, 75, (1981); Bernreuther, W. and W. Wetzel, Nucl. Phys. B197, 228, (1982); Marciano, W.J., Phys. Rev. D29, 580, (1984).

(32) Yoshino, T. and K. Hagiwara, Z. Phys. C24, 185, (1984).

(33) Celmaster, W. and R.J. Gonsalves, Phys. Rev. D20, 1420, (1979).

(34) Kuhn, J.H., Acta. Phys. Polon. B12, 347, (1981).

(35) Richardson, J.L. Phys. Lett. 82B, 272, (1979).

(36) Bachas, C., Phys. Rev. D33, 2723, (1986).

(37) Particle Data Group, Phys. Lett. 170B, 1, (1986).

(38) Celmaster, W., Phys. Rev. D19, 1517, (1979).

(39) Miller, K.J. and M.G. Olsson, Phys. Rev. D25, 2283, (1978).

(40) Martin, A., Phys. Lett. 93B, 338, (1980).

(41) Quigg, C. and J.L. Rosner, Phys. Lett. 72B, 462, (1978).

(42) Kuhn, J.H. and S. Ono, Z. Phys. C21, 395 and C24, 404(E), (1984).

(43) Rosner, J.L., Quarkonium, Nato Series Lectures, (1979).

(44) De Rujula, A., H. Georgi and S.L. Glashow, Phys. Rev. D12, 147, (1975).

(45) Quigg, C. and J.L. Rosner, Phys. Rep. 56, 167, (1979).

(46) Martin, A.D., New Particles '85 Conf., Madison, p.204.

(47) Applequist, T. and H. D. Politzer, Phys. Rev. Lett. 34, 43, (1975); De Rujula, A. and S.L. Glashow, Phys. Rev. Lett. 34, 46, (1975).

(48) Barbieri, R., R. Gatto and R. Kogerler, Phys. Lett. 60B, 1976, (1976).

(49) The hadronic width is obtained by subtracting the leptonic and radiative widths from the total width.

(50) Hiltin, D., in Proceedings of the 1983 International Symposium on Lepton and Photon Interactions at High Energy, Ithaca.

(51) Lepage, G.P., see ref. 45.

(52) Barbieri, R., M. Caffo, R. Gatto and E. Remiddi, Phys. Lett. 95B, 83, (1980).

(53) McClary, R. and N. Byers, Phys. Rev. D28, 1692, (1983).

(54) Martin, A.D., M.G. Olsson and W.J. Stirling, Phys. Lett 147B, 203, (1984).

(55) Oreglia, M., (private communication).

(56) Baglin, C. et al., contribution to the VIIth European Symposium on Antiproton Interactions Durham, UK, (1984).

(57) Duke, D.W. and D. Kimel, Phys. Rev. D25, 2960, (1982).

(58) Barbieri, R., M. Caffo, R. Gatto and E. Remiddi, Nucl. Phys. B192, 61, (1981).

(59) Barbieri, R., R. Gatto and E. Remiddi, Phys. Lett 61B, 465, (1976).

(60) Goulay, A.R. and G. A. Watson, Computational Methods for Matrix Eigenproblems (Wiley, New York, 1971).

(61) Schwarz, H.R., Numer. Math. 12, 231, (1968).

APPENDIX A

Fourier Transform of the Perturbative Potential

Our objective here is to determine the Fourier transform of the QCD perturbative expansion for the static potential given, in massless quark theory, by eq. (2.1) or with the inclusion of heavy quarks loops, by eq. (2.28).

We shall first consider eq. (2.1) for massless quark loops.

1. The Fourier transformation of the potential V(q) reads

$$V(r) = \frac{1}{(2\pi)^3} \int d^3q\, e^{-i\vec{q}\cdot\vec{r}}\, V(\vec{q}) \qquad (A1)$$

$$= \frac{1}{2\pi^2 r} \int_0^\infty dq\, \sin(qr) q V(q) \quad ,$$

where $r = |\vec{r}|$ and $q = |\vec{q}|$. Reading from eq. (2.1) we see that the q-dependence essential results in terms of the form

$$qV(q) = \frac{x}{q} + y\,\frac{\ell n q}{q} \qquad (A2a)$$

where

$$x = -4\pi^2 C_F a\left\{1 + a\left[C_A\left(\frac{11}{12}\ell n\mu^2 + \frac{31}{37}\right) - T_F n_f\left(\frac{1}{3}\ell n\mu^2 + \frac{5}{9}\right)\right]\right\} \qquad (A2b)$$

$$y = -4\pi^2 C_F a^2\left[T_F n_f \frac{2}{3} - C_A \frac{22}{12}\right] \qquad (A2c)$$

neglecting higher-order terms.

Defining the Fourier sine transform as

$$g(r) = \int_0^\infty dq\, \sin(qr) f(q) \; ; \quad r > 0 \quad , \qquad (A3)$$

then useful transformations are:

$f(q)$	$\longrightarrow$	$g(r)$	
$1/q$		$\pi/2$	(A4a)
$\ell nq/q$		$-\pi/2(\gamma_E + \ell nr)$	(A4b)
$\ell n(1 + a^2q^2)/q$		$-\pi Ei(-r/a)$	(A4c)

where γ_E is Euler's constant and Ei(-x) is the exponential integral.

Using the tranformation (A4a) and A4b), then eq. (2.1) can be written,

$$V(r) = -\pi C_F \frac{a}{r}\left[1 + a\left(b_o \ell n\mu r + b_o\gamma_E + \frac{31}{37}C_A - \frac{5}{9}T_F n_f\right)\right] \qquad (A5)$$

which proves the result of eq. (2.6). We consider next eq. (2.28) where heavy quark loops are included.

2. The additional q-dependence of eq. (2.28) over that of eq. (2.1) is through the vacuum polarisation term, eq. (2.29). We only need concentrate on this term as the rest of the analysis follows that of the massless case. We have noted that an accurate approximation to the vacuum polarisation is given by eq. (2.31), over the whole range of x, and so we can then write,

$$\begin{aligned} F(x) &\simeq -\frac{1}{3}\ell n(x + e^{-5/3}) \\ &\equiv -\frac{\ell n(m_q^2/q^2)}{3} - \frac{\ell n(1 + q^2e^{-5/3}/m_q^2)}{3} \end{aligned} \qquad (A6)$$

Using transformations (A4a) and (A4b) for the first term of eq. (A.6) and (A4c) for the second term, we find

$$T_F \sum_{q=1}^{n_f} F\left(\frac{m_q^2}{q^2}\right) \underset{F.T.}{\rightarrow} T_F\frac{2}{3}\sum_{q=1}^{n_f}\left[\gamma_E + \ell n(m_q r) - Ei(-m_q e^{5/6} r)\right] \qquad (A7)$$

which proves eq. (2.32).

APPENDIX B

Numerical Solution Of The 3-Dimensional Schrodinger Equation

To analyse quarkonia data via non-relativistic quantum mechanics one must solve Schrodinger's equation for a spherically symmetric potential, and in general this task must be performed numerically. The basic strategy, after reducing the 3-dimensional problem to a radial equation, is to map this radial dimension into a finite region and by using a finite difference approximation for the relevant derivatives convert this into a matrix equation whose eigenvalues and eigenvectors can be found using well established computer library routines. We examine the accuracy of this method of solution by comparing numerical solutions with the analytical solutions that exist for the Coulomb and 3-dimensional Harmonic oscillator potentials. We first of all consider the method of solution.

B.1 Reduction to a Matrix Equation

In 3-dimensions the Schrodinger equation is written in the form

$$-\frac{1}{2\mu}\nabla^2\Psi(r) + \left[V(r) - E\right]\Psi(r) = 0 \quad , \tag{B1}$$

where μ is the reduced mass of the system

$\underline{r}$ is the relative co-ordinate ($r \equiv |\underline{r}|$)

$\Psi(r)$ is the 3-dimensional wavefunction

E is the energy eigen value

V(r) is the central, velocity independent potential

and $\hbar = c = 1$.

We wish to describe charmonium, bottomonium and toponium states of the form $q\bar{q}$, that is states containing a quark and antiquark of the same species. Hence the reduced mass is given by

$$2\mu \equiv m_q$$

The 3-dimensional equation (B1) is easily converted to a single co-ordinate radial equation by recognising that the interaction potential depends on the radial dimension, r. Reducing the 3-dimensional wavefunction

$$\Psi(r) = R(r)Y_{\ell m}(\theta,\phi) \equiv \frac{u(r)}{r}Y_{\ell m}(\theta,\phi) \qquad (B2)$$

where R(r) [or u(r)] is the radial wavefunction and $Y_{\ell m}(\theta,\phi)$ are the spherical harmonics.

In terms of u(r), (B1) reduces to

$$\frac{d^2u}{dr^2} + \left[m_q(E - V(r)) - \frac{\ell(\ell+1)}{r^2}\right]u(r) = 0 \qquad (B3)$$

where u(r) is normalised such that

$$\int_0^\infty u^2(r)\,dr = 1 \quad , \qquad (B4)$$

and vanishes for r at zero and infinity.

At this point it is convenient to make the following substitution,

$$\lambda = m_q E \qquad (B5a)$$

$$\Phi(r) = m_q V(r) + \frac{\ell(\ell+1)}{r^2} \qquad (B5b)$$

which simplifies eq. (B3) to

$$\frac{d^2u}{dr^2} + \left[\lambda - \Phi(r)\right]u(r) = 0 \quad . \qquad (B6)$$

The numerical methods require that the region from zero to infinity in r be mapped into a finite interval in order to obtain a matrix equation. This is accomplished by the following substitution:

$$t \equiv \frac{1}{(1 + r/r_o)} \tag{B7}$$

where the dimensional constant is chosen to be $r_o = 1\ GeV^{-1}$. The transformation to 't space' involves first derivatives which are eliminated by the replacement

$$\phi(t) \equiv tu(t) \tag{B8}$$

The resulting equation and boundary conditions now read

$$\frac{d^2\phi}{dt^2} + \left[\lambda - \Phi(t)\right]\frac{\phi(t)}{t^4} = 0 \quad , \tag{B9a}$$

$$\phi(0) = \phi(1) = 0 \quad . \tag{B9b}$$

In this form, the equation can be easily transformed into a matrix equation by dividing the range of t from zero to one into n+2 points, a distance of h = 1/(n+1) apart, and labelled by the subscript j. The boundary conditions are trivially given by

$$\phi_o = \phi_{n+1} = 0 \quad , \tag{B10}$$

and we use the following finite difference expression to approximate the second derivative in eq. (B.9a)

$$\frac{d^2\phi_j}{dt^2} = \frac{1}{12h^2}(-\phi_{j-2} + 16\phi_{j-1} - 30\phi_j + 16\phi_{j+1} - \phi_{j+2}) + O(h^4) \tag{B11}$$

Although a lower order expression exists, it implementation would require a very large number of points to obtain accurate answers. The use of eq. (B.11) requires the additional input of ϕ_{-1} and ϕ_{n+2} to fully define the second derivative within the range of t. These values are found by using the symmetry of u(r) and our transformation equations, and can be seen to correspond to negative values of r.

To obtain the symmetry of the radial wavefunction we note that in order for eq.(B.3) to be extended to negative r, V(r) must be an even function of r. This leads to the fact that the eigenfunctions of the Schrodinger equation will have a definite parity

$$u(-r) = (-1)^{\ell+1} u(r) \tag{B12}$$

Employing the transformation equation, eq. (B.7), we find

$$\phi_{-1} = (-1)^{\ell} \phi_1 + O(h^2) \tag{B13a}$$

$$\phi_{n+2} = (-1)^{\ell+1} \phi_n + O(h^3) \tag{B13b}$$

The errors of $O(h^2)$ and $O(h^3)$ respectively in the above two equations are due to the approximations introduced when going to negative values of r, from positive values, through the transformation equations. Since u(r) behaves as a power of r at the origin, it is important that it is accurately predicted by (B.13b). However, the exact behaviour at large r is unimportant as it is lost in noise about zero.

Our Schrodinger equation is now represented by a complete set of equations in j, where j = 1, ..., n,

$$(\phi_{j-2} - 16\phi_{j-1} + 30\phi_j - 16\phi_{j+1} + \phi_{j+2}) + \frac{12h^2}{(jh)^4}\left[\Phi(jh) - \lambda\right]\phi_j = 0 \quad , \tag{B14}$$

with the auxillary and boundary conditions given by eqs. (B.10), (B.13a) and (B.13b). This set of equations is now linear in ϕ_j and can be written as the matrix equation;

$$S\phi = 0 \quad , \tag{B15}$$

where S is an nxn band symmetric matrix (i.e. $s_{ij} = 0$ for $|i-j| > 2$) and ϕ is an n-dimensional column vector. All the boundary conditions are contained in S. However, eq. (B.15) is not a true eigenvalue equation, as its j-th diagonal element behaves like:

$$30 + \frac{12h^2}{(jh)^4}\,\Phi(jh) - \lambda \tag{B16}$$

To set eq. (B.15) in a form $(A - \lambda I)\,\underline{x} = 0$ we therefore need to remove the coefficient $12h^2/(jh)^4$ which is done, while maintaining the symmetry structure of the matrix, by considering the diagonal matrix K such that $k_{jj} = j^2$. We then write

$$S\phi = 0 = (KSK)(K^{-1}\phi) \tag{B17}$$

The j-th diagonal elements of the matrix $(h^2/12)KSK$ can then be written as

$$30\frac{j^4h^2}{12} + \phi(jh) - \lambda \tag{B18}$$

leaving us with a true eigenvalue problem

$$Ax = \lambda x \tag{B19a}$$

with

$$x = K^{-1}\phi \tag{B19b}$$

The eigenvalues and eigenvectors are then obtained from eq. (B.19) using standard library routines for matrix problems as outlined below.

B.2 Calculation Of The Eigenvalues And Eigenvectors

The eigenvalues of the matrix A are obtained in a two step process. First, the band five symmetric matrix is reduced to tridiagonal form by a series rotations in such a way that there are no non-zero elements generated outside the band for each rotation. This procedure is known as Given's method [60] although a modification by Schwarz [61] is used and maintains the band character in general. Once the matrix is in tridiagonal form the eigenvalues are then easily obtained [60]. Let T be the tridiagonal symmetric matrix and we wish to solve the characteristic equation for λ

$$\det(T - \lambda I) = 0 \quad . \tag{B20}$$

Let $P_r(\lambda)$ denote the determinant of the leading principal minor of $T - \lambda I$. Thus

$$P_r(\lambda) = \det \begin{vmatrix} d_1-\lambda & e_1 & & & \\ e_1 & d_2-\lambda & e_2 & & \\ & \cdot & \cdot & \cdot & \\ & & \cdot & \cdot & \\ & & e_{r-1} & d_{r-1}-\lambda & e_{r-1} \\ & & & e_{r-1} & d_r-\lambda \end{vmatrix} \qquad \text{(B21)}$$

Defining $P_0(\lambda)=1$, then by inspection $P_1(\lambda)= d_1 - \lambda$ and expanding $P_r(\lambda)$ by its final row, we obtain a recursion formula which eventually yields $P_n(\lambda)$, the characteristic polynomial

$$P_r(\lambda) = (d_r-\lambda)P_{r-1}(\lambda) - e_{r-1}^2 P_{r-2}(\lambda) \qquad \text{(B22)}$$

Using eq. (B.22) we can evaluate the numbers $P_0(\lambda),..,P_n(\lambda)$ for some value of λ. The Sturm sequence property [60] then tells us that the number of agreements in sign of successive members of the sequence $\{P_r(\lambda)\}$ is equal to the number of eigenvalues strictly greater than λ. Thus the number of eigenvalues in a specific interval $[\lambda_1, \lambda_2]$ can be determined and by bisection of this interval, any given eigenvalue can be determined to prescribed accuracy.

The process of inverse iteration [60] is used to obtain the eigenvectors and also to increase the accuracy of the eigenvalues. We consider for the nxn matrix A that there exist n linearly independent eigenvectors $\underline{x}_1, \underline{x}_2, \ldots, \underline{x}_n$, then an arbitrary vector y can be written as a sum over these, in the form

$$y = \sum_{i=1}^{n} c_i x_i \qquad \text{(B23)}$$

Multiply y by $(A - qI)^{-1}$ gives

$$(A - qI)^{-1} y = \sum_{i=1}^{n} \frac{c_i x_i}{(\lambda_i - q)} \qquad \text{(B24)}$$

By choosing q to be near an eigenvalue, then after several iterations of this equation, y approaches the corresponding eigenvector.

B.3 Accuracy of the Matrix Technique

In order to test the accuracy of the procedure, we consider two potentials with behaviours which more than span the quarkonium potential we consider. Namely the Coulomb and the 3-dimensional oscillator potentials, for which analytic solutions exist for eigenvalues and eigenvectors of the Schrodinger equation. We calculate several of the lowest lying S and P wave energy levels and wavefunctions, for a variety of quark masses and test the accuracy of the results against the choice of dimension of the matrices. We give results for n=49 and n=99, where we would expect the latter to give more accurate predictions.

B.3.1 Coulomb Potential

The potential has the simple form $V(r) = -1/r$ resulting in an energy level structure dependent upon the principal quantum number, n,

$$E_n = -m_q/4n^2 \qquad \text{(B25)}$$

having set $\hbar = c = e = Z = 1$. Of particular relevance in the calculation of quantities like the ratio of leptonic widths of two levels in the charmonium system is the value of the S wavefunction at the origin. For the Coulomb potential the first three S wave radial wavefunctions are expressed as:

$$R_{1S}(0) = m_q^{1.5}/\sqrt{2} \qquad \text{(B26a)}$$

$$R_{2S}(0) = m_q^{1.5}/4 \qquad \text{(B26b)}$$

$$R_{3S}(0) = m_q^{1.5}/(3\sqrt{6}) \qquad \text{(B26c)}$$

We show in Table B1 the comparison of theoretical and calculated values for the first five S and first five P wave energy levels and also the first three S wave radial wavefunctions at the origin.

The calculation is done first with n=99 and then with n=49 to investigate the errors introduced by the matrix method. The quark masses that we have used are relevant for the charmonium and bottomonium spectroscopy and we also anticipate a toponium spectrum for a top quark mass of 40 GeV. For this potential all but the lowest lying S states of toponium are accurately predicted, signalling that for these states even a matrix of 99 x 99 is insufficient in size which is due to the singular behaviour of the potential at the origin. It is precisely this short distance singular region which is most sensitive to these lowest lying toponium S states. Increasing the size of the matrix A proves to be very impractical as the time taken for the routine, which determines the eigenvalues of a tridiagonal matrix, is approximately proportional to n^3, where n is the dimension of the matrix. However, we do not expect QCD-like potentials (which incorporate softening logarithmic terms) to be as singular as the Coulomb potentials as $r \to o$, and so more accurate predictions are obtained for the same size of matrix.

B.3.2 3-Dimensional Harmonic Potential

The potential has the simple form $V(r) = r^2/4$ giving an energy level structure dependent upon both the principal quantum number, n, and the orbital angular momentum, ℓ,

$$E_{n\ell} = (2n - \ell - 1/2)/\sqrt{m_q} \qquad (B27)$$

Again for the first three S wave radial wavefunctions evaluated ar r = o, we have the analytic result;

$$R_{1S}(0) = \left(\frac{\sqrt{m_q}}{2\pi}\right)^{0.75} 2\sqrt{\pi} \qquad \text{(B28a)}$$

$$R_{2S}(0) = (8)^{-1.5}\left[\left(\frac{\sqrt{m_q}}{2\pi}\right)^{\frac{1}{2}} 2\right]^3 2\sqrt{\pi} \qquad \text{(B28b)}$$

$$R_{3S}(0) = (384)^{-1.5}\left[\left(\frac{\sqrt{m_q}}{2\pi}\right)^{\frac{1}{2}} 12\right]^3 2\sqrt{\pi} \qquad \text{(B28c)}$$

A comparison of the analytic and computed values is shown in Table B2. In contrast to the Coulomb potential, the predictions for the toponium spectroscopy are very accurate due to the fact that the oscillator potential is finite at r = o; and indeed for all three quark mass values the predictions shown in Table B2 differ by less than 0.5% from the theoretical results.

As the work in this thesis requires a substantial amount of computing, in that a single fit to quarkonia data using a potential with a number of free parameters requires of the order of a few thousand solutions of the Schrodinger equation, matrices of dimensions greater than 99 x 99 prove to be too time consuming, as noted earlier. Indeed from the predictions in Tables B1 and B2, we see that for the states and mass range that we will be interested in, a matrix of dimensions 49 x 49 is adequate and sufficiently economic although specific predictions for quantities requiring only a single solution of the matrix equation were performed with n=99.

	m_q = 1.5 GeV			m_q = 5 GeV			m_q = 40 GeV		
	Exact	n=49	n=99	Exact	n=49	n=99	Exact	n=49	n=99
E_{1S}	-0.375	-0.37495	-0.3750	-1.25	-1.248	-1.2495	-10.0	-9.351	-9.792
E_{2S}	-.09375	-.09379	-.09357	-0.3125	-0.3123	-0.3124	-2.5	-2.418	-2.474
E_{3S}	-.04166	-.04201	-.04170	-0.1389	-0.1389	-0.1389	-1.111	-1.087	-1.103
E_{4S}	-.02344	-.02264	-.02361	-.07813	-.07828	-.07813	-0.625	-0.6148	-0.6217
E_{5S}	-.015	-.01926	-.01682	-.05	-.0511	-.05006	-0.40	-0.3948	-0.3983
E_{1P}	-.09375	-.09377	-.09375	-0.3125	-0.3125	-0.3125	-2.5	-2.5006	-2.5
E_{2P}	-.04166	-.04186	-.04169	-.1389	-.1389	-.1389	-1.111	-1.1114	-1.1111
E_{3P}	-.02344	-.02351	-.02358	-.07813	-.07826	-.07813	-0.625	-0.6251	-0.625
E_{4P}	-.015	-.01936	-.01656	-.05	-.0510	-.05005	-.40	-.4001	-.40
E_{5P}	-.0104	0.03199	-.0099	-.03472	-.03724	-.03494	-.2778	-.2779	-.2778
R_{1S}	1.299	1.295	1.297	7.9057	7.7918	7.8532	178.9	140.5	162.2
R_{2S}	0.4593	0.4580	0.4585	2.7951	2.7583	2.7774	63.25	52.4	58.3
R_{3S}	0.25	0.2456	0.2502	1.5215	1.5015	1.5119	34.4	28.9	31.9

Table B.1 : Predictions for the Coulomb potential for a variety of quark masses, showing the sensitivity to the dimensions of the matrix, and compared to the exact analytic value.

	m_q = 1.5 GeV			m_q = 5 GeV			m_q = 40 GeV		
	Exact	n=49	n=99	Exact	n=49	n=99	Exact	n=49	n=99
E_{1S}	1.2247	1.2247	1.2247	0.6708	0.6708	0.6708	0.2372	0.2372	0.2372
E_{2S}	2.8577	2.8575	2.8577	1.5653	1.5652	1.5652	0.5534	0.5534	0.5534
E_{3S}	4.4907	4.4886	4.4906	2.4597	2.4590	2.4596	0.8696	0.8695	0.8696
E_{4S}	6.1237	6.1141	6.1231	3.3541	3.3512	3.3539	1.1859	1.1853	1.1858
E_{5S}	7.7567	7.7233	7.7544	4.2485	4.2389	4.2479	1.5021	1.5005	1.5020
E_{1P}	2.0412	2.0412	2.0412	1.1180	1.1180	1.1180	0.3953	0.3953	0.3953
E_{2P}	3.6742	3.6735	3.6742	2.0125	2.0123	2.0125	0.7115	0.7115	0.7115
E_{3P}	5.3072	5.3030	5.3070	2.9069	2.9056	2.9068	1.0277	1.0275	1.0277
E_{4P}	6.9402	6.9231	6.9391	3.8010	3.7963	3.8013	1.3440	1.3431	1.3439
E_{5P}	8.5732	8.5170	8.5694	4.6957	4.6801	4.6947	1.6602	1.6577	1.6600
R_{1S}	1.0399	1.0402	1.0399	1.6334	1.6342	1.6335	3.5624	3.5674	3.5635
R_{2S}	0.3677	0.3678	0.3677	0.5775	0.5781	0.5776	1.2595	1.2636	1.2604
R_{3S}	0.2388	0.2374	0.2374	0.3751	0.3732	0.3729	0.8181	0.8169	0.8140

Table B.2 : Predictions for the 3-dimensional Harmonic Oscillator potential for a variety of quark masses, showing the sensitivity to the dimension of the matrix, and compared to the exact analytic value.

APPENDIX C

Computer Program Listing

We reproduce a listing of the computer program used in this work. The program uses the methods developed in Appendix B to solve the Schrodinger equation for a given input potential, which as seen in Chapter 3 contains 5 variable parameters that can be adjusted in order to obtain optimum agreement with quarkonia data values. A minimising routine is used to obtain the fit parameters by minimising the value of χ^2 as defined in eq. (3.13). Comment cards within the program describe the details.

```
C     ************************************************************
CCCCC *                                                          *
CCCCC *       TO SOLVE THE SCHRODINGER EQUATION FOR A            *
CCCCC *       GIVEN INTERQUARK POTENTIAL AND OBTAIN              *
CCCCC *       A FIT TO THE QUARKONIA DATA                        *
CCCCC *                                                          *
CCCCC ************************************************************
C
C***  MINIMISING ROUTINE WHICH CALLS A SUBROUTINE FCN AND
C***  MINIMISES THE VALUE OF F WITHIN FCN
C
      CALL MINTSD
      STOP
      END
      SUBROUTINE FCN(NPAR,G,F,X,IFLAG)
      IMPLICIT REAL*8 (A-H,O-Z)
      COMMON/ABCD/PI,XH,EUL,XLAM,BETA0,BETA1,BLER,NF,KQ
      DIMENSION A(5,99),DA(99),E(99),E2(99),R(10),WU(10),VEC(99),D(
     ^30),INT(99),WORK(1000),B(3,99),AP(5,99),RADL(0:200),ST(6)
      DIMENSION AQ(6,3),QMASS(6,10),QDATA(16),QERR(16),YTHEO(23)
      DIMENSION X(30),G(30),VRG3(99),VRG2(40),VRG1(40),ERROR(40)
      DIMENSION VRG4(99),VRG6(40),ABJ(20),WF(40),WD(40),WS(60)
      DATA ST/1.0D-01,1.0D-02,1.0D-03,1.0D-04,1.0D-05,1.0D-06/
C***  QUARKONIA DATA VALUES
      DATA QDATA/3.663D+00,3.068D+00,0.457D+00,0.432D+00,9.452D+00
     ^,0.567D+00,0.900D+00,0.448D+00,0.809D+00,0.439D+00,0.328D+00,
     ^8.0D+01,0.6693D+00,3.439D-06,0.5424D+00,1.1D-06/
      DATA QERR/2.D-03,2.D-03,10.D-03,0.06D+00,2.5D-03,3.D-03,
     ^2.5D-03,2.5D-03,6.D-03,0.03D+00,0.03D+00,0.1D+00,
     ^0.020D+00,0.3439D-06,0.020D+00,0.12D-06/
      IF(IFLAG.GT.1)GOTO 1010
      EUL=0.5772D+00
C***  QCD SCALE PARAMETER (XLAM)
      XLAM=0.20D+00
      EMA=1.0D+00/1.37D+02
      NF=4
      PI=3.1415926D+00
```

```
      BETA0=(33.0-2.*NF)/6.
      BETA1=(153.-19.*NF)/12.
      BLER=(BETA0+(1.0/3.0))*EUL+(93.0/37.0)-(5.0/6.0)
C   ***  DIMENSION OF THE MATRIX (KQ)
      KQ=49
      XH=1.0/(KQ+1.0)
      XH2=XH**2
      CALL SUB1(VRG1,ERROR,VRG6)
      CALL SUB4(VRG4)
1010  CONTINUE
      CALL SUB3(VRG3,VRG4,X)

C   ***  EVEN NAN = P-WAVES,ODD NAN = S-WAVES.
      DO 1000 NAN=1,6

      N=KQ
      IA=5
      IXB=3
      M1=3
      MB1=1
      EPS1=0.0D+00
      LMB1=-1
      LWORK=1000
      NA=KQ
      IAA=5
      MA1=3
C   ***  X(1) = CHARM QUARK MASS
C   ***  X(2) = BOTTOM QUARK MASS
C   ***  X(7) = TOP QUARK MASS

      IF((NAN.EQ.1))THEN
      MB2=2
      MM12=2
      UM=X(1)
      ELSE IF(NAN.EQ.2)THEN
      MB2=1
      MM12=1
      UM=X(1)
      ELSE IF(NAN.EQ.3)THEN
      MB2=3
      MM12=3
      UM=X(2)
      ELSE IF(NAN.EQ.4)THEN
      MB2=2
      MM12=2
      UM=X(2)
      ELSE IF(NAN.EQ.5)THEN
      MB2=2
      MM12=2
      UM=X(7)
      ELSE IF(NAN.EQ.6)THEN
      MB2=1
      MM12=1
      UM=X(7)
      END IF
C   ***  TO DETERMINE THE BAND FIVE SYMMETRIC MATRIX A
C   ***  (ONLY THE UPPER TRIANGLE ELEMENTS ARE GIVEN)
      DO 10 J=3,KQ
       A(1,J)=XH2*(J*(J-2))**2/12
10    CONTINUE
      DO 20 J=2,KQ
       A(2,J)=-4*XH2*(J*(J-1))**2/3
20    CONTINUE
      IF((NAN.EQ.2).OR.(NAN.EQ.4).OR.(NAN.EQ.6))THEN
      A(3,1)=(29*XH2/12)+(UM*(VRG3(1))+(2/(KQ**2)))
      A(3,KQ)=(31*XH2*KQ**4/12)+(UM*(VRG3(KQ))+2*KQ**2)
      DO 30 J=2,KQ-1
      PU=J*XH
      QU=1-PU
      A(3,J)=5*XH2*J**4/2+(UM*(VRG3(J))+(2*(PU/QU)**2))
30    CONTINUE
      ELSE IF((NAN.EQ.1).OR.(NAN.EQ.3).OR.(NAN.EQ.5))THEN
      A(3,1)=(31*XH2/12)+(UM*(VRG3(1)))
```

```
      A(3,KQ)=(29*XH2*(KQ**4)/12)+(UM*(VRG3(KQ)))
      DO 29 J=2,KQ-1
      PU=J*XH
      QU=1-PU
       A(3,J)=(5*XH2*J**4/2)+(UM*(VRG3(J)))
29    CONTINUE
      END IF
C   ***  ROUTINE TO TRI-DIAGONALISE THE BAND FIVE MATRIX A
      CALL F01BWF(N,M1,A,IA,DA,E)
      DO 100 L=1,KQ
       E2(L)=E(L)**2
100   CONTINUE
C   ***  ROUTINE TO FIND EIGENVALUES OF TRIDIAGONAL MATRIX
C   ***  DIAGONAL ELEMENTS ARE IN DA
C   ***  OFF-DIAGONAL ELEMENTS ARE IN E
      CALL F02BFF(DA,E,E2,N,MB1,MB2,MM12,EPS1,X02AAF(X),
     ^EPS2,IZ,R,WU)
      DO 710 JJJ=1,MB2
       QMASS(NAN,JJJ)=R(JJJ)/UM+2*UM
710   CONTINUE
      IF((NAN.EQ.2).OR.(NAN.EQ.4).OR.(NAN.EQ.6))GOTO 2001
      DO 700 III=1,MB2
      IFAIL=1
      D(1)=-1.0D+00
      DO 11 J=3,KQ
       AP(1,J)=XH2*(J*(J-2))**2/12
11    CONTINUE
      DO 21 J=2,KQ
       AP(2,J)=-4*XH2*(J*(J-1))**2/3
21    CONTINUE
      IF((NAN.EQ.2).OR.(NAN.EQ.4).OR.(NAN.EQ.6))THEN
      AP(3,1)=(29*XH2/12)+(UM*(VRG3(1))+(2/(KQ**2)))
      AP(3,KQ)=(31*XH2*KQ**4/12)+(UM*(VRG3(KQ))+2*KQ**2)
      DO 31 J=2,KQ-1
      PU=J*XH
      QU=1-PU
      AP(3,J)=5*XH2*J**4/2+(UM*(VRG3(J))+(2*(PU/QU)**2))
31    CONTINUE
      ELSE IF((NAN.EQ.1).OR.(NAN.EQ.3).OR.(NAN.EQ.5))THEN
      AP(3,1)=(31*XH2/12)+(UM*(VRG3(1)))
      AP(3,KQ)=(29*XH2*(KQ**4)/12)+(UM*(VRG3(KQ)))
      DO 32 J=2,KQ-1
      PU=J*XH
      QU=1-PU
       AP(3,J)=(5*XH2*J**4/2)+(UM*(VRG3(J)))
32    CONTINUE
      END IF

C   ***  TO FIND THE EIGENVECTORS OF THE INITIAL MATRIX
C   ***  THE EIGENVECTOR IS OUTPUT IN VEC
      RMU=R(III)
      CALL F02SDF(NA,MA1,LMB1,AP,IAA,B,IXB,.TRUE.,1.0D-04,RMU,VEC,D,INT,
     ^WORK,LWORK,IFAIL)
      RNMU=RMU+D(30)
      DO 95 K=1,KQ
      WT=K*XH
      RADL(K)=VEC(K)*K**2/(1-WT)
      IF(ABS(RADL(K)).LT.1.0D-25)THEN
      RADL(K)=0.0D+00
      END IF
95    CONTINUE
      IOUT=0
      DO 800 N=1,10
150   CONTINUE
      RADL(0)=0.0D+00
      RADL(KQ+1)=0.0D+00
C   ***  TO RENORMALISE THE WAVEFUNCTION ***

      XSIMP=0.0D+00
      LSIM=1
      DO 200 M=1,KQ+1
       TR=M*XH
```

```
        IFAC=3+LSIM
        IF((M.EQ.0).OR.(M.EQ.KQ+1))THEN
        IFAC=1
        END IF
        XSIMP=XSIMP+IFAC*(RADL(M)*(1-TR)/TR**2)**2
        LSIM=-LSIM
200     CONTINUE
        XSIMP=XSIMP*XH/3
        IF(IOUT.EQ.1)GOTO 220
        IF(IOUT.EQ.2)GOTO 888
        IF(XSIMP.GT.1.0D+00)THEN
        GOTO 210
        ELSE IF(XSIMP.LT.1.0D+00)THEN
        IOUT=1
        GOTO 220
        END IF
210     CONTINUE
        DO 300 J=1,KQ
         RADL(J)=RADL(J)/1.0D+01
300     CONTINUE
        GOTO 150
220     CONTINUE
        IF(XSIMP.LT.1.0D+00)THEN
        DO 400 K=1,KQ
         RADL(K)=RADL(K)*(N+1)/N
400     CONTINUE
        ELSE IF(XSIMP.GT.1.0D+00)THEN
        DO 410 K=1,KQ
         RADL(K)=RADL(K)*(N-1)/N
410     CONTINUE
        GOTO 801
        END IF
800     CONTINUE
801     CONTINUE
        PM=N-1.0D+00
        IOUT=2
        DO 950 N=1,5
        ZMAX=PM+11.0D+00*ST(N)
        DO 900 YK=PM,ZMAX,ST(N)
        GOTO 150
888     CONTINUE
        IF(XSIMP.LT.1.0D+00)THEN
        DO 910 K=1,KQ
         RADL(K)=RADL(K)*(YK+ST(N))/YK
910     CONTINUE
        ELSE IF(XSIMP.GT.1.0D+00)THEN
        DO 920 K=1,KQ
         RADL(K)=RADL(K)*(YK-ST(N))/YK
920     CONTINUE
        GOTO 949
        END IF
900     CONTINUE
949     CONTINUE
        PM=YK-ST(N)
950     CONTINUE
        AQ(NAN,III)=RADL(KQ)+(RADL(KQ)-RADL(KQ-1))

700     CONTINUE
2001    CONTINUE
1000    CONTINUE
C   ***  TO CALCULATE THE RUNNING COUPLING CONSTANT FOR CC,BB,TT.
        GG2=BETA0**2/BETA1
        GG4=(GG2/2)**(1./GG2)
        GG5=BETA0**2*DLOG((2*X(7))/XLAM)
        GG6=BETA0**2*DLOG((2*X(1))/XLAM)
        GG7=BETA0**2*DLOG((2*X(2))/XLAM)
        GG8=BETA1*DLOG(2./GG2)
        PP=BETA1/(GG4+GG8)
        QP=BETA1/(GG7+GG8)
        XS=BETA1/(GG5+GG8)
        WF(1)=PP
```

```
      DO 845 JK=1,40
       WF(JK+1)=PP/(1.+PP*DLOG((WF(JK)+1)/WF(JK)))
       IF(ABS(WF(JK+1)-WF(JK)).LT.1.0D-04)THEN
       P4=WF(JK+1)
       GOTO 846
       END IF
845   CONTINUE
846   CONTINUE
      WD(1)=QP
      DO 847 JK=1,40
       WD(JK+1)=QP/(1.+QP*DLOG((WD(JK)+1)/WD(JK)))
       IF(ABS(WD(JK+1)-WD(JK)).LT.1.0D-04)THEN
       P6=WD(JK+1)
       GOTO 848
       END IF
847   CONTINUE
848   CONTINUE
      WS(1)=XS
      DO 83 JK=1,60
       WS(JK+1)=XS/(1.+XS*DLOG((WS(JK)+1)/WS(JK)))
       IF(ABS(WS(JK+1)-WS(JK)).LT.1.0D-04)THEN
       P8=WS(JK+1)
       GOTO 84
       END IF
83    CONTINUE
84    CONTINUE
      APC=BETA0*PI*P4/BETA1
      APB=BETA0*PI*P6/BETA1
      APT=BETA0*PI*P8/BETA1
C  ***  ARRAY YTHEO DEFINES THE PREDICTIONS OF THE SCHRODINGER EQ.
      YTHEO(1)=QMASS(1,2)-QMASS(1,1)
      YTHEO(2)=QMASS(1,1)
      YTHEO(3)=QMASS(2,1)-QMASS(1,1)
      YTHEO(4)=(AQ(1,2)*QMASS(1,1)/(AQ(1,1)*QMASS(1,2)))**2
      YTHEO(5)=QMASS(3,1)
      YTHEO(6)=QMASS(3,2)-QMASS(3,1)
      YTHEO(7)=QMASS(3,3)-QMASS(3,1)
      YTHEO(8)=QMASS(4,1)-QMASS(3,1)
      YTHEO(9)=QMASS(4,2)-QMASS(3,1)
      YTHEO(10)=(AQ(3,2)*QMASS(3,1)/(AQ(3,1)*QMASS(3,2)))**2
      YTHEO(11)=(AQ(3,3)*QMASS(3,1)/(AQ(3,1)*QMASS(3,3)))**2
      CORC=1.-16*APC/(3*PI)
      CORB=1.-16*APB/(3*PI)
      CORT=1.-16*APT/(3*PI)
      YTHEO(12)=QMASS(5,1)
      YTHEO(13)=QMASS(5,2)-QMASS(5,1)
      YTHEO(14)=(4.*EMA*AQ(5,1)/(3.*QMASS(5,1)))**2*CORT
      YTHEO(15)=QMASS(6,1)-QMASS(5,1)
      IF(IFLAG.EQ.3)THEN
      PRINT'(''OLAMDA QCD='',D15.6)',XLAM
      PRINT'(''OC MASS='',D15.6)',X(1)
      PRINT'(''OB MASS='',D15.6)',X(2)
      PRINT'(''OC1='',D15.6)',X(3)
      PRINT'(''OC2='',D15.6)',X(4)
      PRINT'(''ORO='',D15.6)',X(5)
      PRINT'(''OAA='',D15.6)',X(6)
      PRINT'(''OT MASS='',D15.6)',X(7)
      DO 740 JK=1,15
       PRINT 741,JK,YTHEO(JK)
741    FORMAT(I6,D20.10)
740   CONTINUE
      END IF

C  ***  ARRAY ABJ CALCULATES CHI**2 FOR QUARKONIA DATA
      F=0.0D+00
      DO 730 LMN=2,12
       ABJ(LMN)=((YTHEO(LMN)-QDATA(LMN))/QERR(LMN))**2
730   CONTINUE
      DO 630 LMN=2,12
       F=F+ABJ(LMN)
630   CONTINUE
```

```
      IF(IFLAG.EQ.3)THEN
      DO 631 LMN=2,12
       PRINT 632,LMN,QDATA(LMN),QERR(LMN),ABJ(LMN)
632    FORMAT (I6,3D15.6)
631   CONTINUE
      PRINT'(''OCHI**2 FROM QUARKONIA='',D15.6)',F
      END IF

      CALL SUB2(VRG6,VRG2,X)
C  ***  ARRAY BZ CALCULATES CHI**2 FOR POTENTIAL AT SHORT DISTANCES
      BZ=0.0D+00
      DO 725 N=1,10
      BZ=BZ+((VRG1(N)-VRG2(N))/ERROR(N))**2
725   CONTINUE
      F=F+BZ
      IF(IFLAG.EQ.3)THEN
      PRINT'(''OCHI**2 FROM POTENTIAL='',D15.6)',BZ
      PRINT'(''OTOTAL CHI**2='',D18.6)',F
      PRINT'(''O    R          VS                PHENOM.          CHI**2'')'
      DO 728 N=1,10
      QM=0.01D+00
      YAF=N*QM/XLAM
      PRINT 729,YAF,VRG1(N),VRG2(N),((VRG1(N)-VRG2(N))/ERROR(N))**2
729   FORMAT (4D15.6)
728   CONTINUE
      END IF
      RETURN
      END

C  ***  SUB1 CALCLATES REGULARISED AND UNREGULARISED SHORT DISTANCE
C  ***  PART OF THE POTENTIAL

      SUBROUTINE SUB1(VRG1,ERROR,VRG6)
      IMPLICIT REAL*8 (A-H,O-Z)
      COMMON/ABCD/PI,XH,EUL,XLAM,BETA0,BETA1,BLER,NF,KQ
      DIMENSION A1R(40),Q1A(40),ALPHA(40),VRG1(40),ERROR(40),FX(40)
      DIMENSION VRG6(40),FY(40)
      ISTEP=500
      DO 100 N=1,10
      JSIM=-1
      TOT=0.0D+00
      AXH=0.01D+00
      PU=N*AXH/XLAM
      XMC=1.5D+00
      VEX=5.0D+00/6.0D+00
      ZMC=XMC*EXP(VEX)
      BEG=ZMC*PU
      FIN=3.0D+01
      AH=(FIN-BEG)/ISTEP
      DO 200 IA=1,ISTEP+1
       Q=BEG+((IA-1)*AH)
       IFAC=3+JSIM
       IF((IA.EQ.1).OR.(IA.EQ.ISTEP+1))THEN
       IFAC=1
       END IF
       TEG=EXP(-Q)/Q
       TOT=TOT+IFAC*TEG
       JSIM=-JSIM
200   CONTINUE
      TOT=TOT*AH/3
      A1R(N)=BLER+(LOG(XMC*PU)/3.0)+TOT/3.0
      Q1A(N)=EXP(-A1R(N)/BETA0)*(1.0/PU)
      BB2=BETA0**2/BETA1
      BB4=(BB2/2)**(1./BB2)
      ZL0=BETA0**2*LOG((Q1A(N)/XLAM)+BB4)
      ZL1=BETA0**2*LOG(Q1A(N)/XLAM)
      ZL2=BETA1*LOG(2./BB2)
      XX=BETA1/(ZL1+ZL2)
      FX(1)=XX
      DO 300 JK=1,40
       FX(JK+1)=XX/(1.+XX*DLOG((FX(JK)+1)/FX(JK)))
       IF(ABS(FX(JK+1)-FX(JK)).LT.1.0D-04)THEN
       C2=FX(JK+1)
```

```
        GOTO 301
        END IF
300     CONTINUE
301     CONTINUE
        RHO=BETA0*C2/BETA1
        ALPHA(N)=PI*RHO
        VRG1(N)=-4*ALPHA(N)/(3*PU)
        ERROR(N)=(3*ALPHA(N)/PI)**2*VRG1(N)
        YY=BETA1/(ZL0+ZL2)
        FY(1)=YY
        DO 305 JK=1,40
        FY(JK+1)=YY/(1.+YY*DLOG((FY(JK)+1)/FY(JK)))
        IF(ABS(FY(JK+1)-FY(JK)).LT.1.0D-04)THEN
        C4=FY(JK+1)
        GOTO 306
        END IF
305     CONTINUE
306     CONTINUE
        PFR=BETA0*C4*PI/BETA1
        VRG6(N)=-4*PFR/(3*PU)
100     CONTINUE
        END

C   ***  SUB2 CALCULATES THE TOTAL INTERQUARK POTENTIAL TO BE
C   ***  COMPARED AGAINST THE PERTUBATIVE POTENTIAL

        SUBROUTINE SUB2(VRG6,VRG2,X)
        IMPLICIT REAL*8 (A-H,O-Z)
        COMMON/ABCD/PI,XH,EUL,XLAM,BETA0,BETA1,BLER,NF,KQ
        DIMENSION VRG6(40),VRG2(40),X(30)
        DO 100 N=1,10
        BXH=0.01D+00
        PU=N*BXH/XLAM
        VRG2(N)=VRG6(N)+X(6)*PU+PU*(X(3)+PU*X(4))*DEXP(-PU/X(5))
100     CONTINUE
        END

C   ***  SUB3 CALCULATES THE TOTAL INTERQUARK POTENTIAL TO
C   ***  SCHRODINGERS EQUATION WITH.

        SUBROUTINE SUB3(VRG3,VRG4,X)
        IMPLICIT REAL*8 (A-H,O-Z)
        COMMON/ABCD/PI,XH,EUL,XLAM,BETA0,BETA1,BLER,NF,KQ
        DIMENSION X(30),VRG3(99),VRG4(99)
        DO 100 N=1,KQ
        PU=N*XH
        QU=1-PU
        RAB=QU/PU
        IF((RAB/X(5)).GT.1.0D+02)THEN
        A2=X(6)*RAB
        ELSE IF((RAB/X(5)).LT.9.999D+01)THEN
        A2=X(6)*RAB+RAB*(X(3)+X(4)*RAB)*DEXP(-RAB/X(5))
        END IF
        VRG3(N)=VRG4(N)+A2
100     CONTINUE
        END

C   ***  SUB4 CALCULATES THE TOTAL SHORT DISTANCE POTENTIAL TO
C   ***  LARGE DISTANCES.

        SUBROUTINE SUB4(VRG4)
        IMPLICIT REAL*8 (A-H,O-Z)
        COMMON/ABCD/PI,XH,EUL,XLAM,BETA0,BETA1,BLER,NF,KQ
        DIMENSION A1R(99),Q1A(99),ALPHA(99),X(30),VRG4(99),FX(60)
        ISTEP=500
        DO 100 N=1,KQ
        JSIM=-1
        TOT=0.0D+00
        PU=N*XH
        QU=1-PU
        XMC=1.5D+00
        VEX=5.0D+00/6.0D+00
        ZMC=XMC*EXP(VEX)
        BEG=ZMC*QU/PU
```

```
      FIN=3.0D+01
      IF(N.LE.5)THEN
      TOT=0.0D+00
      GOTO 250
      END IF
      AH=(FIN-BEG)/ISTEP
      DO 200 IA=1,ISTEP+1
       Q=BEG+((IA-1)*AH)
       IFAC=3+JSIM
       IF((IA.EQ.1).OR.(IA.EQ.ISTEP+1))THEN
       IFAC=1
       END IF
       TEG=EXP(-Q)/Q
       TOT=TOT+IFAC*TEG
       JSIM=-JSIM
200   CONTINUE
      TOT=TOT*AH/3
250   CONTINUE
      RAB=QU/PU
      A1R(N)=BLER+(LOG(XMC*RAB)/3.0)+TOT/3.0
      Q1A(N)=EXP(-A1R(N)/BETA0)*(1.0/RAB)
      BB2=BETA0**2/BETA1
      BB4=(BB2/2)**(1./BB2)
      ZL1=BETA0**2*(LOG((Q1A(N)/XLAM)+BB4))
      ZL2=BETA1*LOG(2./BB2)
      XX=BETA1/(ZL1+ZL2)
      FX(1)=XX
      DO 300 JK=1,60
       FX(JK+1)=XX/(1.+XX*DLOG((EX(JK)+1)/EX(JK)))
       IF(ABS(FX(JK+1)-FX(JK)).LT.1.0D-04)THEN
       C2=FX(JK+1)
       GOTO 301
       END IF
300   CONTINUE
301   CONTINUE
      RHO=BETA0*C2/BETA1
      ALPHA(N)=PI*RHO
      VRG4(N)=-4*ALPHA(N)/(3*RAB)
100   CONTINUE
      END
```

Example :

We reproduce the output from a sample fit to the $c\bar{c}$ and $b\bar{b}$ data, for Λ = 0.2 GeV. This corresponds to the fit shown in Table 3.1. The total χ^2 is split into contributions from the quarkonia data values and from the fit to the perturbative form of the potential, as indicated by eq.(3.13), and we indicate the χ^2 contribution from each point in the sum of eq.(3.7) for χ^2_V .We also make $t\bar{t}$ predictions for m(1S) = 80 GeV in numbers 13,14 and 15. These correspond to m(2S) - m(1S), Γ_1 and m(1P) - m(1S) respectively, as shown in Table 4.2.

```
LAMDA QCD=    0.200000D+00
C MASS=     0.136620D+01
B MASS=     0.478836D+01
C1=    -0.112602D+01
C2=     0.118634D+01
RO=     0.697543D+00
AA=     0.216293D+00
T MASS=     0.405169D+02
     1     0.6096214067D+00
     2     0.3067956555D+01
     3     0.4265091276D+00
     4     0.4942728914D+00
     5     0.9451998927D+01
     6     0.5713666616D+00
     7     0.9028976918D+00
     8     0.4456103005D+00
     9     0.7901707914D+00
    10     0.3868182799D+00
    11     0.3191472569D+00
    12     0.8000098631D+02
    13     0.6693949403D+00
    14     0.3541652031D-05
    15     0.5478684594D+00
     2   0.306800D+01    0.200000D-02    0.471861D-03
     3   0.457000D+00    0.100000D-01    0.929693D+01
     4   0.432000D+00    0.600000D-01    0.107720D+01
     5   0.945200D+01    0.250000D-02    0.184297D-06
     6   0.567000D+00    0.300000D-02    0.211864D+01
     7   0.900000D+00    0.250000D-02    0.134346D+01
     8   0.448000D+00    0.250000D-02    0.913706D+00
     9   0.809000D+00    0.600000D-02    0.984831D+01
    10   0.439000D+00    0.300000D-01    0.302548D+01
    11   0.328000D+00    0.300000D-01    0.870790D-01
    12   0.800000D+02    0.100000D+00    0.972806D-04
CHI**2 FROM QUARKONIA=    0.277114D+02
CHI**2 FROM POTENTIAL=    0.163976D+01
TOTAL CHI**2=       0.293511D+02
      R          VS          PHENOM.          CHI**2
 0.500000D-01  -0.444733D+01  -0.445672D+01  0.691914D-02
 0.100000D+00  -0.267907D+01  -0.270183D+01  0.532290D-01
 0.150000D+00  -0.203589D+01  -0.206254D+01  0.748599D-01
 0.200000D+00  -0.169897D+01  -0.172075D+01  0.468744D-01
 0.250000D+00  -0.149192D+01  -0.150113D+01  0.747895D-02
 0.300000D+00  -0.135290D+01  -0.134293D+01  0.760110D-02
 0.350000D+00  -0.125469D+01  -0.121964D+01  0.797586D-01
 0.400000D+00  -0.118311D+01  -0.111782D+01  0.230781D+00
 0.450000D+00  -0.113018D+01  -0.103034D+01  0.443297D+00
 0.500000D+00  -0.109106D+01  -0.952813D+00  0.688961D+00
```